

ELECTRON SPIN RESONANCE IN TRANSITION METAL IONS

THESIS

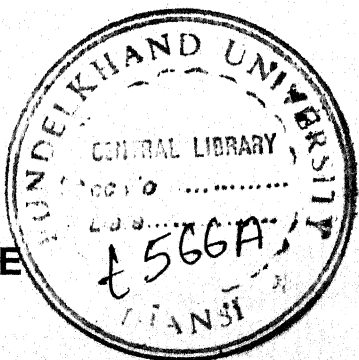
Submitted to the

Bundelkhand University,
Jhansi, U.P. (INDIA)

*For the Degree of
Doctor of Philosophy in Physics*

-:By:-

RAJNEESH KHARE



Under The Supervision Of

Dr. N.L. Shukla

Reader & Head, Physics Department

Atarra P.G. College

Atarra (Banda), U.P.

(Supervisor)

(2002)

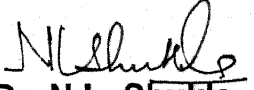
For
My Mummy Ji

Certificate

This is to certify that the present thesis entitled "Electron Spin Resonance in Transition Metal Ions" embodies the unaided research work of Rajneesh Khare. This work was carried out under my supervision and has not been submitted elsewhere for a degree.

Mr. Rajneesh Khare has attended the research center, P.G. Department of Physics, Atarra P.G. College, Atarra (Banda), more than 300 days.

Date: 25.12.2002


Dr. N.L. Shukla
Reader & Head
Department of Physics
Atarra P.G. College
Atarra (Banda), U.P.
Supervisor

ACKNOWLEDGEMENT

At this moment I thank first and foremost Goddess Durga Ji for making me blessed with this research work.

I express my deepest sense of gratitude and regards to Dr. N.L. Shukla for his kind guidance and keen interest, which made this present work possible. I am equally thankful to Dr. S.K. Mishra, Head, Department of Physics, D.B.S. College, Kanpur, for his great help during the various stages of the work.

I am highly thankful to Dr. D.N. Pandey, Ex. Principal, Atarra P.G. College, Atarra, for his encouragement during the progress of the work.

I am also thankful to Prof. K.N. Pathak, Vice Chancellor, Punjab University, Chandigarh, and Prof. B.N. Mishra, Retd. Prof. of Physics, Allahabad University, Allahabad, for their kind guidance and help.

I have been greatly benefited by discussion with Dr. D.C. Dwivedi, Dr. Vikas Mishra and Mr. Anurag Mishra, Department of Physics, D.B.S. College, kanpur. I convey my sincere thanks to them.

I also convey my special thanks to Mr. Bharat Morbhatt and Mr. Ajay Pratap Srivastava for helping and boosting me during difficult moments of research work.

I take this opportunity to express my respects and regards to Smt. Kusum Lata Shukla (Respected Aunty Ji) and convey my thanks to all family members of Dr. N.L. Shukla who have shown a lot of affection and given unlimited contribution for my progress.

I wish to express my deep sense of indebtedness to my mother Smt. Rajeshwari Khare and Father Sri. K. M. Khare as they are the source of inspiration to me.

I convey a special thanks to my elder brother Flt. Lt. Rajeev Khare, Bhabhi Smt. Rashmi Khare and dear Ratnam Khare who have always supported and backed me up in the hard moments of life.

In the end, I can not forget to thanks my dear friends Brajpal, Avineesh, Abhay and Rajesh for their help and moral support for all the time.

Dated : 25.12.02

Rajneesh Khare

(Rajneesh Khare)

List of Publications

1. *Effect of exposure to Lithium and Iodine Vapours of transition ions doped ceramics.* Presented in the fourth Conference of International Academy of Physical Science, Feb. 25-27(2001), Chitrakoot, N. L. Shukla, R. K. Shukla, Bharat Morbhatt, S.K. Mishra, Rajneesh Khare, Vikas Mishra and A. P. Srivastava.
2. *Experimental investigations on $(ZrO_2)_{0.8}(Y_2O_3)_{0.2}$ ceramic compound.* Presented in the fourth conference of International Academy of Physical Science, Feb 25-27 (2001). Chitrakoot, N. L. Shukla, R. K. Shukla, Bharat Morbhatt, S. K. Mishra, Vikas Mishra, Rajneesh Khare and A. P. Srivastava.
3. *EPR study of Mn^{+2} : $Cd(1m)_6(No_3)_2$.* Presented in the 2nd National Seminar on new dimensions of Higher Physics and Information Technology, Dec 16-17 (2001), Kanpur, N.L. Shukla, A. P. Srivastava, Rajneesh Khare and Bharat Morbhatt.
4. *Intensities of Various spectra in Mn^{2+} : $NaNO_2$.* Presented in the fifth conference of International Academy of Physical Science, April 07- 09 (2002), Jhansi, N. L. Shukla, A. P. Srivastava, Rajneesh Khare and Abhishek Richharia.

CONTENTS

	Page
Chapter- 1	
Introduction	1
References	7
General References	9
Chapter -2 Theoretical Cosideration of Electron Spin Resonance	
2.1 Introduction	11
2.2 Crystal field effects	12
(i) Weak crystal field	13
(ii) Intermediate crystal field	13
(iii) Strong crystal field	14
2.3 Hyperfine Interaction	14
2.4 The Spin Hamilton	14
2.5 Covalency Effects and Super hyperfine structure	17
2.6 Kramer's Theorem and the Jahn-Teller [J-T] Effect	18
2.7 Spin-Lattice and Spin-Spin Relaxations	19
2.8 ESR of liquids	20
2.9 Power ESR spectra	23
2.10 The Expected Power lineshapes	27
(i) Patterns without hyperfine splitting	27
(ii) Patterns with hyperfine splitting	29

2.11 (1) Computation of Resonance field	30
(2) Method for S= 1/2 Ions	31
Figures 2.1 -2.4	33
References	37

CHAPTER-3 Experimental Techniques

3.1 Electron Spin Resonance (ESR)	42
3.2 X-ray Diffraction (XRD)	43
3.3 Scanning Electron Microscope (SEM)	45
Figure 3.1 - 3.4	47
Referenes	51

CHAPTER-4 Experimental Investigations on $(\text{ZrO}_2)_{0.8} (\text{Y}_2\text{O}_3)_{0.2}$ Ceramic Compounds

4.1 Introduction	52
4.2 Experimental	53
4.3 Results and Disussion	55
(a) X-ray diffraction studies	55
(b) Scanning electron microscopy studies	57
(c) Electron Spin Resonance Studies	58
I. Pure Sample SZYP	58
II. Titanium Deped Sample SZYTi	59
III. Nickel Deped sample SZY Ni	60
IV. Cobolt deped sample SZYCo	60
4.4 Conclusion	61
Tables 4.I - 4.IV	62

Figures 4.1(a)- 4.3(d)	67
References	79
CHAPTER -5 ESR study of Copper Amino Acid Complexes	
5.1 Introduction	81
5.2 Polycrystalline Sample study	82
5.3 Glass Study	90
5.4 Solution study of the samples	100
5.5 Conclusion	112
Table 5.I - 5.VII	114
Figure 5.1 - 5.10	121
References	131
CHAPTER- 6 The angular variation and temperature variation of line widths and temperature variation of Spin- Hamiltonian parameters in $Mn^{+2} : NaNo_2$.	
6.1 Experimental observations	135
6.2 Discussion	140
(1) Temperature variation of D and E and Phase	140
(2) Line Widths	152
Tables 6.I - 6.III	166
Figures 6.1 - 6.10	169
References	179

Chapter- 1

Introduction

CHAPTER - 1

INTRODUCTION

The electron Spin Resonance (ESR) has become one of the most powerful tools for studying the wide varieties of Physical, chemical and Biological effects and also for the study of magnetic behaviour of paramagnetic substances. It was first observed by E.J. Zavoisky [1] in -1945 at USSR. Later on Cummerow and Halliday [2], Bleaney and Penrose [3] obtained well resolved resonance spectra of paramagnetic ions of the first transition series. A. Abragam, B. Bleaney, J.H.E. Griffiths, K.W.H. Stevens and their co-workers did the major developmental work in the techniques of ESR at the Clarendon laboratory, Oxford.

If a static magnetic field is applied to a system of free electrons ($L=0$, $S=1/2$), the electrons align themselves either parallel or antiparallel to the applied magnetic field. On applying electromagnetic field of frequency ν in a direction perpendicular to a d.c. magnetic field, the transitions of the electrons from lower level to upper level according to the selection rule $\Delta M_S = \pm 1$ take place and a sharp absorption of Power occurs provided the relation

$$h\nu = g\beta H \quad (1.1.1)$$

is satisfied. Mostly the population ratio of the two energy states is given by the Maxwell-Boltzmann distribution relation :

$$\frac{n_1}{n_2} = e^{-\Delta E / kT} \quad (1.1.2)$$

where n_1 and n_2 are the number of free electrons in the upper and lower states respectively and ΔE is the energy separation between the two states. In case of single spin system the population of the ground state is slightly in excess of the population of the upper state. Factually for a temperature of about 300^0 K and magnetic field 3000 gauss, the excess population in the ground state is only about 0.07 percent; yet the whole phenomenon of ESR depends upon this difference. If this resonance absorption of the radiation is to continue, there must be some other mechanism, apart from the stimulated emission which allows the electrons of the upper state to lose energy and drop to lower state, otherwise after sometime the population of the lower state will be zero and absorption will cease. Spin-lattice interaction, spin-spin interaction and exchange interaction are the important processes by which electrons lose energy and come to ground state and the absorption becomes a steady process [4].

The Hyperfine splitting of an electron Spin Resonance line is obtained when the interaction between the unpaired electron and the magnetic nucleus takes place within the molecule. It is of extreme importance in determining the distribution of unpaired electron density and leads us to reach the valuable information regarding the intra and inter molecular interactions. The total Hamiltonian of the system inclusive of ESR and Hyperfine processes is given by

$$\mathcal{H} = g\beta\bar{H} \cdot \bar{S}_z + A \bar{S} \cdot \bar{I} \quad (1.1.3)$$

assuming the ion to be free. But the unpaired electron is not always free and is bound in the molecule by a number of forces. The above Hamiltonian will be modified for a macroscopic body containing a paramagnetic as well as a large number of diamagnetic components. A brief discussion is given in chapter two of the thesis.

The substances possessing a resultant electronic magnetic moment exhibit the phenomenon of ESR. The materials possessing this property are transition elements, electrons trapped in radiation damages, impurities in semiconductors, free radicals and many other biological materials. The ESR study gives the various significant informations about the system which are mentioned below :

- (i) The phenomenon of Electron Spin Resonance under certain conditions is found useful in providing the information about the bulk properties like susceptibility and specific heat of the system.
- (ii) The resonance spectrum is extremely sensitive to the surroundings of the paramagnetic ion in the system. Thus it also provides information about the symmetry of the surroundings, the nature and the strength of the bonding between the ion and its immediate diamagnetic neighbour.
- (iii) The width of the resonance lines in a fully resolved spectrum depends on a number of factors such as (a) spin-lattice interaction (b) spin-spin interaction and (c) exchange interaction etc. The study of the width of the ESR lines provides complete

information about the strength and nature of these magnetic as well as non-magnetic interactions present in the system.

- (iv) Electronic transitions provide resonance spectra which help to obtain reliable interpretation about the nuclear spin of the paramagnetic ion. The values of nuclear dipole and nuclear quadrupole moments may also be found approximately.
- (v) From the analysis of the observed hyperfine structure we can draw conclusions concerning the nature of the sample and the character of the delocalization of the molecular orbital of the unpaired electron.

Thus there are various parameters of ESR spectrum e.g. lineshape, line width, g-value, intensity of the signal and hyperfine splitting constant etc, from which a variety of informations about the paramagnetic molecule can be obtained. Apart from these points, the informations derived from the ESR spectrum also depends upon the nature and form of the specimen used.

Concentrated specimens used for ESR study usually provide single line spectrum [5-8]. In the case of polycrystalline samples, one gets linewidth and g-value averaged out over all possible orientations of the crystallites present in the samples. The Hyperfine structure [9-15] is studied in the diluted solutions of the complexes. When magnetically diluted single crystals are used for ESR study [16-20] we obtain most significant in-

formations. Results of directional anisotropies in line width and g-value which are obtained only from single crystal study, give informations about the configurations of the ions present in the complexes. A. Abragam, et al. have developed most of the theory on crystal fields and electron spin resonance [21,22,23]. It is not always possible to grow a magnetically dilute single crystal. However, it has been shown possible to obtain the similar type of informations from Powder, and glass state ESR spectra [8-22]

Among the transition group elements, Copper is of great importance because of the reason that most of the discoveries associated with microwave spectra of solid state have been first observed in Cu^{+2} salts [28-30]. McGarvey [9], Cohn [10], Kozyrev[11], Kivelson and Wilson [15], Chary and Sastry [24], Misra and Sharma [25-27], have investigated the paramagnetic resonance spectra of the transition metal ions.

The present thesis consists of Six Chapters including first chapter of Introduction.

In Chapter II, a description of the various theories used for the estimation of different ESR parameters have been discussed.

Chapter III describes the experimental setup of the techniques of ESR along with X-RD and SEM which are being employed to study magnetic, structural and electrical properties of the samples.

Chapter IV is based on Ti, Ni, and Co transition metal ions doped in $(\text{ZrO}_2)_{(0.8)} (\text{Y}_2\text{O}_3)_{(0.2)}$ ceramic compound using ESR, XRD and SEM techniques.

The results obtained are presented and discussed.

Chapter V consists of ESR studies of Cu^{2+} -Amino Acids complexes in polycrystalline solution and glassy state. The spin Hamiltonian parameters and line width studies have been carried out at LNT and RT.

Chapter VI consists the ESR studies of Mn^{2+} ion doped in diamagnetic lattice ($\text{Mn}^{2+} \text{: NaNO}_2$). The angular and temperature variation of line widths and spin Hamiltonian parameters have been studied.

REFERENCES

1. E.J. Zavoisky, J. Phys. (USSR) 9 (1945) 211; ibid 10 (1946) 197.
2. R.L. Cummerow and D. Halliday, Phys. Rev. 70 (1946) 433.
3. B. Bleaney and R.P. Penrose, Nature 157, (1946) 339.
4. G.E. Pake, Spin resonance, W.A. Benjamin Inc. New York (1962).
5. H. Kumagai, K. Ono, I. Hayashi, H. Abe, I. Shimada, H. Shono, H. Ibamato and S. Tachimori, J. Phys. Soc. Japan, 9 369 (1954).
6. C. Maclean and G.J.W. Kor, Appl. Sci. Res. 48, 425 (1955).
7. B.N. Misra and S.K. Gupta, J. Mag. Resonance, 12 126 (1973).
8. F.K. Neubuhl, J. Chem. Phys, 33 1074 (1960).
9. B.R. McGarvey, J. Chem. Phys 60, 71 (1956).
10. M. Cohn and J. Townsend, Nature, 173, 1090 (1954).
11. B.M. Kozyrev, Disc. Faraday Soc; 19, 135 (1955).
12. B.B. Garrett and L.O. Morgan, J. Chem. Phys; 44, 890 (1966).
13. B.N. Misra, S.D. Sahrma and S.K. Gupta IL Nuovo Cimento 19, 129 (1974).
14. M.P. Eastman, G.R. Kooser, M.R. Das and J.H. Freed J. Chem. Phys; 51, 2690 (1969).
15. D. Kivelson and R. Wilson, J. Chem. Phys 44, 154, 4440, 4445 (1966).

16. B. Bleaney and D.J.E. Ingram, Proc. Roy. Soc. A205, 336 (1951).
17. M. Weger and W. Low; Phys Rev. 111. 1526 (1958).
18. H.C. Box and H.G. Freund, J. Chem. Phys. 40, 817 (1968).
19. B. Bleaney, K.D. Bowers and D.J.E. Ingram, Proc. Roy. Soc. A228, 147 (1955).
20. R. Janakiraman and G.C. Upreti J. Chem. Phys. 54, 2336 (1971).
21. A. Abragam and B. Bleaney, Electron Spin resonance of Transition Ions, Clarendon Press, Oxford (1970).
22. D. Kivelson and R. Neiman, J. Chem. Phys. 35, 156 (1961).
23. K.D. Bowers and J. Owen, Reports on Progress in Physics, 18, 304 (1955).
24. M.N. Chary and B.A. Sastry, Indian J. Pure and Appl. Phys. 15, 172 (1977).
25. B.N. Misra and S.D. Sahrma, J. Chem. Phys. 63, 5322, (1975).
26. B.N. Misra and S.D. Sharma, J. Mag. Reso. 24. 1 (1976).
27. B.N. Misra and S.D. Sharma, Indian J. Pure and Appl. Phys. 15, 719 (1977).
28. D.J.E. Ingram, Proc. Phys. Soc. A62, 664 (1949).
29. B. Bleaney and D.J.E. Ingram, Proc. Roy. Soc., A63, 408 (1950).
30. B. Bleaney, K.D. Bowers and D.J.E. Ingram, Proc. Phys. Soc. A64, 758 (1951).

GENERAL REFERENCES

1. D.J.E. Ingram, 'Spectroscopy at radio and microwave frequencies : Butter worth London (1955).
2. W. Gordy, 'Theory and Application of Electron Spin Resonance' (John Wiley and sons, Inc, 1972).
3. C. P. Poole Jr. and H.A. Farach, 'The Theory of magnetic resonance (John Wiley and sons Inc. 1972).
4. W. Low ' Paramagnetic resonance in solids' (Academic press New York and London 1960).
5. A. Abragam, B. Bleany, ' Electron Paramagnetic resonance of Transition Ions (Clarendon press, Oxford 1970).
6. C. J. Ballhausen, Introdution to ligand field theory (McGraw Hill Book Co. Inc. New Delhi 1962).
7. M.W. Porter and R.C. Spiler, Barker Index of crystals, Haffer Cambridge (1956).
8. R. W. G. Wyckoff, Crystal Structure, (Vol. 3, Interscience Publ. 1965).
9. K.A. Muller and H. Thomas, 'Structural Phase Transitions I' (Springer Verlag Berlin , Heidelberg, New York 1981).
10. F. J. Owens, C.P. Poole Jr. and H.A. Farach, Magnetic Resonance of Phase Transitions, Academic Press(1979).
11. A CarRington and A. D. McLachlen, Introduction to Magnetic Resonance

(Chapman and Hall, 1979).

12. J. E. Wertz and J. R. Bolton, Electron Spin Resonance ; Elementary theory and Practical Applications, McGraw Hill (1972).
13. J.W. Orton, Electron Paramagnetic Resonance, Ilitte Books Ltd. London (1968).
14. B. D. Cullity, Elements of X-ray diffraction, Addison- Wisley Pub. Company, Inc. California (1978).
15. Kaiser and L. Kavad, Electron Spin Resonance of first row transition Metal Complex ions, John Wiley (1968).
16. R. K. Watts : Points Defect's in crystals, John Wiley and Sons (1977) .



Chapter -2

Theoretical Consideration of Electron Spin Resonance

CHAPTER -2

2.1 INTRODUCTION

When a free ion with a resultant angular \bar{J} is subjected to a static magnetic field \bar{B} then it has $2\bar{J} + 1$ energy levels and the energies of the various states are given as :

$$E_{M_J} = g \cdot \beta B M_J \quad (2.1.1)$$

where $M_J = J, J-1, \dots, -J+1, -J$, B is the static magnetic field. g is the spectroscopic splitting factor and β is Bohr magneton. The electrons in the unfilled 3d, 4d, 4f, 5d and (5f, 6d) shells are responsible for paramagnetism in iron, Palladium, rare earth, platinum and actinide group complexes. A resonance absorption line corresponding to the energy difference ΔE between the E_{M_J} levels differing in M_J value by ± 1 should be observed. Therefore, the resonance condition becomes :

$$\Delta E = h\nu = g \beta B \quad (2.1.2)$$

The resonance condition for free electron is shown in fig. 2.1 .

The intensities of these transition are given by the square of the matrix element connecting M_J^{th} and $(M_J+1)^{\text{th}}$ levels. The intensities are governed by the following relation.

$$[\text{Intensity}]_{M_J \leftrightarrow M_J \pm 1} \propto [J(J+1) - M_J(M_J \pm 1)] \quad (2.1.3)$$

Thus transitions with different $M_J \leftrightarrow M_J \pm 1$ values will have different intensities. For the case of $J = 5/2$ the five transitions corresponding to $\Delta M_J = \pm 1$ would have intensities in 5:8:9:8:5: Ratio.

2.2 CRYSTAL FIELD EFFECTS

The energy levels of ions in a crystalline environment differ from the free ion energy levels. When a metal ion is placed in a crystalline field, the degeneracy of the d-orbitals will be removed by the electrostatic interactions. The spin degeneracy will remain until a magnetic field is applied. When the species contains more than one unpaired electron, the spin degeneracy can also be resolved by crystal field. Thus the spin levels may be split even in the absence of a magnetic field ; this phenomenon is called zero-field splitting. The theoretical explanation of zero-field splitting in S-state ions was given by Van Vleck and Penny [1], Sharma et. al. [2], Narayana [3], Chatterjee et. al. [4], and Watanable [5].

The EPR splitting of energy levels occurs under the effect of two types of fields ; crystal field around the ion and the applied magnetic field. The crystal field is also called the internal splitting field and the energy splitting caused by this field are called 'Crystal field splitting' or ' Internal field splitting' or ' Zero field splitting' (ZFS) since it happens in the absence of external magnetic field. For the paramagnetic ion in a crystal, there are two types of interactions, interactions between the paramagnetic ions (dipolar) and interactions between the paramagnetic ion and the nearest neighbours (ligand field). Former interaction is large in concentrated paramagnetic complexes but can be reduced effectively to a negligibly small value by dilution i.e. by doping small amounts of paramagnetic complex in an isomorphous diamagnetic host. Thus each ion may be considered

isolated from other paramagnetic ions and to be independent. The latter interactions of paramagnetic ion with diamagnetic ligands modify the magnetic properties of the paramagnetic ions. The crystal field (CF) theory assumes that the ligands influence the magnetic ion through the electric field which they produce at its site and their orbital motions get modified. The crystal field interaction is affected by the electrostatic screening by the outer electronic shells. Depending upon its magnitude relative to other interactions, the crystalline field interaction is generally classified into three categories.

2.2. (i) Weak Crystal Field

When the crystal field interaction is weaker than the spin-orbit coupling (this is the case with the rare-earth and certain actinide compounds). It is due to the fact that the unfilled shell, 4f or 5f lies fairly deep within the ion and is shielded by the closed 5s and 5p or 6s and 6p shells respectively.

2.2 (ii) Intermediate Crystal Field

When the crystal field interaction is greater than spin-orbit coupling but is less than the coulombic interaction between electrons. The best example of these are hydrated salts of the iron group. This situation is described by regarding the orbital motion as clamped due to crystal field and making it unable to respond to an applied magnetic field. This is known as "quenching of orbital angular momentum" and the magnetic properties are all due to spin which is affected only weakly by crystal field through spin-orbit coupling.

2.2. (iii) Strong Crystal Field

The crystal field is said to be strong when the crystal field interaction is of the order of coulombic interaction between electrons. For the 4d and 5d transition group ions there is a tendency of covalent bonding due to which the orbitals of the metal ion and neighbouring ligands overlap appreciably. In this case due to strong covalent bonding the crystal field assumption remains no longer valid.

2.3 HYPERFINE INTERACTION

Hyperfine interaction are mainly magnetic dipole interactions between the electronic magnetic moment and the nuclear magnetic moment of the paramagnetic ion. The origin of this can be understood simply by assuming that the nuclear moment produces a magnetic field B_N at the magnetic electrons and the modified resonance condition is :

$$\Delta E = h\nu = g\beta [B + B_N] \quad (2.3.1.)$$

The hyperfine interaction is highly characteristic one. Identification of paramagnetic and its isotopes in characteristic by the hyperfine structure (HFS) in the ESR spectra is the simplest method. The interaction of the magnetic electron with nuclei of the ligands gives rise to super hyperfine structure (SHFS) on the HFS in the ESR spectra.

2.4 THE SPIN HAMILTONIAN

The ESR, the unpaired electron is not isolated or free, but frequently interacts with a variety of nuclei and electrons. Therefore the right handside in eqn. (2.1.2) becomes the sum of various terms. The state of affairs may be expressed from the quantum mechanical view point in terms of a Hamiltonian.

The electronic interactions which contribute to the total energy of the ion may be described by the following Hamilton. [6 - 10].

$$\mathcal{H} = \mathcal{H}_0 + \mathcal{H}_{cr} + \mathcal{H}_{s-o} + \mathcal{H}_{s-s} + \mathcal{H}_z + \mathcal{H}_{h-f} + \mathcal{H}_q + \mathcal{H}_n + \mathcal{H}_e \quad (2.4.1)$$

Where

\mathcal{H}_0 = Free ion energy [$\sim 10^5$ cm $^{-1}$]

\mathcal{H}_{cr} = Electrostatic energy ($\sim 10^4$ cm $^{-1}$)

\mathcal{H}_{s-o} = Spin orbit interaction energy ($\sim 10^2 - 10^3$ cm $^{-1}$)

\mathcal{H}_{s-s} = Spin-spin interaction energy (~ 1 cm $^{-1}$)

\mathcal{H}_z = Interaction of electron with the external field or Zeeman energy = $\beta B (L + 2S)$ (~ 1 cm $^{-1}$)

\mathcal{H}_{h-f} = Dipole-dipole interaction between the electron and nuclear-magnetic moments ($\sim 10^{-1}$ cm $^{-1}$ - 10^{-3} cm $^{-1}$)

\mathcal{H}_q = Quadrupole interaction between electron and nucleus ($\sim 10^3$ cm $^{-1}$)

\mathcal{H}_n = Nuclear Zeeman energy = $g_N \beta_N B.I.$ ($\sim 10^4$ cm $^{-1}$)

\mathcal{H}_e = Energy of exchange effects between electrons.

Practical ESR spectroscopy concerns itself mainly with the \mathcal{H}_{s-s} , \mathcal{H}_z , and \mathcal{H}_{h-f} i.e. the fine structure, Zeeman splitting and hyperfine interactions as the nuclear Zeeman and quadrupole interactions are usually small. The best way to consider all the energy contributions is to express them in the following form including the nuclear Zeeman and quadrupole terms [10].

$$\mathcal{H} = \beta \bar{B} \cdot \bar{g} \cdot \bar{S} + \bar{S} \cdot \tilde{D} \cdot \bar{S} + \bar{S} \cdot \tilde{A} \cdot \bar{I} - \beta_N \bar{B} \tilde{g}_N \bar{I} + \bar{I} \cdot \tilde{Q} \cdot \bar{I} \quad (2.4.2)$$

Where \bar{S} and \bar{I} are the electronic spin and nuclear spin operators respectively and are equivalent to \bar{J} operators from mathematical point of view and \bar{g} , \tilde{D} , \tilde{A} , \tilde{Q} , and \tilde{g}_N are all second rank tensor quantities. The first term represents Zeeman interaction with the applied field B , the presence of orbital momentum is taken into account by allowing the splitting factor \bar{g} to differ from the spin-only value 2.0023. \tilde{D} in the second term represents the crystal field splitting. The third term expresses the hyperfine interaction between S and I . The fourth term express the nuclear Zeeman interaction and the last term expresses the quadrupole coupling between nuclear spin I and the electric field gradient. In principal axes system (Tensors in diagonalised eqn. Form) eqn. 2.4.2. can be written as (neglecting the nuclear Zeeman interaction).

$$\begin{aligned} \mathcal{H} = & \beta (g_x B_x S_x + g_y B_y S_y + g_z B_z S_z) + D [S_z^2 - 1/3 S (S+1)] + \\ & E (S_x^2 - S_y^2) + A_x S_x I_x + A_y S_y I_y + A_z S_z I_z + Q' [I_z^2 - 1/3 (I+1)] + Q'' (I_x^2 - I_y^2) \end{aligned} \quad (2.4.3.)$$

$$\text{where } D = D_z - 1/2 [D_x + D_y], E = 1/2 (D_x - D_y)$$

$$Q' = Q_z - 1/2 [Q_x + Q_y], Q'' = 1/2 [Q_x - Q_y]$$

and g_x , g_y , g_z and A_x , A_y , A_z are the components of g and A tensors respectively along principal axes. In Eqn. (2.4.3.) the Parameters "D" and "E"

are generally known as fine structure parameters and are the measure of the ZFS of energy states described by the spin-Hamiltonian. "D" and "E" represent the axial and rhombic parts of the crystal field splitting respectively. For the so called axial symmetry

$$E = Q_z = 0 \text{ and } g_x = g_y; g_z = g_x = g_{\perp}, A_z = A_x \text{ and } A_x = A_y = A_{\perp}$$

2.5 COVALENCY EFFECTS AND SUPER-HYPERFINE STRUCTURE

A detailed examination reveals that the approximation of ligand ion in CF theory is not strictly valid, and the overlap of the wave functions of the ligand ions with that of the metal ion must be taken into account. Stevens [11] considered this problem for the first time for the complexes of the ions from 4d and 5d groups which are bonded in a strongly covalent manner. Owen [12, 13] studied the same for some ions from 3d group. The main effects of the covalency on ESR can be listed as follows :

- 1- The covalent bond reduces the orbital contributions to the g - factor. The evidence for reduction of the orbital contribution has been obtained from the spectra Ti^{3+} in alum [14], Fe^{2+} in MgO [15, 16] and ZnF_2 [17] and Co^{2+} in MgO [18, 19] and ZnF_2 [17].
- 2- The hyperfine interaction parameter 'A' is reduced. The experimental evidence comes from the work of Title [20] who studied the spin resonance of Mn^{2+} in a variety of host lattices and proved that the hyperfine constant "A" decrease linearly with the increase of covalency.
3. There may be an additional SHFS structure on the HF lines due

to interaction between the magnetic electrons and the surrounding nuclei. The effect was first found by Owen and Stevens in ammonium chlororidate [21], and subsequently for a number of transition metal ions in ZnF_2 Tinkham [17] and by several other workers [22-25] in various host lattices.

2.6 KRAMER'S THEOREM AND THE JAHN-TELLER [J-T] EFFECT

The Kramer's theorem [26] states that in a crystalline field of any symmetry, a system having an odd number of electrons will always posses at least a two-fold spin degeneracy which can be lifted by the application of a magnetic field. These states were reffered to as Kramer's doublet and assures the observation of ESR in the so called Kramers' (odd number of electrons).

According to J-T effect [27-28], a symmetrical non-linear molecule having a degenerate electronic energy level can not have stable configuration and will therefore distort to a configuration of lower symmetry and thus the degeneracy of the electronic state is lifted, or in other words the disposition of the nuclei adjusts in such a way that the symmetry of a complex gets lowered.

Van Vleck [29] estimated that for iron group, a splitting of few hundred cm^{-1} and for rare earth group about $10^2 cm^{-1}$ may be caused by J-T effect. In the case of paramagnetic ions embedded in diamagnetic hosts, the symmetry of the ligand field is also reduced due to Jahn-Teller effect. This effect is prominently noticeable in the case of Cu^{2+} in trigonal field [30-32] and Fe^{2+} in octahedral field [15-16].

2.7 SPIN-LATTICE AND SPIN-SPIN RELAXATIONS

In ESR three processes are commonly described for transferring energy from the excited spin system to the lattice [spin lattice relaxation (SLR)] direct, Raman and Orbach process. In the direct process for the two level system, relaxation occurs through transfer of energy from a single spin to a single vibrational mode of the crystalline lattice which has essentially the same frequency [33]. When relaxation is by the direct process, $T_1 \propto 1/B^2T$ [34] (where T_1 is the SLR time) and is independent of the spin concentration. Therefore, the temperature and magnetic field can serve as variables either for the study or for the control of T_1 . Actually, the "direct" process is important only at low temperatures.

At high temperature, the indirect or Raman process predominates. Here a phonon is inelastically scattered in the process of flipping a spin. Energy is conserved and this process was strongly temperature dependent with $T_1 \propto 1/T^7$ for $T < \theta_D$, $T_1 \propto 1/T^2$ for $T > \theta_D$ where θ_D is the Debye temperature [35]. Experimental results are in fair agreement with theory at high temperature but not at low temperature where the direct process is important.

In the orbach process, there are two transitions one after the other which occur via an intermediate state. When electron is transferred from a level m to level n in the ground manifold of states by absorbing energy equal to $h\nu$, then by stimulated transition, it goes to a level q which is higher in energy than n by an amount Δ . Spontaneous transition then takes place from level p to m which release a phonon of energy equal to $(h\nu + \Delta)$. The relaxation rate is given by

$$\frac{1}{T_1} \propto e^{-\Delta/kT} \quad (2.7.1)$$

Where k is the Boltzmann factor. This relaxation process is active in the case of rare - earth ions.

The theory of spin-spin relaxation (S-SR) has been developed by Van Vleck [36], Pryce and Stevens [37] where two main types of interactions between the ions have been recognized ; the dipole-dipole and the exchange interaction. The dipoles are close enough so that they experience various local fields resulting from the dipolar fields of their neighbours. In the case of exchange interaction, the energy transfer takes place by means of mutual spin flips between neighbouring spins. As the spins are in thermal equilibrium among themselves and if the equilibrium is disturbed, it is re-established exponentially with a time constant T_2 called the S-SR time. The resonance line width is proportional to $1/T_2$.

2.8 ESR OF LIQUIDS

The paramagnetic complexes in liquid solutions can be considered as micro-crystals tumbling in a random way as they jostled by the molecular motions of the solvent [38]. Considering the effect of only motional modulation of anisotropic g and A tensors on the line-width Kivelson [39] developed the theory of ESR line width in dilute solutions. Because of the tumbling motion, the orientation of micro-crystals varies with respect to the external magnetic field. The spin Hamiltonian under this condition can be written as :

$$\mathcal{H}_{\text{spin}} = \mathcal{H}^{(0)} + \mathcal{H}^{(1)} + F(t) \quad (2.8.1)$$

Where

$$\begin{aligned} \mathcal{H}^{(0)} &= g_0 \beta_0 S_z H_z \\ \mathcal{H}^{(1)} &= h A_0 S_z + \frac{1}{2} A_0 [I^+ S^- + I^- S^+], \\ g_0 &= 1/3 (g_x + g_y + g_z) \\ A_0 &= 1/3 (A_x + A_y + A_z) \end{aligned}$$

$F(t)$ is the time dependent part of the Hamiltonian and depends upon the anisotropy of g and A . Assuming that the spectral line are well resolved, that the Zeeman term is the largest term in energy and the lines-shapes are Lorentzian, Wilson and Kivelson [40] gave the expression of line-width ΔH as

$$\Delta H = a_1 + a' + a_2 + a_3 + a_4 \quad (2.8.2)$$

$$a_1 = a_0 + a = 1/43 [(\Delta \gamma H_0)^2] (4 + 3u) + 1/40 b^2 [I+1]$$

$$\times (3 + 7u) 1/8 b^2 (I+1) (A_0 / \omega_0) uf - 1/30$$

$$= \Delta \gamma H_0 b_1 (I+1) (A_0 / \omega_0) (1+u),$$

$$a_2 = \frac{1}{13} (b \Delta \gamma H_0) (4+3u) - \frac{2}{43} (\Delta \gamma H_0)^2 (4 + 3u + 3uf) (A_0 / \omega_0)$$

$$= \frac{1}{20} b^2 I(I+1) (A_0 / \omega_0) (4+3u+7uf) + \frac{1}{40} b^2 (A_0 / \omega_0) (3+2u)$$

$$[2I(I+1)-1],$$

$$a_3 = A_0 = \frac{b^2}{20} (5-u) + \frac{1}{8} b^2 (A_0 / \omega_0) uf = \frac{1}{30} (\Delta \gamma / H_0 b)$$

$$= (A_0 / \omega_0) (7+5u+12uf)$$

$$a_4 = \frac{1}{10} b^2 (A_0 / \omega_0) (1+u+uf)$$

In these expressions

$$u = (1 + \omega_0^2 \tau_e^2)^{-1}, \quad f = \omega_0^2 \tau_e^2 u,$$

$$b = \frac{2}{3} (A_{||} - A_{\perp}) \text{rad/sec}, \quad \Delta\gamma = \beta_0 \Delta g / h, \quad \Delta g = g_{||} - g_{\perp}$$

Where ω_0 is the microwave frequency in rad/sec and τ_c is the orientational correlation time expressed as:

$$\tau_c = \frac{4 \pi r^3 \eta}{3 kT} \quad (2.8.3)$$

and η is the viscosity of the solution, a_0 is called the residual line-width due to some unspecified mechanisms. The most important of these mechanisms is the spin rotational relaxation mechanism, a relaxation mechanism because of the interaction of the rotational magnetic moment of paramagnetic molecule with its spin or nuclear magnetic moment. Atkins and Kivelson [41], following Hubbard theory [42], gave the following expression for the line-width due to this mechanism :

$$a_0 \approx a_{RS} = \frac{2}{\sqrt{3}} \frac{h}{\beta_0 g} \frac{1}{12\pi r^3} / \Delta g^2 + 2\Delta g_{\perp}^2 / \frac{kT}{\eta} \quad (2.8.4)$$

Where $\Delta g_{||} = g_{||} - 2.0023$, $\Delta g_{\perp} = g_{\perp} - 2.0023$, r the molecular radius of the equivalent rotating sphere in the solution and the remaining symbols have their usual meaning.

Among many suggestions to explain the observed line-width an idea analogous to electric field fluctuation mechanism in solids [43, 44] was applied in the case of liquids. In this process the electric fields constituting the crystal or molecular binding fields are modulated by the molecular vibrations and by collisions with surrounding diamagnetic molecules, and these fluctuations of electric field affect the spin by means of spin-orbit interactions. The lattice vibrations in crystals replace the Brown-

ian motion in solutions as the source of modulation. Kivelson developed [43] the contributions of three most significant electric field fluctuation mechanisms in solutions as:

$$W(1) = 64(\lambda/\Delta)^2 = \left(\frac{\phi' q_0}{\Delta r_0}\right)^2 \frac{(\omega_0 \tau_e)^2 \tau_e^{-1}}{1 + \omega_0^2 \tau_e^2} \quad (\text{Van Vleck direct}) \quad (2.8.5)$$

$$W(2) = 32(\lambda/\Delta)^2 = \left(\frac{\phi' q_0}{\Delta r_0}\right)^2 \tau_e^{-1} \quad (\text{Van Vleck Roman}), \quad \omega_0^2 \tau_e^2 \leq 1, \quad (2.8.6)$$

$$W(3) = 16(\lambda/\Delta)^2 = \left(\frac{\phi' q_0}{\Delta r_0}\right)^2 \left(\frac{\Delta}{\delta}\right)^2 \frac{\tau_e^{-1}}{[\exp(h\delta/kT-1)]} \quad (\text{Orbach}) \quad (2.8.7)$$

$$\delta^2 \tau_e^2 \geq 1$$

Where λ = spin orbit coupling constant for a given ion, Δ = crystal field splitting parameter, r_0 = characteristic intermolecular distance, τ_e = mean correlation time for intermolecular fluctuations, q_0 = typical root-mean-square value of q_i ; q_i 's are the amplitudes of intermolecular oscillations, $h\delta$ = exciting energy of the first excited state.

$$\phi' = \sum |(hV_{CF} / \delta q_i) r_0|$$

is a potential indicating the approximate magnitude of the crystal or molecular binding field. However, out of these three electric field fluctuation mechanisms only Orbach process was found to be useful.

2.9 POWDER ESR SPECTRA

In the polycrystalline samples the polycrystals (crystallites) randomly oriented with respect to the static magnetic field [46-48]. Consequently, ESR corresponding to all possible orientations of these small

crystallites are obtained. The individual ESR signals usually overlap because of finite individual line widths to form what we normally call a "powder ESR pattern". For discussing the powder line-shapes, we consider a spherical coordinate system shown in Fig. 2.1 in which the orientation of the paramagnetic species defined by the orthogonal axes, x, y and z; θ and ϕ are the angles specifying the orientation of \mathbf{B} in this coordinate system. Now, the number of crystallites with a magnetic field orientation between θ and $\theta + d\theta$ and between ϕ and $\phi + d\phi$ proportional to the solid angle $d\Omega$ [49] where-

$$d\Omega \propto \sin\theta d\theta d\phi = d \cos\theta d\phi \quad (2.9.1)$$

The powder ESR pattern then the ensemble average of the resonance condition over all equally probable elements of solid angle ($d\Omega$) summed over all allowed transitions. The ESR absorption at field H in the magnetic field interval dH may be expressed in terms of a normalized "shape function" [59] $S(H)$ given by

$$S(H)dH \propto (4\pi)^{-1} \sum_r f_r^{H+dH} P_r(\Omega) d\Omega(H_r) \quad (2.9.2)$$

Eqn. (2.9.2) integrated over those elements of solid angle $d\Omega(H_r)$ such that $H < H_r < H + dH$, where H_r is the appropriate resonance condition corresponding to r th transition. In general, $d\Omega_r$ is a multivalued function of H_r , there being more than one value of $\cos\theta$ and ϕ for some resonance fields H_r . $P_r(\Omega)$ is the transition probability for the r th component and is normally independent of Ω except in the case where we have strong-anisotropy [51-54]. Thus, $P_r(\Omega)$ may be taken out-

side the integral sign of Eqn. (2.9.2) in most situations, and the ESR powder pattern for each resonance transition to be multiplied by one of these factors before adding all pattern together to get the total absorption line-shapes.

However, in situations where all elements of solid angle not equally probable, [55], an additional factor such as $p(\Omega)$ must be included in Eqn. (2.9.2), where $P(\Omega) d\Omega$ gives the probability of a site being oriented in an element of solid angle $d\Omega$ at Ω .

The resonance conditions described above represented idealized δ -function line-shapes, which are seldom observed in the actual spectra. Several line broadening mechanisms operative in actual situations. Line-broadening from dipole-dipole interactions can be expressed empirically by a normalized "Gaussian Function" of the following [56].

$$Y_G(H-H_r) = \left(\frac{\ln 2}{\pi}\right)^{1/2} \frac{y_0}{\Delta H} \exp\left[-\frac{(-\ln 2)(H-H_r)^2}{\Delta H^2}\right] \quad (2.9.3)$$

Where $y_G = \left(\frac{\ln 2}{\pi}\right)^{1/2} \frac{1}{\Delta H}$ and H_r represents the resonant field corresponding to an appropriate resonance condition. The quantity ΔH referred to as the half-width at half-maximum (HWHM) of a pure absorption line in the absence of microwave power saturation. The equation for the corresponding first derivative of the Gaussian Function is:

$$Y'_G(H-H_r) = -\frac{2}{\pi} \frac{(\ln 2)^{3/2}}{\Delta H^3} \cdot (H-H_r) \exp\left[-\frac{(-\ln 2)}{\Delta H}(H-H_r)^2\right] \quad (2.9.4)$$

The peak-to-peak width of the derivative line-shape (AH_{pp}) is related to ΔH by the following relation :

$$\Delta H = (\ln 2 / 2)^{1/2} \Delta H_{PP} \quad (2.9.5)$$

Line broadening from "Exchange Interaction" can often be approximated theoretically by a normalized Lorentzian function, characterized by the following expression [57]:

$$Y_L(H - H_r) = 1/\pi \cdot \frac{\Delta H}{\Delta H^2 + (H - H_r)^2} \quad (2.9.6)$$

The corresponding first derivative line-shape is:

$$Y'_L(H - H_r) = -\left(\frac{2}{\pi}\right) \frac{\Delta H (H - H_r)}{[\Delta H^2 + (H - H_r)^2]^2} \quad (2.9.7)$$

For Lorentzian line ΔH and (ΔH_{PP}) are related by the following relation:

$$\Delta H = \frac{(\sqrt{3} \Delta H_{PP})}{2} \quad (2.9.8)$$

Dilute paramagnetic systems (such as radical species diluted in a liquid) often exhibit spectral line-shapes which can normally be approximated by a Lorentzian function. Moreover, in some systems, the presence of more than one independent line-broadening mechanism complicates the spectral shape, and then each component line-width should be given by Eqns. (2.9.3-2.9.5) and (2.9.6.-2.9.8), respectively. Although not common, a combination of Lorentzian and Gaussian lines was sometimes observed due to the presence of several types of interaction in the spin system. Such combinations are often represented by a "Voigt" shape function [57].

To account for the above broadening mechanism, an additional term representing the appropriate line line-shape, e.g. Eqn. (2.9.2- 2.9.4) and

(2.9.5-2.9.7), should be added to in Eqn. (2.9.2), which then involves a double integral. If we neglect the dependence of the lines- shapes functions on orientation [58], which normally is unimportant in the powder lines-shape calculations [59], we can take the line- broadening terms outside of the integral sign in Eqn. (2.9.2), thus giving a convolution of the ideal delta function line-shape.

Since analytical solutions to most powder ESR pattern problems generally impossible to carry out in practice , Eqn. (2.9.2) quite often solved numerically by using a computer. It might be said that without high-speed digital computers that are available these days, this task would be nearly impossible. As a consequence powder ESR spectrometry would have been more limited in its applications than it is today. The normal procedure for obtaining solutions to Eqn. (2.9.2) comprises summation of all contributions to the shape function, $S(H)$,over a grid in $(\cos \theta, \phi)$ space by various numerical integration algorithm [60].

The next section illustrates the powder patterns expected for several systems under different symmetry conditions.

2.10 THE EXPECTED POWDER LINE-SHAPES

2.10.(i) Pattern without Hyperfine Splitting:

For paramagnetic systems with axial symmetry the shape function $S(H)$ can be expressed as:

$$S(H) dH \propto \sin \theta d\theta \quad (2.10.1)$$

Or

$$S(H) \propto \sin \theta / (dH/d\theta) \quad (2.10.2)$$

Eqns. (2.10.1) and (2.10.2) reflect the fact that very large number of radicals with axes nearly perpendicular to the field direction will be present in the system and only a few radicals will have their axis aligned close to the field direction. This means that we expect to see two "extrema" in the powder spectra.

The resonance field (H_r) is given by:

$$H_r = \frac{h\nu}{\beta} \frac{1}{(g_{\parallel} \cos^2 \theta + g_{\perp} \sin^2 \theta)} \quad (2.10.3)$$

Eqn. (2.10.3) shows the expected angular variation of H_r (Fig. 2.2). Differentiating Eqn. (2.10.3), in order to evaluate $dH/d\theta$, we write Eqn. (2.10.2) into the form

$$S(H) \propto \left(\frac{h\nu}{\beta} \right)^2 \frac{1}{H_r^3 (g_{\perp}^2 - g_{\parallel}^2) \cos \theta} \quad (2.10.4)$$

We see, therefore, that due to the presence of " $\cos \theta$ " term in the denominator of Eqn. (2.10.4), $S(H)$ rises monotonically from a finite value determined by g_{\parallel} to infinity, i.e., at a field determined by g_{\parallel} , as $\theta \rightarrow 90^\circ$. This behaviour is shown by the s-function line-shape in fig. 2.2(a) where the powder patterns obtained for various amounts of line broadening are also depicted. The two extrema, therefore, correspond to g_{\parallel} and g_{\perp} , respectively, so that the resonance field lies between $h\nu/g_{\parallel}\beta$ and $h\nu/g_{\perp}\beta$. The corresponding first derivative spectra would be of the type shown in Fig. 2.2. (c). Levedev [61] gives a more complete

description of such theoretical line-shapes for systems with axial symmetry.

For powder specimens with an orthorhombic g-tensor, there are three turning points in the ESR spectrum corresponding to the three principal g-tensor components, g_{xx} ; g_{yy} and g_{zz} ; g_{yy} being the intermediate in the spectrum [49]. The diagnostic features of the absorption line-shapes and its first-derivative for such a situation are shown in Fig. 2.3.

2.10.(ii) Patterns with Hyperfine Splitting:

The simple line-shapes patterns in Fig. 2.2 and Fig. 2.3 are modified in the presence of electron-nuclear hyperfine interaction. Assuming the unpaired electron to be interacting with a set of magnetically equivalent $I=2$ nuclei, the line-shape pattern of Fig. 2.2(c) becomes modified to that shown in Fig. 2.4.(a). The powder pattern becomes more complicated when interacting magnetic nuclei have spin $I > 1/2$, for example, for $I=3/2$, and an isotropic hyperfine interaction, the pattern would be according to Fig. 2.4.(c).

In several simple situations it may be possible to determine some or all of the components of g and A simply from the experimentally observed spectra. Otherwise, the extraction of rather precise Hamiltonian parameters usually rests on the "Computer Simulation" until the best fit is achieved between experimental and calculated lineshapes.

2.11.1 COMPUTATION OF RESONANCE FIELDS

The ESR transitions result from a matching of energy levels of a spin in a magnetic field by the microwave quantum used. Thus the validity of the phenomenological SH used may be testified by comparing the observed and computed values of resonance fields with the help of solution of SH matrix (with the known values of parameters) as and subsequently matching the possible energy level differences to the microwave quantum. The SH matrix can be solved either by perturbation method or by exact numerical diagonalization on digital computers. The perturbation methods are applicable to the cases where the Zeeman term is dominant and are thus of limited applicability only to cases with small ZFS and small hyperfine interaction. The energy levels given in the fine structure in the ESR are labeled by quantum numbers M_S and those giving the hyperfine structure by m_I . Though the labelling is done as if these are pure quantum numbers, they have no other meaning except their use for labelling. In the perturbation expressions which involve these numbers and treat them as pure quantum numbers an error is introduced due to their real value being defined for $\Delta M_S = \pm 1$ and $\Delta m_I = 0$. The transitions possible in violation of the above rules are termed as forbidden transitions and may involve $\Delta M_S = \pm 2, \pm 3$ etc. and $m_I = \pm 1, \pm 2$ etc.

The resonance fields are calculated from the exact solution of SH matrix and by finding and interval $(H, H + \delta H)$ by interactive procedure such that for a value H_j of the magnetic field $F_j / \{ |E_j - E_{j+\Delta M_j}| - \frac{\hbar v}{\beta} \} \leq 0$ and

for $(H_j - \delta H)F_j \geq 0$ where E_j are the levels involved in the transition, ΔM is a positive or negative integer including zero depending on the transition under consideration being "allowed" or "forbidden", $h\nu$ is the microwave quantum and δH is a small number pre-selected based on the experimental accuracy of the resonance fields ($\delta H \sim 10^{-1} - 10^{-3}$ Gauss). The value H_j thus computed corresponds to the resonance field position for the transition under consideration. The process is repeated until the total number of observed transitions have been considered and their position computed (in Gauss).

2.11.2 METHOD FOR S=1/2 IONS

For $S = 1/2$ and $I = 3/2$ or $7/2$ for example Cu^{2+} , Co^{2+} and VO^{2+} the fine structure terms are dropped from the SH and it assumes the simpler form:

$$\mathcal{H} = \beta \vec{S} \cdot \vec{g} \cdot \vec{H} + \vec{I} \cdot \vec{A} \cdot \vec{S} + \vec{I} \cdot \vec{P} \vec{I} - \beta_N \vec{H} \vec{g}_N \cdot \vec{I} \quad (2.11.2.1)$$

In most of the cases the last two terms are found to be very small and may generally be dropped from the spin Hamiltonian. For axial symmetry the SH (II-2.7) is sometimes written in terms of more customary symbols in the following form [49]:

$$\begin{aligned} \mathcal{H} = & g_0 \beta S_z H_z + \beta g_{\perp} (S_x H_x + S_y H_y) + A S_z I_z + B (S_x I_x + S_y I_y) + \\ & + O [3I_z^2 - I(I+1)] + \gamma \beta_N \vec{H} \cdot \vec{I} - R_z I_z H_z - R_{\perp} (H_x I_x + H_y I_y) \end{aligned} \quad (2.11.2.2)$$

Bleaney [50] in his classic paper has obtained the expressions for

the resonance fields applying perturbation method and Low [9] has given the expressions for resonance fields for both the allowed and the forbidden transitions. Extensive discussion of the perturbation method and the above SH may be found in literature [12,48]. For the analysis of Cu^{2+} ($S=1/2$, $I=3/2$) and V^{2+} ($S=1/2$, $I=7/2$) ESR spectra spin Hamiltonian paramagnetics are obtained. The parameters thus obtained were next refined by obtaining minimizing F . Here $F = \sum_i (H_o^i - H_r^i)^2$, where H_o^i and H_r^i are the experimentally observed and calculated resonance field values respectively and H_r^i are computed by the method described earlier through the exact numerical diagonalization of a SH matrix 8×8 for Cu^{2+} and 16×16 for V^{2+} .

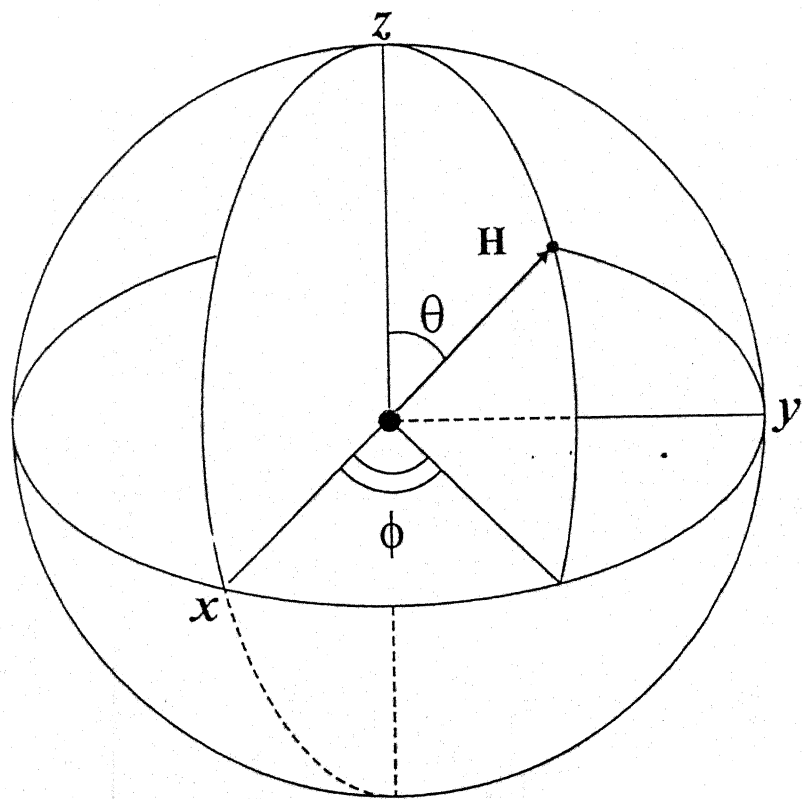
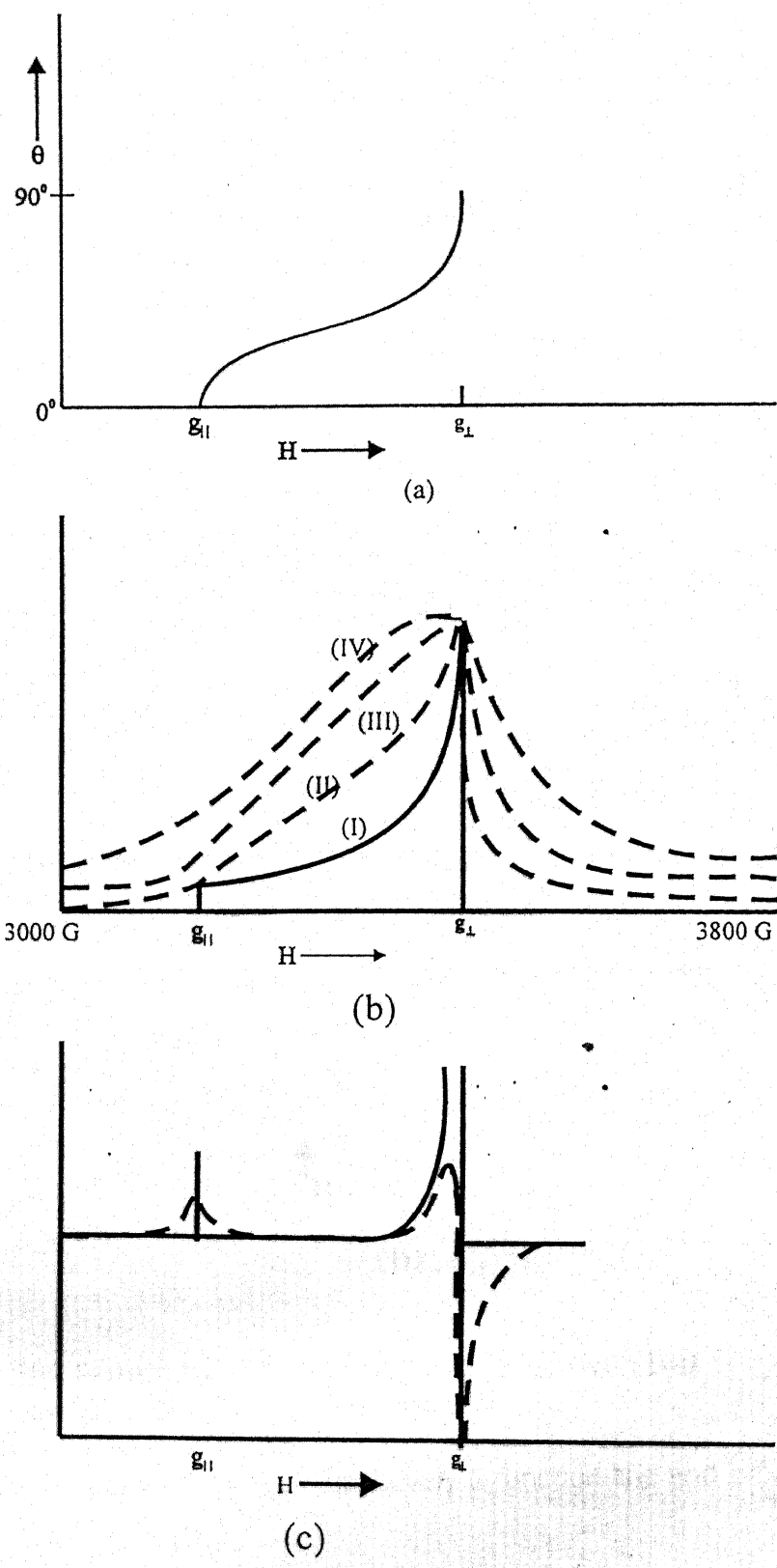


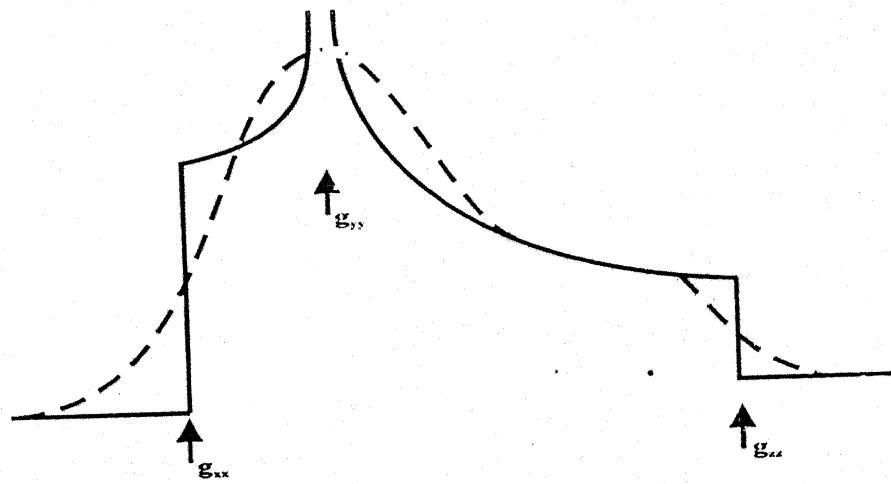
Fig2.1.

Axis system and polar coordinates showing the orientation of H

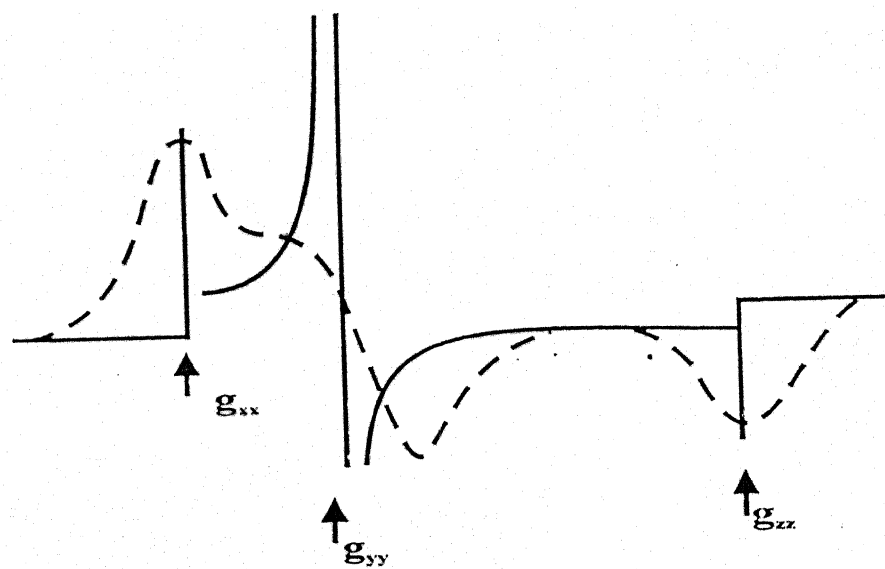


g. 2.2: Powder EPR Pattern for a system ($S=1/2, I=0$) with axial symmetry ($g_{\parallel} > g_{\perp}$)

- (a) Angular dependence of the resonance field position.
- (b) Absorption line shapes: The δ -function line shape (I) is broadened by Lorentzian shape functions of width 10G (II), 50G (III) and 100G(IV) respectively.
- (c) Derivative line shape: Solid is the δ -function line shape.



(a)



(b)

Fig. 2.3: Powder EPR Pattern for an orthorhombic g-tensor with $I=0$

(a) Absorption Curves

(b) Derivative Curves

The solid and broken lines are respectively δ -function line and broadened line.

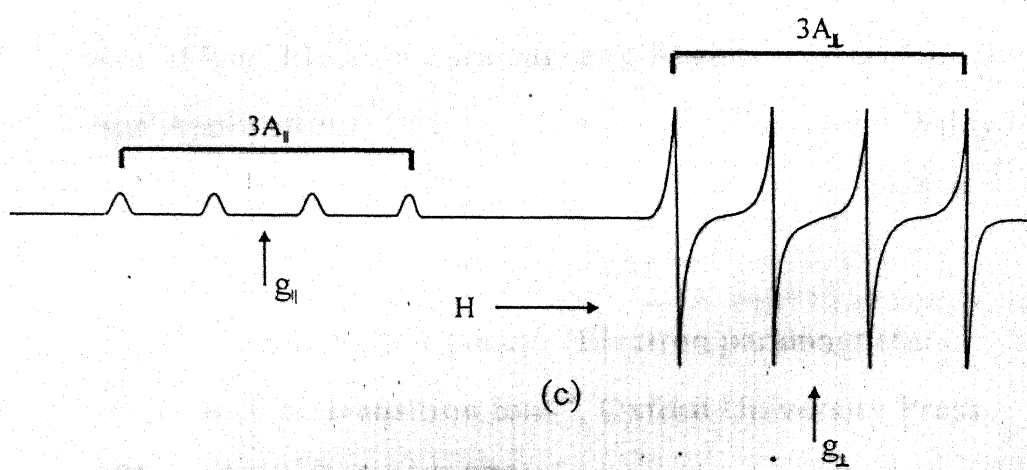
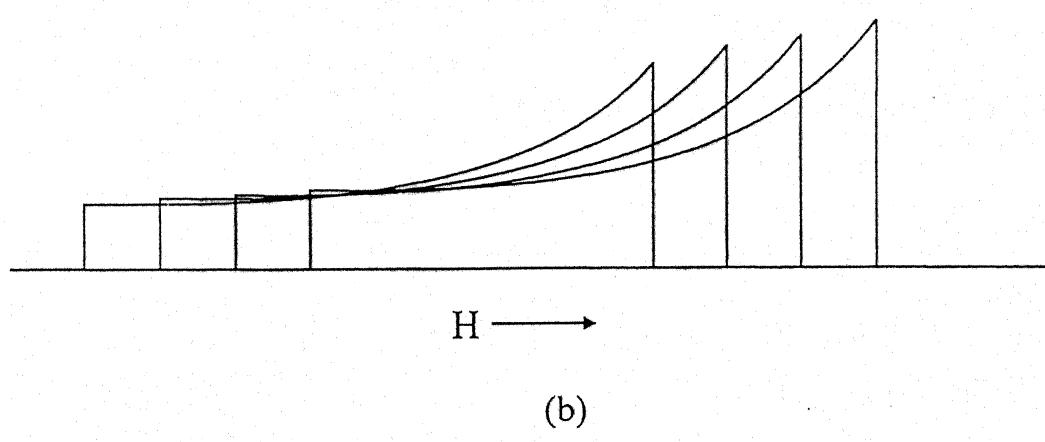
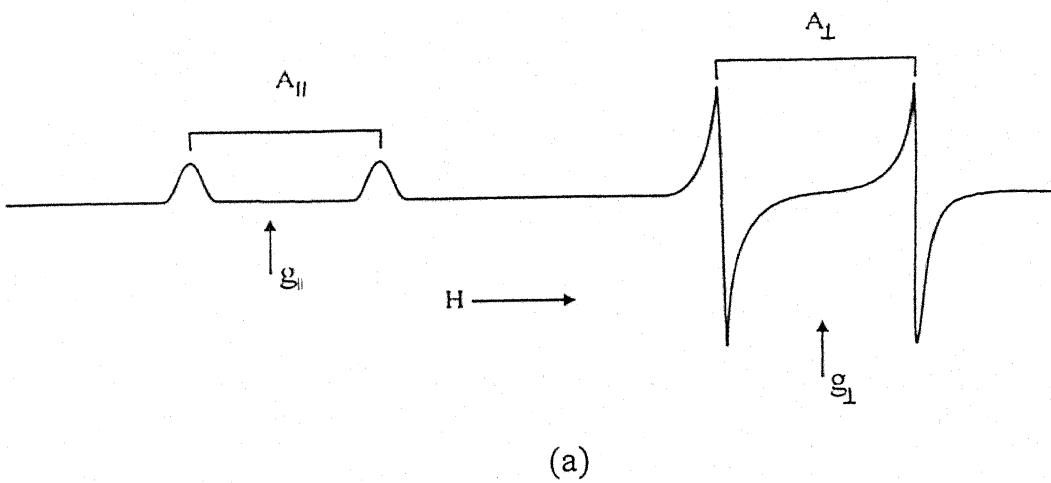


Fig. 2.4: Powder patterns for an $S = 1/2$ axial symmetry system ($g_{\parallel} > g_{\perp}$) with isotropic A- tensor:

- (a) Derivative line showing hyperfine interaction with $I = 1/2$.
- (b) Idealised absorption positions for hyperfine interaction with $I = 3/2$
- (c) Derivative line corresponding to (b) including some line broadening.

REFERENCES

1. J.H. Van Vlack and W.G. Penny, Phil. Mag., 17, 961 (1934).
2. R.R. Sharma, T.P. Das and R. Orbach, Phys. Rev., 149, 257 (1966); 388 (1967) and 171, 378 (1968).
3. P.A. Narayana, Phys. Rev. Lett., B10 2676 (1974).
4. R. Chatterjee, M.R. Smith and H.A. Buckmaster, Canad. J. Phys., 54, 1224 (1976).
5. H. Watanabe, Progr. Theor. Phys., 18, 405 (1957).
6. A Abragam and M.H.L. Pryce, Proc. Roy. Soc., A205, 135 (1951).
7. S.A. Al'tshuler, B.M. Kozyrev. "Electron Paramagnetic Resonance", Academic Press, New York (1964).
8. R.S. Anderson, "Electron Spin Resonance", Methods of Experimental Physics, 3, 441 (1962).
9. R.S. Alger, Electron Paramagnetic Resonance, Techniques and Applications, Inter-science Publications, John Wiley and Sons, New York, London, Sydney (1968).
10. A. Abragam and B. Bleaney, "Electron paramagnetic Resonance of Transition Ions", Oxford University Press (Clarendon), Oxford (1970).
11. K.W.H. Stevens, Proc. Roy. Soc, A219, 542 (1953).

12. J. Owen., Discus, Faraday. Soc., 19., 127 (1955).
13. J. Owen, Proc. Roy., Soc., A227, 183 (1955).
14. B. Bleaney, G.S. Bogle., A.H. Cooke, H.J. Duffus, M.C.M. O'Brien and K.W.H. Stevens, Proc., A 68, 57 (1955).
15. W. Low. Ann. New York Acad. Sci., 72, 69 (1958).
16. W. Low. Phys. Rev., 101, 1827 (1956).
17. M. Tinkham, Proc. Roy. Soc., A 236, 535 and 549 (1956).
18. W. Low. Phys. Rev. 109, 865 (1958).
19. W. Low and D. Shaltiel, J. Phys. Chem. Solids, 6, 315 (1958).
20. R.S. Title, Phys. Rev., 131, 623 (1963).
21. J. Owen and K.W.H. Stevens, Nature, 171, 836 (1953).
22. S. Ogawa, J. Phys. Soc. Japan, 15, 1475 (1960).
23. J.E. Drumheller, J. Chem. Phys. 38, 970 (1963).
24. W.J., Weighle and W.H. Tanttila, J. Chem. Phys., 41, 274 (1964).
25. T.L. Estle and W.C. Holton, Phys. Rev., 150, 159 (1968).
26. H.A. Kramers, Proc. Amsterdam Acad. Sci., 33, 959 (1930).
27. H.A. Jahn and E. Teller, Proc. Roy. Soc., A161, 220 (1937).
28. H.A. Jahn, Proc. Roy. Soc., A 164, 117 (1938).
29. J.H. Van Vleck, J. Chem. Phys., 7, 72 (1939).
30. B. Bleaney and K.D. Bowers, Proc. Ph'ys. Soc., A65, 667

(1952).

31. D. Biji and A.C. Ross-Innes, Proc. Phys. Soc., **A66**, 954 (1953).
32. B. Bleaney, K.D. Bowers, and R.S. Trenam, Proc. Roy. Soc., **A 228**, 157 (1955).
33. J.A. Giordamine, L.E. Alsop, F.R. Nash and C.H. Townes, Phys. Rev., **109**, 302 (1958).
34. G.E. Pake, "Paramagnetic Resonance", Benjamin, New York (1962)
35. W. Low, "Paramagnetic Resonance in Solids", Solid state Physics Suppl., 2, 150 (1960).
36. J.H. Van Vlack, Phys., Rev., **74**, 1168 (1948).
37. M.H.L., Pryce and K.W.H. Stevens, Proc. Phys Soc., **A63**, 36 (1950).
38. H.M. McConnell, J. Chem., Phys., **25**, 709 (1956).
39. D. Kivelson, J. Chem. Phys., **27**, 1087 (1957); **33**, 1094 (1960).
40. R. Wilson, D. Kivelson, J. Chem. Phys., **44**, 154, 4440, 4445 (1966).
41. P.S. Hubbard, Phys. Rev., **131**, 1155 (1962).
42. J.H. Van Vleck, Phys. Rev., **57**, 426 (1940).
43. R. Orbach, Proc. Phys. Soc., **A77**, 821 (1961).

44. D. Kivelson, *J. Chem. Phys.*, 45, 1324 (1966).
45. F.J. Adrian, *J. Colloid Interface Sci.*, 26, 317 (1968).
46. P.H. Kasai and R.J. Bishop, Jr. in "Zeolite Chemistry and Washington, E.C." (1976), p. 350.
47. W.N. Delgass, G.L. Haller, R. Kellerman and J.H. Lunsford, "Spectroscopy in Heterogeneous Catalysis", Academic Press, New York (1979), p. 183.
48. F.K. Kneubuhl, *J. Chem. Phys.*, 33, 1074 (1960).
49. C.P. Slichter, "Principles of Magnetic Resonance" (second revised and expanded edition), Springer-Verlag, Berlin (1980), p. 259.
50. C.A. McDowell, P. Raghunthan and J.C. Tait, *J. Chem. Phys.*, 59, 5858 (1973).
51. B. Blaney, *Proc. Phys. Soc., London* 75, 621 (1960).
52. T. Vangard and R. Assa, "Paramagnetic Resonance", Vol., 2, Ed. W. Low, Academic Press, New York (1963), p. 509.
53. A Isomoto, H. Watari and M. Kotani, *J. Phys. Soc. Japan*, 29, 1571 (1970).
54. H.M. McConnell and B.G. McFarland, *Quart. Rev. Biophys.*, 3, 91 (1970).
55. C.P. Poole, Jr., "Electron Spin Resonance", Interscience, New York (1967), p. 778.

56. Reference 21, p. 783.
57. J. Maruani, Chem. Phys. Lett., PS7PS, 29 (1970).
58. A. Abragam, "The Principles of Nuclear Magnetism", Clarendon Press, Oxford (1961), p. 220.
59. See, for example, (a) R. Lefebvre and J. Maruani, J. Chem. Phys. 42, 1480 and 1496; (b) R. Breslow and F.J. Owens, Chem. Phys. Lett., 16, 20 (1972) and references therein (c).



CHAPTER-3

Experimental

Techniques

CHAPTER -3

3.1 ELECTRON SPIN RESONANCE (ESR)

ESR spectra were recorded on a Varian E-line century series spectrometer model E- 109 at Indian Institute of Technology, Kanpur. The spectrometer operates at X-band frequency (9.4 GHz). All the ESR spectra have been recorded with 100 kHz field modulation. The maximum power available with this spectrometer is 200 MW. The recording of ESR spectra only in absorption mode is possible and the first as well as second derivative of absorption signal can be recorded. The schematic diagram of the ESR spectrometer is shown in Fig. 3.1. Rectangular cavity E-231 which operates in TE_{102} mode with unloaded $Q > 7000$ is used throughout the experiments. The field stability of the spectrometer after stabilization of the order of 10 ppm with temperature coefficient of 2 ppm/ $^{\circ}\text{C}$ is between 300 mT and 1T. The signal to noise ratio with E-231 cavity at 100 kHz field modulation approximately equal to 180.

For ESR studies with single crystals it is required to know the crystal field (X, Y, Z) axis. For this purpose a two axes goniometer (Fig. 3.2) is used which provides a possibility of rotation of the magnetic field in any desired plane of the crystal. The X, Y, Z were determined employing the following method. The crystal was rotated first independently about a horizontal and a vertical axis and a particular orientation was searched where the spread of the fine structure was maximum. Thus knowing one direction of maximal spread in fine structure spread were searched in a plane normal to the first direction of maximal spread. The directions are

referred to Z, Y and X according to the spread of spectrum.

Once the axes is known the crystal is cut to facilitate the angular rotation of the crystal about a desired direction. The Varian model E-229 goniometer permit an accurate rotation of samples in steps of 1° . Powder samples were filled in quartz sample tube with typical outer diameter (OD) 4mm. For liquid samples either such sample tubes or a flat quartz liquid sample cell was used as per need. Spectra of liquid nitrogen temperature (LNT) were recorded with the Varian model E257/WL-257 variable temperature accessory automatically controls the sample temperatures within the range of 573 K to 88 K. It provides a mean to maintain the desired temperature with an accuracy better than 1 K. For attaining the temperature of boiling liquid nitrogen (LNT) a liquid nitrogen quartz Dewar compatible with E-231 cavity, provided with a cold finger, was used.

Typical designs of sample tube and dewar are shown in fig. 3.3. The actual temperature at the sample was measured with the help of an indicator using a copper constant thermocouple in contact with the sample. The overall accuracy of the measured temperature is 1K. The temperature stability at the sample was found to be within $\pm 1K$, after stabilization.

3.2 X-RAY DIFFRACTION (XRD)

The samples were examined by XRD, using ISO Debye Flex Powder Diffractometer Model 2002 from Rich and Scifert Company FRG.

The diffractometer uses $\text{CuK} \alpha$ radiation ($\lambda = 1.5418 \text{ \AA}^0$) obtained from a copper target using an inbuilt Ni-monochromating filter (density 0.019 g/cm^3 , thickness 0.021 mm). The diffractograms were taken in the range $2\theta = 20^\circ$ to 90° for all the samples, with the following conditions.

- i. Scan speed = 3 degree per min. (in 2θ)
- ii. Chart speed = 15 mm per minutes
- iii. Counts per min (CPM) = 10 K
- iv. Time constant = 10 sec.
- v. Accelerating voltage /current = 30 KV/20mA.

The existence of various peaks in the XRD patterns was used to identify the phases present in the samples. The details of identification of phases are based on intensity variation semi empirical method which will be discussed in the relevant chapters. The schematic diagram of the XRD is shown in Fig. 3.4. Diffractometer designed somewhat like a Debye-Scherrer camera, except that a movable counter replaces the strip of film. In both instruments, essentially monochromatic radiation is used and the X-ray detector (film or counter) placed on the circumference of a circle centered on the powder specimen. The essential features of a diffractometer are shown in Fig. 3.4. A powder specimen C in the form of a flat plate, supported on a table H, which can be rotated about an axis o perpendicular to the plane of the drawing. The X-ray source S is, the line focal spot on the target T of the X-ray tube: S also normal to the plane of the drawing and therefore parallel to the diffractometer axis O.

X-ray diverge from this source and diffracted by the specimen to form a convergent diffracted beam which comes to a focus at the slit F and then enter the counter G. A and B are special slits which define and collimate the incident and diffracted beams. The filter is usually placed in a special holder (not shown) in the diffracted, rather than the incidents beam, a filter in the diffracted beam not only serves its primary function (suppression of K radiation) but also decrease background radiation originating in the specimen.

The receiving slits and counter are supported on the carriage E, which may be rotated about the axis 0 and whose angular position 2 may be read on the graduated scale K. The supports E and H are mechanically coupled so that a rotation of the counter through $2x$ degrees automatically accompanied by rotation of the specimen through X degrees. This coupling ensure that the angles of incidence on, and reflection from, the flat specimen will always be equal to one another and equal to half the total angle of diffraction, an arrangement necessary to preserve focusing conditions. The counter may be powerdriven at a constant angular velocity about the diffractometer axis or moved by hand to any desired angular position.

3.3 SCANNING ELECTRON MICROSCOPE (SEM)

The scanning electron micrographs of the samples coated with gold were taken by the JEOL Scanning Electron Microscope JSM-840, equipped with detector connected to a PC on which the KEVEX Quantex

Software installed. By operating the JEOL JSM 840 in analytical mode and detecting the emitted X-Ray by Kevex detector, the quantitative analysis of the samples is made possible. The morphological studies are carried out using SEM studies for all the pure, Ti^{+3} , Ni^{+2} and Co^{+2} doped ceramics.

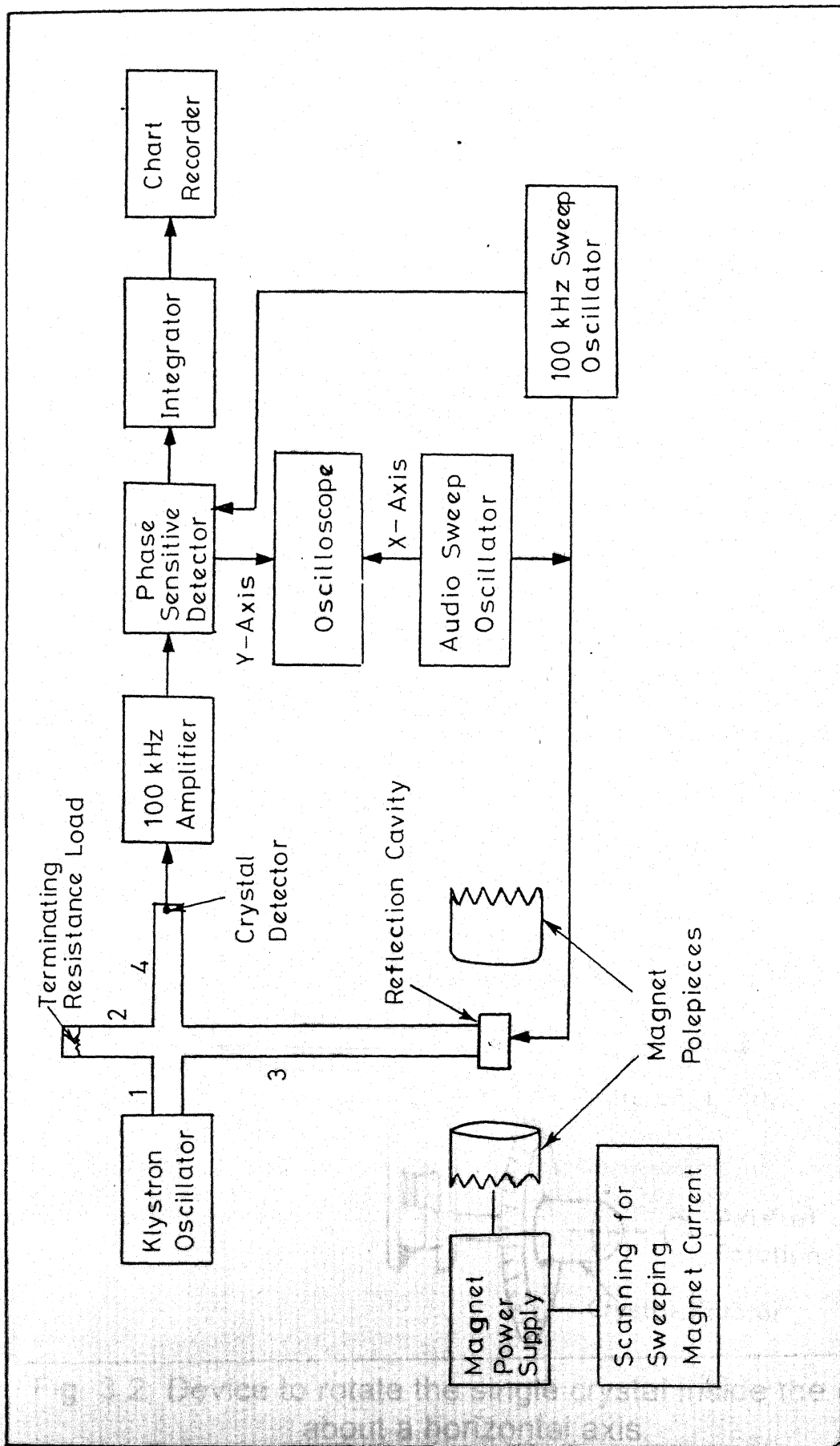


Fig. 3.1: Block diagram of the EPR spectrometer.

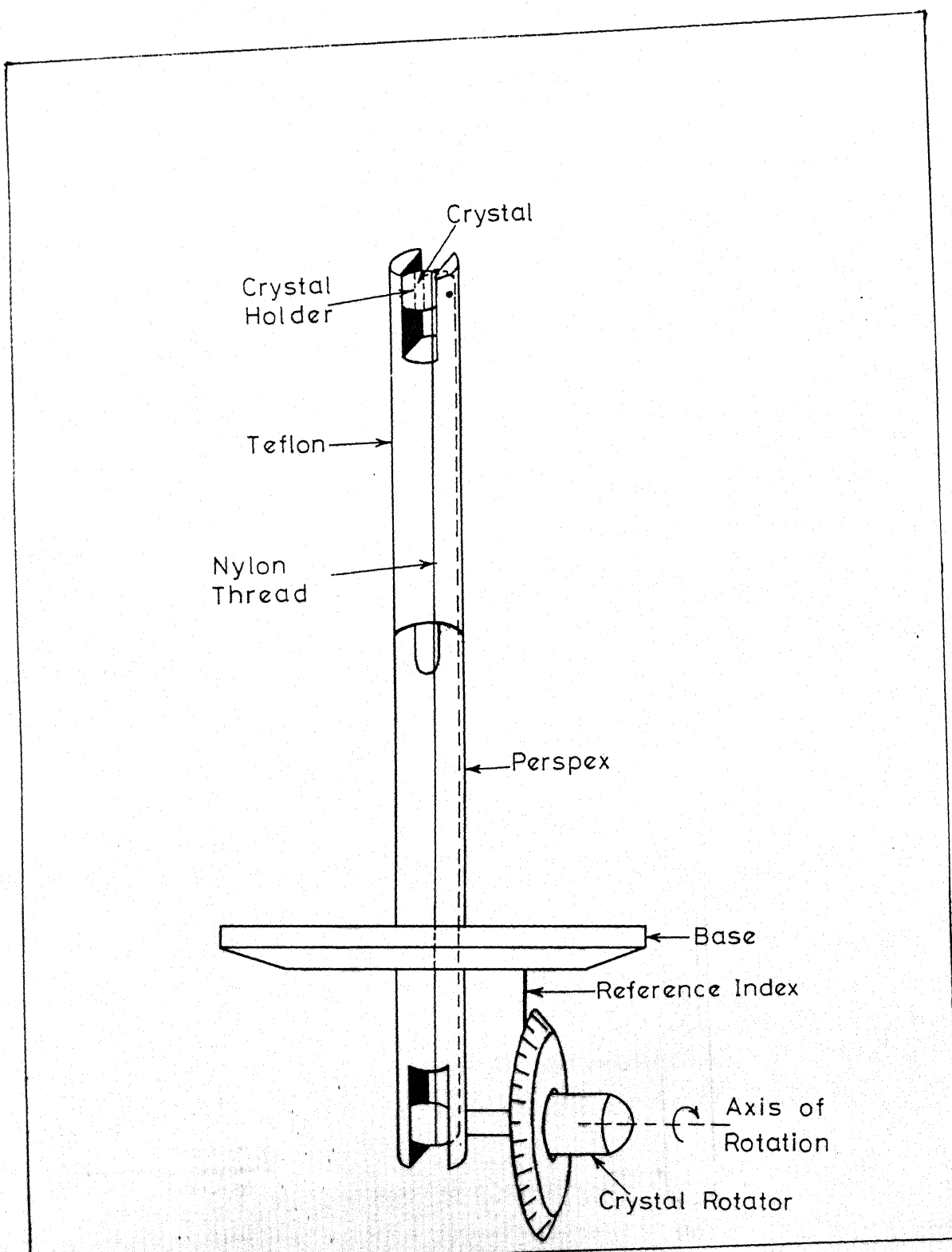


Fig. 3.2: Device to rotate the single crystal inside the cavity about a horizontal axis.

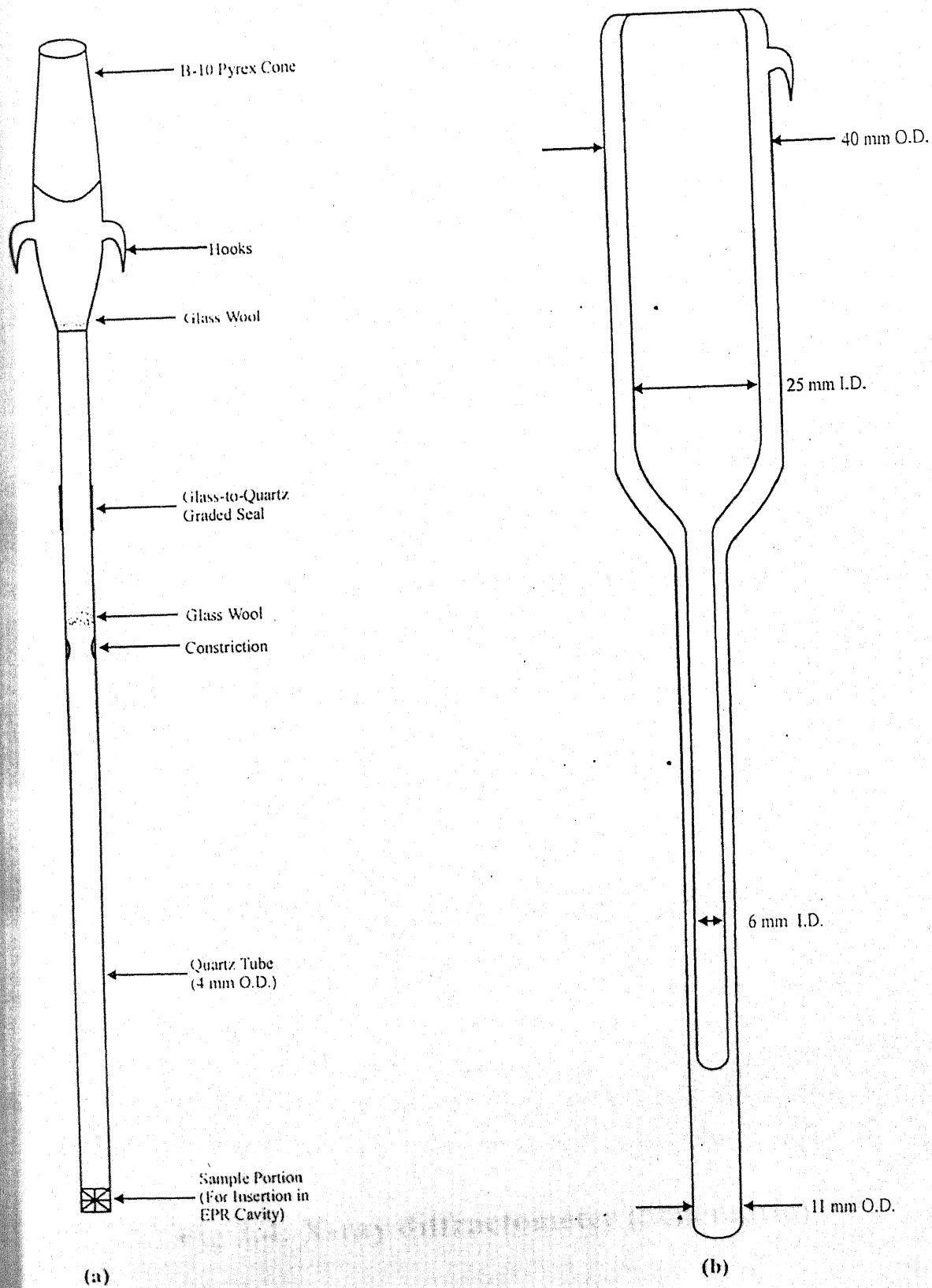


Fig. 3.3 (a) A typical sample tube used in the EPR experiments
(b) Quartz liquid nitrogen dewar used for the EPR measurements.

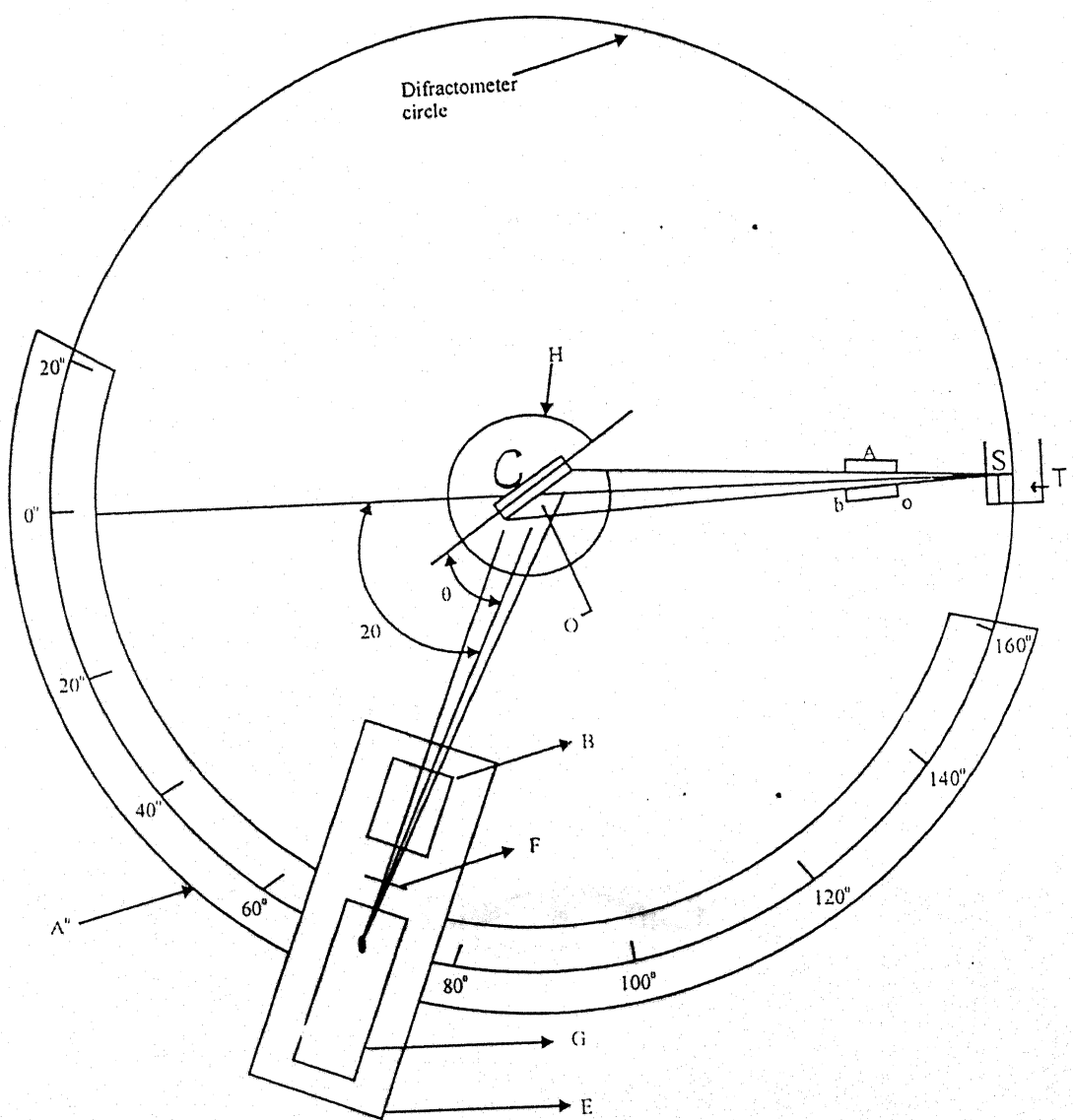


Fig 3.4: X-ray diffractometer (Schematic)

REFERENCES

1. EPR spectrometer manual (model E-109 century Series, VARIAN ASSOCIATE Pub.)
2. Elements of X-ray diffraction, Vol. -V "B.BD Culty, John- John Wiley (1978).
3. Scanning Electron Microscope Users' Manual JEOL, Japan.



CHAPTER-4

Experimental Investigations

on $(\text{ZrO}_2)_{0.8} (\text{Y}_2\text{O}_3)_{0.2}$

Ceramic Compounds

CHAPTER- 4

4.1 INTRODUCTION

Stabilized zirconia (ZrO_2) has been widely used for many years. The ever increasing applications of the oxide in high technology ceramics, particularly in wear parts and as solid electrolytes, has attracted a great deal of attention [1]. Owing to their important applications as high temperature materials, zirconia ceramics have received considerable attention from the view point of their sintering behaviour and control of the microstructures which develop during the sintering process, so that the resulting materials meet the requirements needed for these applications. In order to produce high performance zirconia ceramics, solid state sintering has traditionally been adopted as the favoured fabrication route. This route has often required the use of high firing temperature for the achievement of high density in zirconia materials. Several approaches have proved to be effective in reducing these temperatures. Amongst these approaches, the use of reactive powders such as CaO , Y_2O_3 or rare earths oxides has received particular attention [5]. It has been reported that yitria (Y_2O_3) stabilized zirconia compacts sintered at 1200°C are found to have the highest density [3]. Zirconia-based coatings are commonly used as thermal barrier coatings (TBCs) are increasingly being employed to provide thermal insulation to critical air-cooled mechanical components of gas turbine engines, thereby improving their efficiency [4]. There are three well defined polymorphs in ZrO_2 based ceramic materials namely, monoclinic, tetragonal and cubic phases [5]. It has been stabilized in cubic phase by the addition of variable amounts of

R_2O_3 (R= rare earth or yttrium) or CaO. One of the best stabilizers is Y_2O_3 .

The phase diagram of the ZrO_2 - Y_2O_3 system indicates that the cubic phase exists in the range of composition from 6 to 40 mole % of Y_2O_3 [6]. In the case of ZrO_2 - Y_2O_3 solid solution the stabilization of cubic phase takes place when the concentration of Y_2O_3 is not more than 10 mole %.

In the present chapter, the polycrystalline ceramic samples of $(ZrO_2)_{0.8}$ $(Y_2O_3)_{0.2}$ pure as well as doped with a 1wt% concentration of transition elements (Ti, Ni and Co) were synthesized in order to investigate their structural and magnetic feature using x-ray diffraction (XRD), scanning electron microscopy (SEM) and electron spin resonance (ESR). ESR is hoped to provide information about the valence state of the transition metal ions doped in the ceramic and about the local environment of the doped transition metal ions. The structural information obtained from XRD and Electron microscopy can be correlated with the ESR results together more understanding regarding the microstructural and other properties of the ceramics.

4.2 Experimental

The synthesis of polycrystalline ceramic samples of required stoichiometry in pure as well as doped form has been done using standard high temperature solid state reaction technique. This technique involves grinding of the constituents together followed by pelletization and sintering at high temperature. High purity (99.99%) Zr and Y from Aldrich (USA) in the desired stoichiometry to $(ZrO_2)_{0.8}$ $(Y_2O_3)_{0.2}$ were taken. The transition metal impurities were taken in the following form for the purpose of doping $Ni(NO_3)_2 \cdot 6H_2O$, TiO_2 and cobalt chloride. A fixed concentration

(1 wt %) of the impurity complex was added to the base ceramic. All the constituents were well mixed together in an agate mortar and pestle and then pelletized in the form of thin cylindrical pellets under the application of a pressure of 6 ton/cm². The pelletized materials were kept for sintering at a temperature of 1550°C in a glower furnace for 24 hours. Thus formed materials were then characterized through x-ray diffraction (XRD), scanning electron microscopy (SEM) and electron spin resonance (ESR) techniques in order to investigate their structural and magnetic properties. The sample code and the composition are give in Table 4.(I).

The XRD patterns of all the samples were recorded using a Rich Seifert Isodebyflex 2002 diffractometer and CuK α radiation with monochromator. The recording conditions were scan speed (ss) 3°/min., Time constant T_c = 10 Sec., Count per minute (CPM) = 10K, current/voltage = 20 MA/30KV. The SEM micrographs were taken using a JEOL 840 SEM. All the micrographs were taken at a fixed magnification of x4000 at 15 KV. ESR measurements were done with the help of an X-band ESR spectrometer (Varian E-109) using 100KHz phase sensitive detection. The phase composition of the samples has been evaluated using the XRD studies. The size of grains and mcrphological features have bean studied with the help of SEM. ESR measurements were crried out to examine the magnetic state of the impurity ion and various changes during and after the synthesis of tie samples. The results obtained through the above techniques are presented and discussed here.

4.3 Results and discussion

(a) X-ray diffraction studies :

Fig. 4.1(a) shows the x-ray diffraction (XRD) pattern for sample SZYP. It is evident that the XRD pattern consists of three phases namely, monoclinic, tetragonal and cubic. After indexing the observed XRD pattern d values are calculated. The observed values of d (d_{obs}), calculated values (d_{cal}), the miller indices and relative intensities of the peaks are collated in, Table 4.(II). The values of d_{obs} are calculated using Bragg's formula :

$$d_{obs} = \frac{\lambda}{a \sin \theta} \quad (4.3.1)$$

where λ is the wavelength of $\text{CuK}\alpha$, θ is the diffraction angle and d_{obs} is the interplaner distance.

The values of d_{cal} have been calculated using the following expressions and lattice parameters from literature [7,8] :

$$\text{For cubic} \quad \frac{1}{d_{cal}^2} = \frac{h^2 + k^2 + l^2}{a^2} \quad (4.3.2)$$

$$\text{For tetragonal} \quad \frac{1}{d_{cal}^2} = \frac{h^2 + k^2}{a^2} + \frac{l^2}{c^2} \quad (4.3.3)$$

For monoclinic

$$\frac{1}{d_{cal}^2} = \frac{1}{\sin^2 \beta} \left[\frac{h^2}{a^2} + \frac{k^2 \sin^2 \beta}{b^2} + \frac{l^2}{c^2} - \frac{2hl}{ac} \cos(\beta) \right] \quad (4.3.4)$$

The phase composition for the samples has been evaluated using intensity variation semiempirical method [7,8].

In order to make quantitative analysis of the monoclinic, tetragonal and cubic phases existing in the samples, we have used the following expressions :

$$I_M = \left[\frac{I_m(11\bar{1}) + I_m(111)}{I_m(11\bar{1}) + I_m(111) + I_{t,c}(111)} \right] \times 100 \quad (4.3.5)$$

$$I_T = (1 - I_M) \left[\frac{I_t(400) + I_t(004)}{I_t(400) + I_t(004) + I_c(400)} \right] \times 100 \quad (4.3.6)$$

$$\text{and } I_c + I_M + I_T = 100$$

where IM, IT, and IC are the percentages of monoclinic, Tetragonal and cubic phases respectively. We have assumed that the intensities of various peaks of respective phases represent the amount of the particular phases, for example intensity of reflection(111) represents the amount of monoclinic phase.

Fig 4.1 (b to d) depict the XRD patterns for samples SZYTi, SZYNi, SZYCo. The percentage of phase composition of the samples has been estimated using earlier expressions and the values obtained are given in Table 4.(III).

From the above crystallographic data, we can say that all samples exhibit monoclinic phase as the dominant phase. It is also worthmentioning that in earlier studies ZrO_2 doped with 12 mol % of Y_2O_3 were found to contain almost monoclinic phase [5].

(b) Scanning electron microscopy studies:

The SEM micrographs for all the samples are shown in Fig. 4.2 (a-d). It is evident from the micrographs that all samples comprise two major kinds of phases. One of them being brighter (white), while the other is darker (black). At the time of preparation of these samples for SEM studies, we have observed an interesting fact that during the sputtering of Ag metal upon the samples, there was illumination of light. We can attribute this phenomenon to luminescences of materials. All the samples seem to have the nearly uniform microstructure except sample SZYNi. The average grain size varies from sample to sample. Generally, sintering temperature, duration preparation methods, particle size of unsintered mixture etc. are the parameters which affect the microstructure of the final product. It should be stressed here that we have subjected a fixed heat treatment for sintering to all the samples. Therefore, the variation in average grain size may be attributed to the effect of various dopants.

It may also be noted from these micrographs that all samples display an overall increase in grain-size as compared to the pure sample SZYP. This increase probably results due to the presence of impurity ions which favours the particles assemblage of doped samples. The grain size estimates obtained from the SEM pictures indicate two ranges of particle-size; larger grains ($> 5 \mu m$) and smaller grains ($< 1 \mu m$).

(c) Electron Spin resonance studies :

(I) Pure sample SZYP :

The ESR spectrum of the powdered (finely crushed) undoped sample SZYP comprise a narrow resonance line near $g \approx 2$ superimposed on a broad ESR signal spectrum for pure sample (SZYP). Fig.4.3(a) shows ESR spectrum of SZYP at RT. As mentioned earlier we have used 99.99% pure ZrO_2 for synthesizing the SZYP samples, therefore the presence of any extrinsic paramagnetic impurity is not expected. However the sample indicates the presence of some paramagnetic centres in the synthesized material SZYP. It is not possible to identify the exact nature and cause of these centres. The narrow signal is situated at $g_{eff} = 1.975 \pm 0.005$ and the width of this signal ΔH is $\approx 25 \pm 3$ G. The width of the broad signal is ≈ 290 G and is situated around $g_{eff} \approx 2.05$. These paramagnetic centres may be artefact of synthesis process since these signals are present in all the samples prepared for the present study. The interesting aspect of these signals is that their widths and positions remain essentially temperature independent between RT and LNT. The narrow signal is marked by p and its position is denoted by g_p [Table 4.(IV)] where the parameters obtained from ESR study are collated. As revealed by X-ray the SZYP sample comprise mainly monoclinic and tetragonal phases. The two signals may result from these phases present in the synthesized sample.

(II) Titanium doped sample SZYTi :

The ESR spectrum of titanium doped sample [Fig.4.3(b)] comprises a large number of narrow lines in addition to Titanium has the electronic structure $[A]3d^24s^2$. The two signals Divalent titanium complexes are very unstable. However trivalent titanium observed in SZYTi, with electronic configuration $[A]3d$ forms octahedral paramagnetic complexes which are stable. Titanium has several isotopes vis. ^{44}Ti , ^{47}Ti , ^{48}Ti , ^{49}Ti and ^{50}Ti . Hyperfine splittings may arise only due to ^{47}Ti and ^{49}Ti as they have non-zero nuclear spins I of $5/2$ and $7/2$ respectively and for the even isotopes the nuclear spin is zero. In octahedral and tetrahedral environments Ti^{3+} has an orbital singlet as its ground state and there are low lying excited states. ESR spectra can be observed at RT and LNT and are appropriate to $S=1$ like Ni^{2+} [9-11]. The g factor is expected to be less than g_e ($=2.0023$) ESR is appropriate to $S=1/2$. The observed ESR spectrum in the present case are not appropriate to any of the above two paramagnetic states of Titanium. The observed increase in line width of the broad spectrum as compared to SZYP indicates that Titanium ion is having some exchange interaction with the paramagnetic centre responsible for the broad ESR signal. The presence of a large number of narrow lines on the broad signal may be attributed to superhyperfine interaction between the paramagnetic centre and surrounding ligands which probably involves Titanium nuclear spins. The structure is too complex to be analysed meaningfully.

(III) Nickel Doped sample SZYNi :

The ESR spectrum of nickel doped sample SZYNi is shown in fig [4.3(c)]. There is a very broad ($\Delta H \approx 1350$ G) signal on which a large number of narrow signals are observed to superimpose. The narrow signal at $g_p \approx 1.97$ (characteristic of all simples) is also present and is marked as p in the figure. Ni^{2+} with $3d^8$ configuration is characterized by $S = 1$ because an octahedral crystal field leaves an orbital singlet lowest. Lower symmetry fields raise the spin degeneracy for Ni^{2+} by rather large amounts (\sim few cm^{-1}) [11]. This high sensitivity to low symmetry crystal fields is believed to be the reason for considerable line broadening due to slight imperfections in the host crystals. Appreciable positive g shifts are usually encountered for Ni^{2+} ions in crystalline host [9] The g factor in the present case is estimated to be ≈ 2.5 Since incorporation of Ni^{2+} in the SZYNi lattice in the present case would demand charge compensation which in turn is expected to cause crystal imperfections in the host lattice. Thus broader lines of ESR Spectrum for SZYNi are explained. However, we have no immediate explanations for the hyperfine structure on the broad ESR singal. Also the SEM study has shown significant changes in morphology of SZYP after doping with nickel (SZYNi) as discussed earlier.

(IV) Cobalt Doped Sample ZXYCo.

The Cobalt doped sample[Fig. 4.3(d)] showed ESR signals similar

to the undoped samples. No additional signals could be observed even at LNT. Relaxation time of Co^{2+} ion in octahedral coordination is short at room temperature as a result ESR signals can be observed only below 20K [9-12].

4.4 CONCLUSION

The results of ESR, SEM and X-RD studies of $(\text{ZrO}_2)_{0.8} (\text{Y}_2\text{O}_3)_{0.2}$ samples synthesized by solid state reaction route show that the favourable phases are monoclinic and tetragonal. Small amounts of doped impurities of transition metal ions are not found to change the composition of the system noticeably. The ESR spectra for Ni doped sample has shown the discernible large broadening with a large number of narrow signals whereas the samples with Co have less broadening. The origin of broadening has been traced out to be due to the dipolar effect of impurity ions.

Table 4(I) Samples codes and doped impurity

S.No	Sample	Doped Impurity [#]	Stoichiometry of Samples
1.	SZYp	P	$(\text{ZrO}_2)_{0.8}(\text{Y}_2\text{O}_3)_{0.2}$
2.	SZYTi	TiO_2	"
3.	SZYCo	$\text{Co}(\text{NO}_3)_2$	"
4.	SZYNi	$\text{Ni}(\text{NO}_3)_2$	"

The concentration of each dopant is 1 wt % of $(\text{ZrO}_2)_{0.8}(\text{Y}_2\text{O}_3)_{0.2}$ and P stand for pure.

Table : 4(II) Crystallographic data esimated from XRD studies for SZYP sample.
 (M=monoclinic, T= tetragonal and C= cubic)

hkl	phases	d_{obs} Å	d_{cal} Å	$(d_{\text{obs}} - d_{\text{cal}})$ Å	$(I/I_0)_{\text{obs}}$ %
[110],[011]	M	3.60	3.64	0.05	24
[111]					
[111]	M	3.12	3.16	0.04	77
[111]	T,C	3.02	2.97	0.05	100
[111]	M	2.80	2.84	0.04	76
[200],[002]	M,C	2.59	2.56	0.03	30
[210]	M	2.30	2.28	0.02	8
[102]	M	2.17	2.18	0.01	21
[112]	T	2.06	2.10	0.04	10
[112]	M	1.98	2.01	0.03	20
[022]	M	1.86	1.85	0.01	70
[202],[220]	T,C,M	1.80	1.81	0.01	72
[220]					
[002],[300]	M	1.68	1.69	0.01	16
[013],[221]	M	1.64	1.64	0.00	38
[113],[311]	T,C,M	1.56	1.55	0.01	49
[311],[131]					
[222],[222],[311]	C,M	1.47	1.47	0.00	16

Cont.

[132]	T	1.34	1.37	0.03	6
[104]	M	1.31	1.32	0.01	26
[400],[004]	C,T	1.29	1.28	0.01	16
[400]	C	1.26	1.26	0.00	16
--	--	1.22	1.23	0.01	10
[114]	T	1.21	1.21	0.00	20
[400]	T	1.10	1.10	0.00	11
[004]	T	1.09	1.09	0.00	9

Table 4(III) Shows the relative phase composition.

S.No	Sample's code	Relative concentration of phases (%)		
		M	T	C
1.	SZYP	61	33	6
2.	SZYTi	58	33	9
3.	SZYNi	63	32	5
4.	SZYCo	62	33	5

M= Monoclinic, T = Tetragonal and C = Cubic

Table 4(IV) Parameter derived from ESR studies.

Sample Code	g value	Line width ΔH (Gause)
SZYP	$g_p = 1.975 \pm 0.005$	$\Delta H_p = 23 \pm 3$
	$g_a = 2.05 \pm 0.05$	$\Delta H_a = 290 \pm 20$
SZYTi	$g_p = 1.975 \pm 0.005$	$\Delta H_p = 25 \pm 3$
	$g_a = 3.7536 \pm 0.05$	$\Delta H_a = 1687 \pm 50$
SZYNi	$g_p = 1.975 \pm 0.005$	$\Delta H_p = 25 \pm 23$
	$g_a = 2.544 \pm 0.005$	$\Delta H_a = 1350 \pm 50$
SZYCo	*	*

* Similar to SZYP

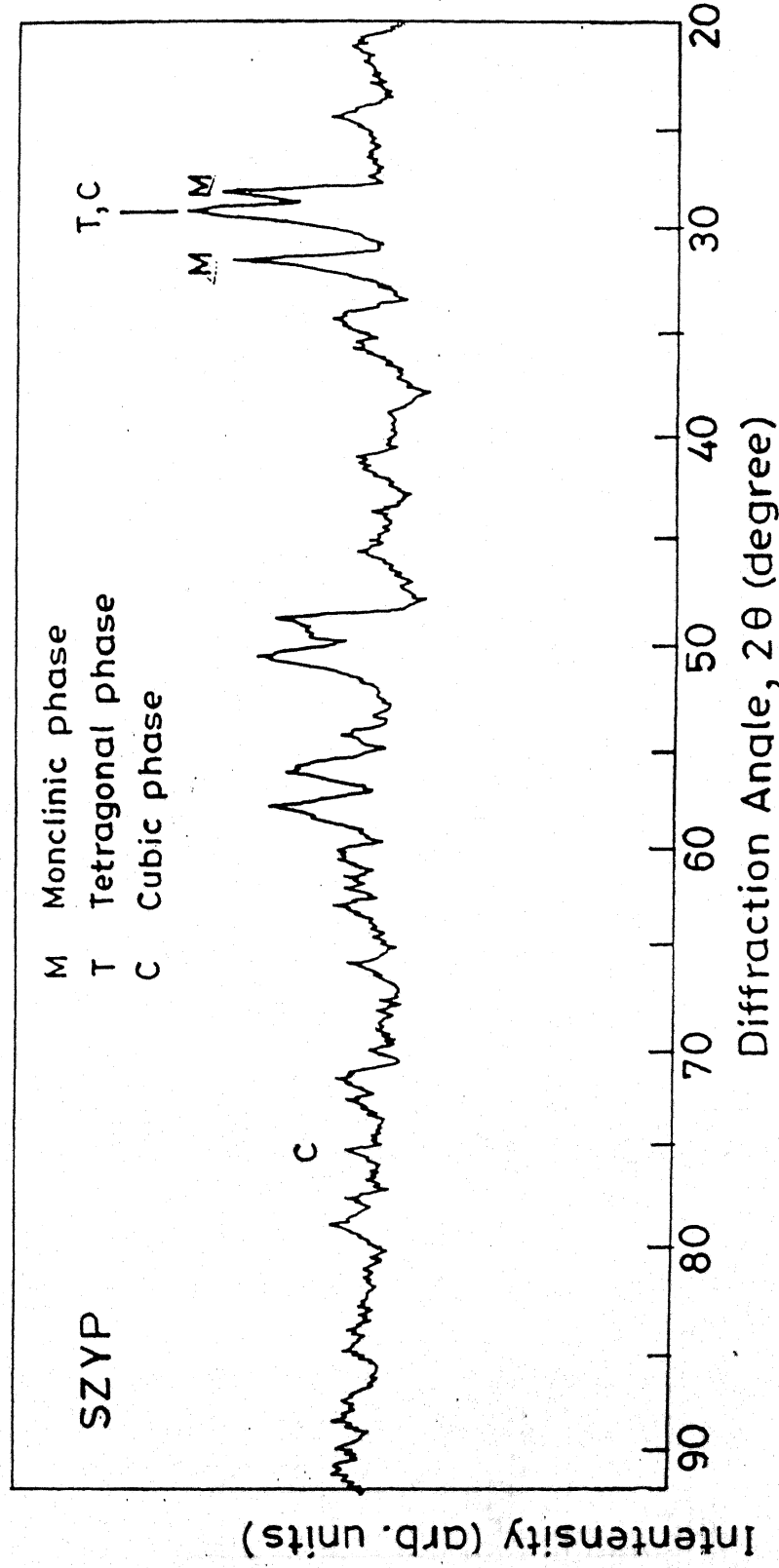


Fig 4.1 (a) X-ray diffraction pattern of Sample SZYP.

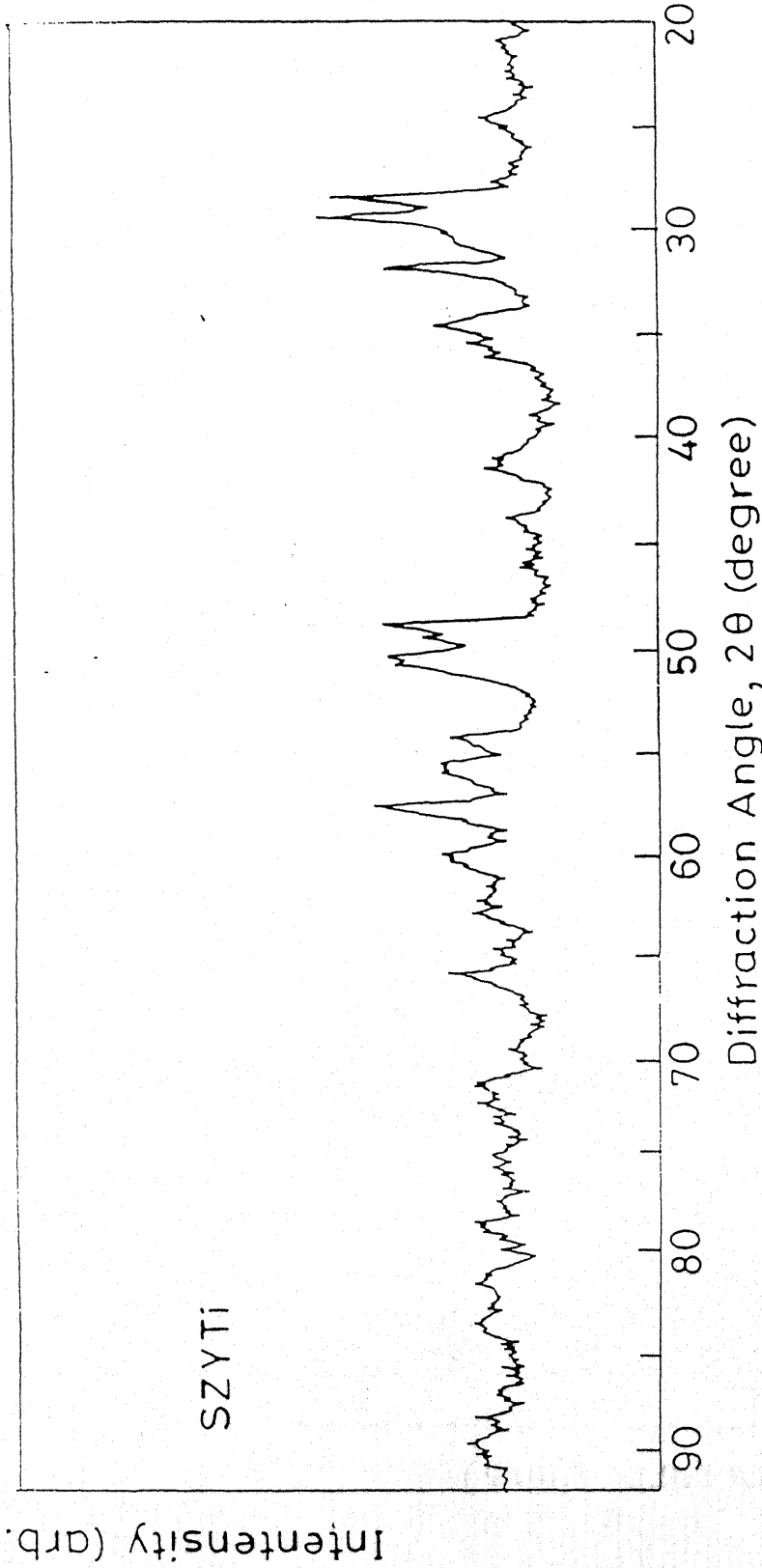


Fig 4.1 (b) X-ray diffraction pattern of Sample SZYTi.

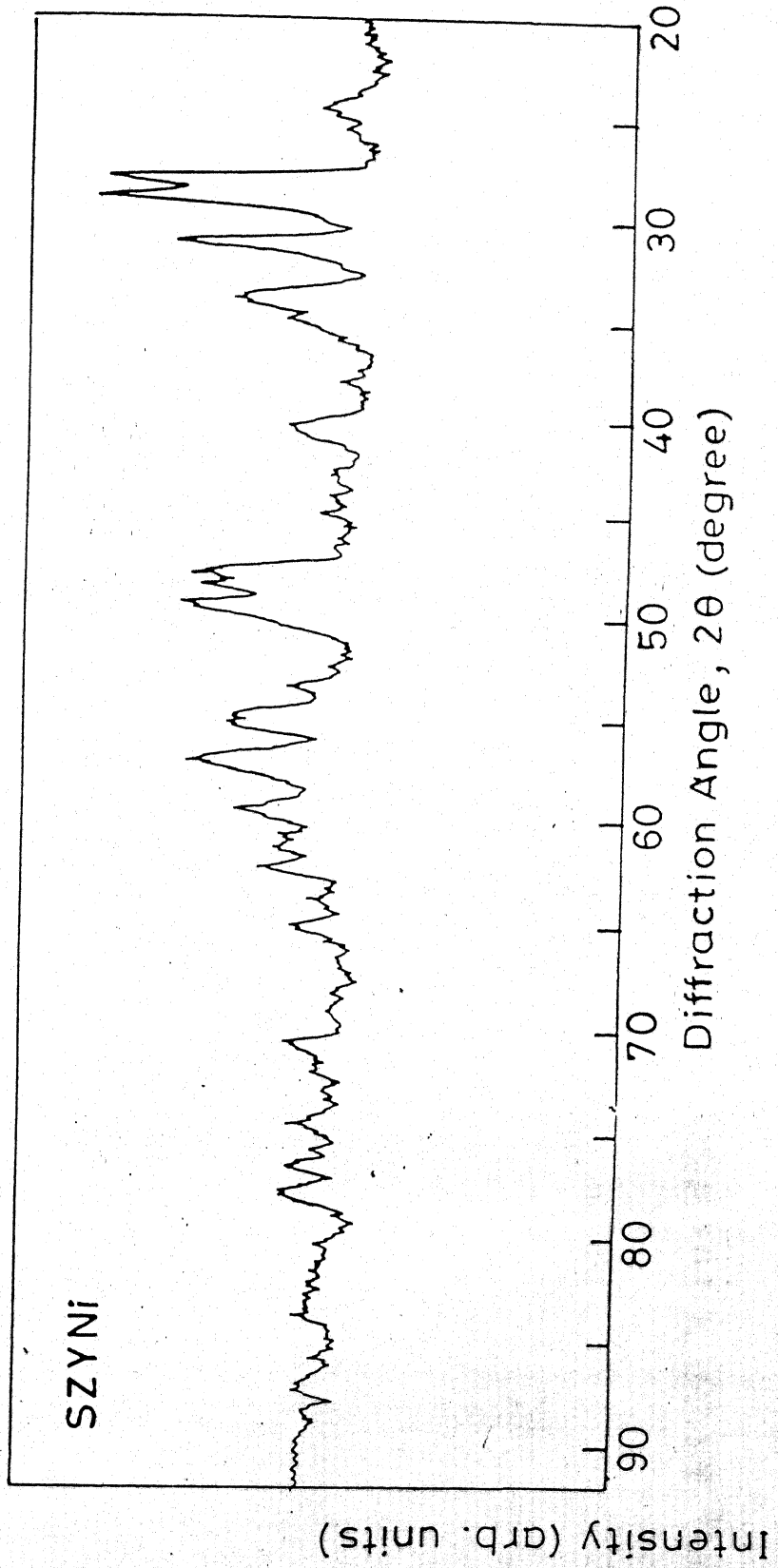


Fig 4.1 (c) X-ray diffraction pattern of Sample SZYNi.

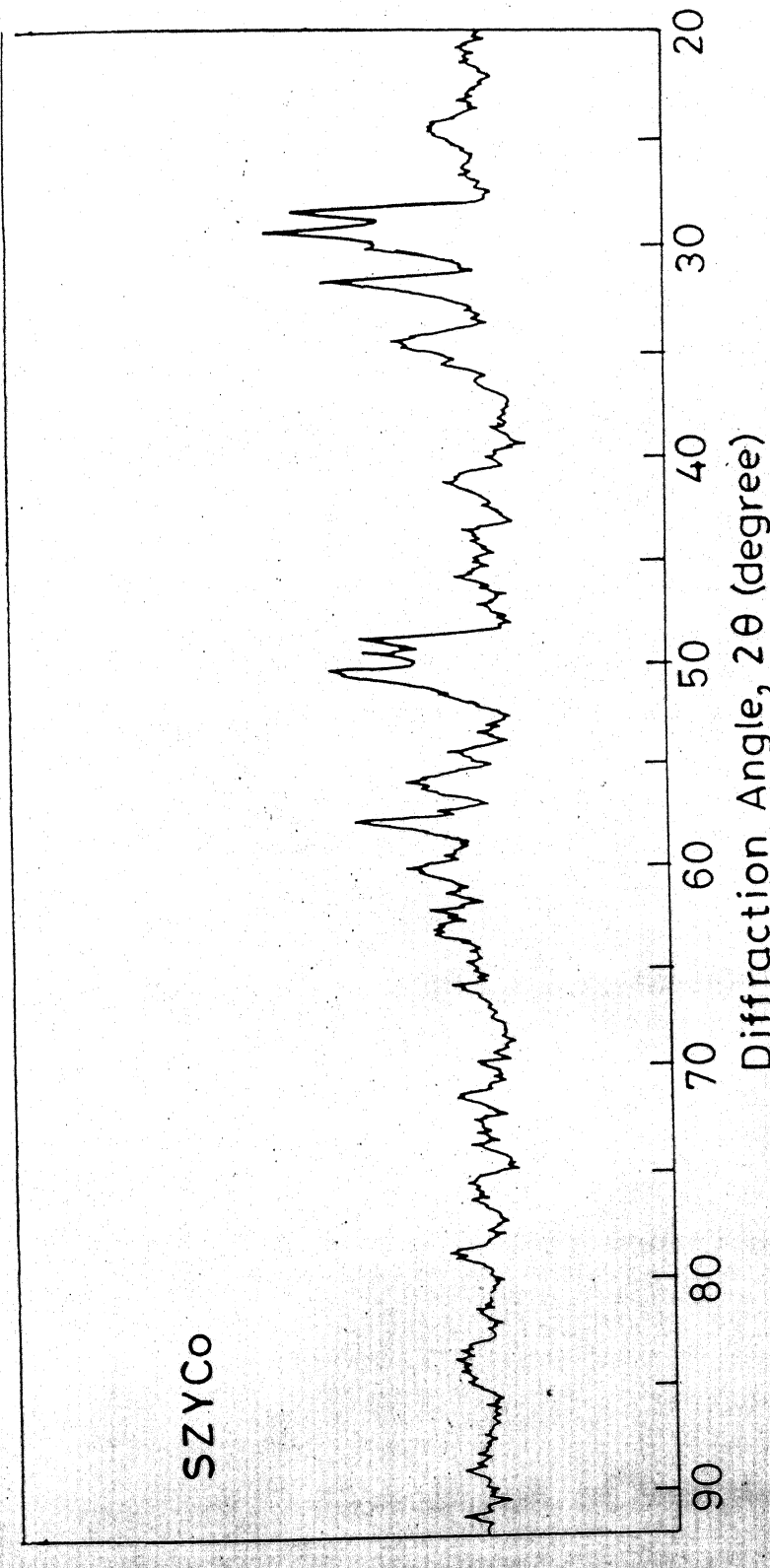


Fig 4.1 (d) X-ray diffraction pattern of Sample SZYCo.

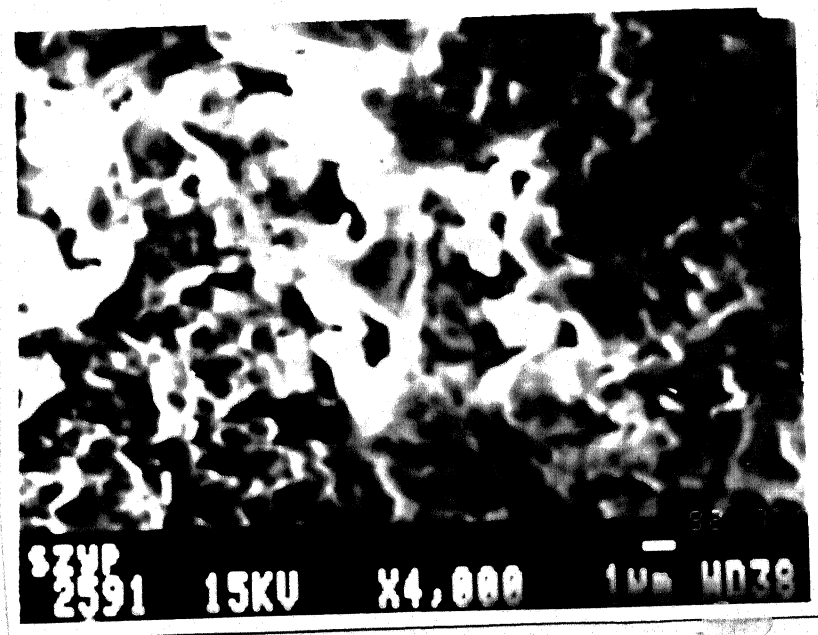


Fig 4.2 (a) SEM Micrograph of Sample SZYP.

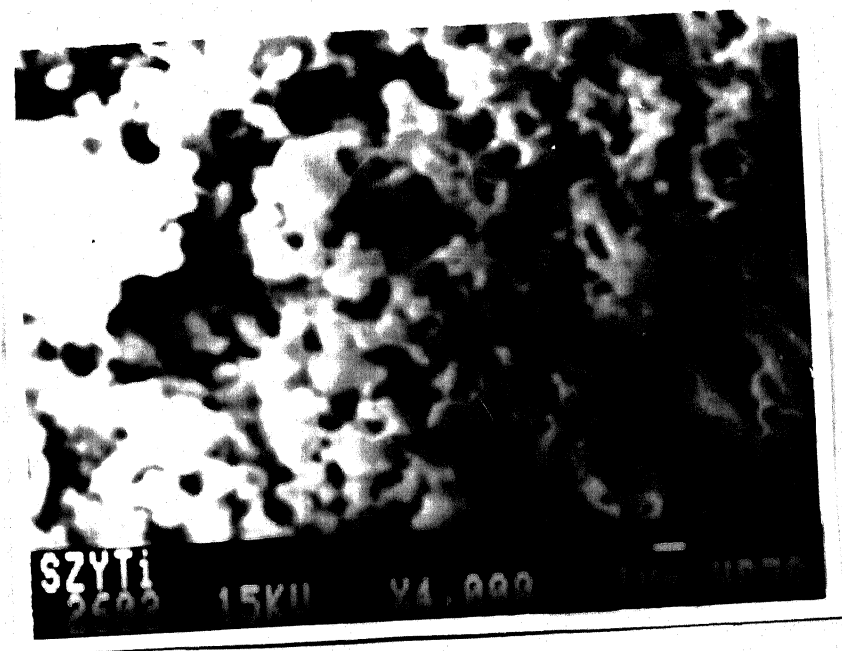


Fig 4.2 (b) SEM Micrographs of Sample SZYTi.

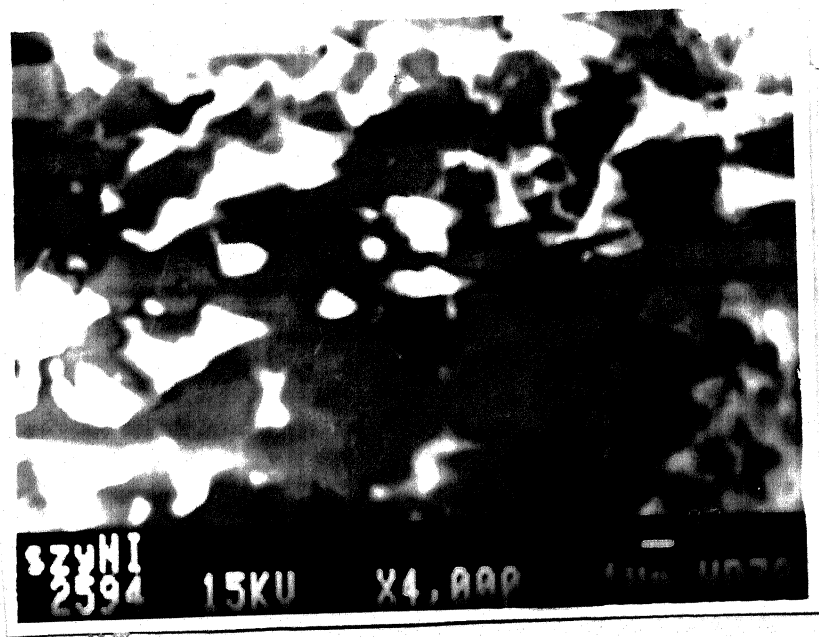


Fig 4.2 (c) SEM Micrograph of Sample SZYNi.

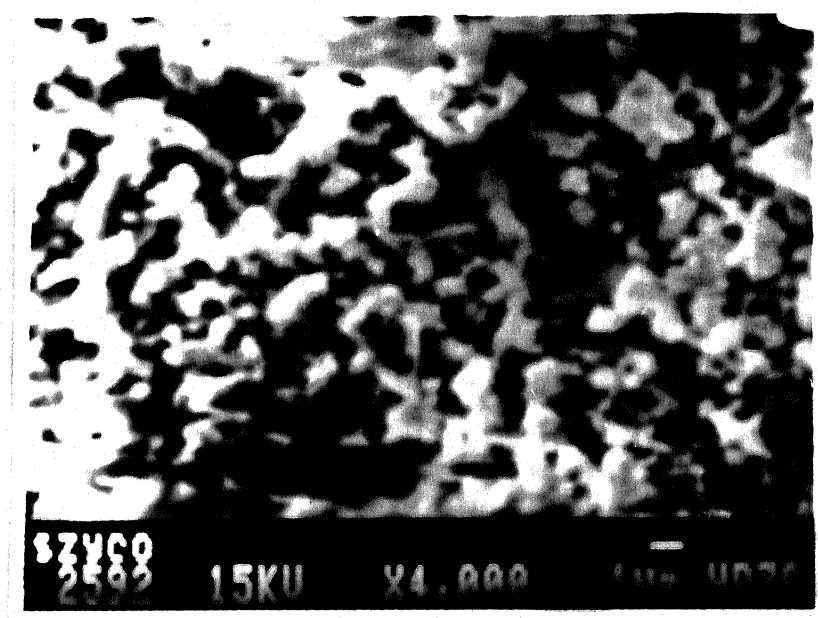


Fig 4.2 (d) SEM Micrograph of Sample SZYCo.

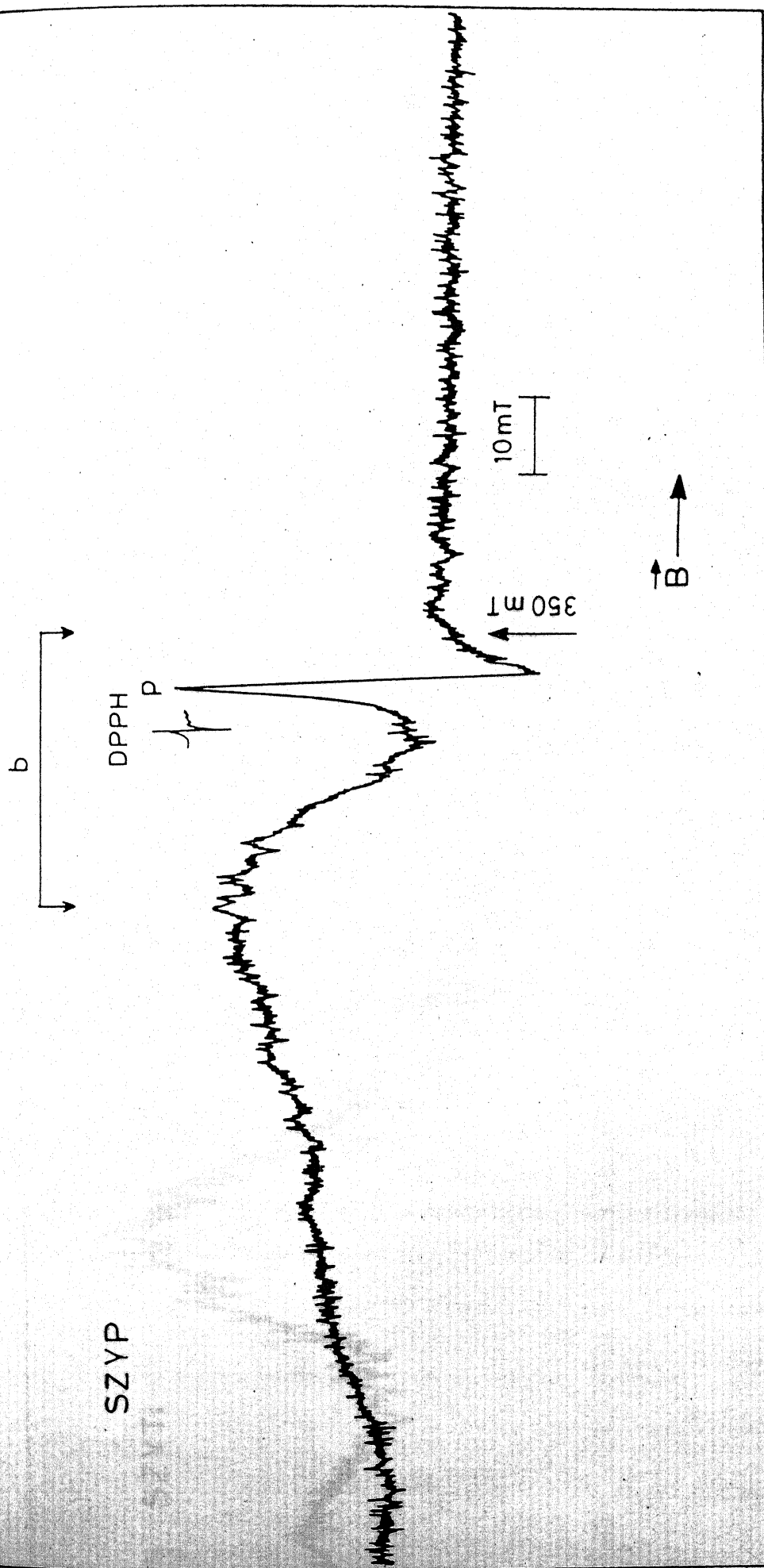


Fig 4.3 (a) ESR spectrum of sample SZYP

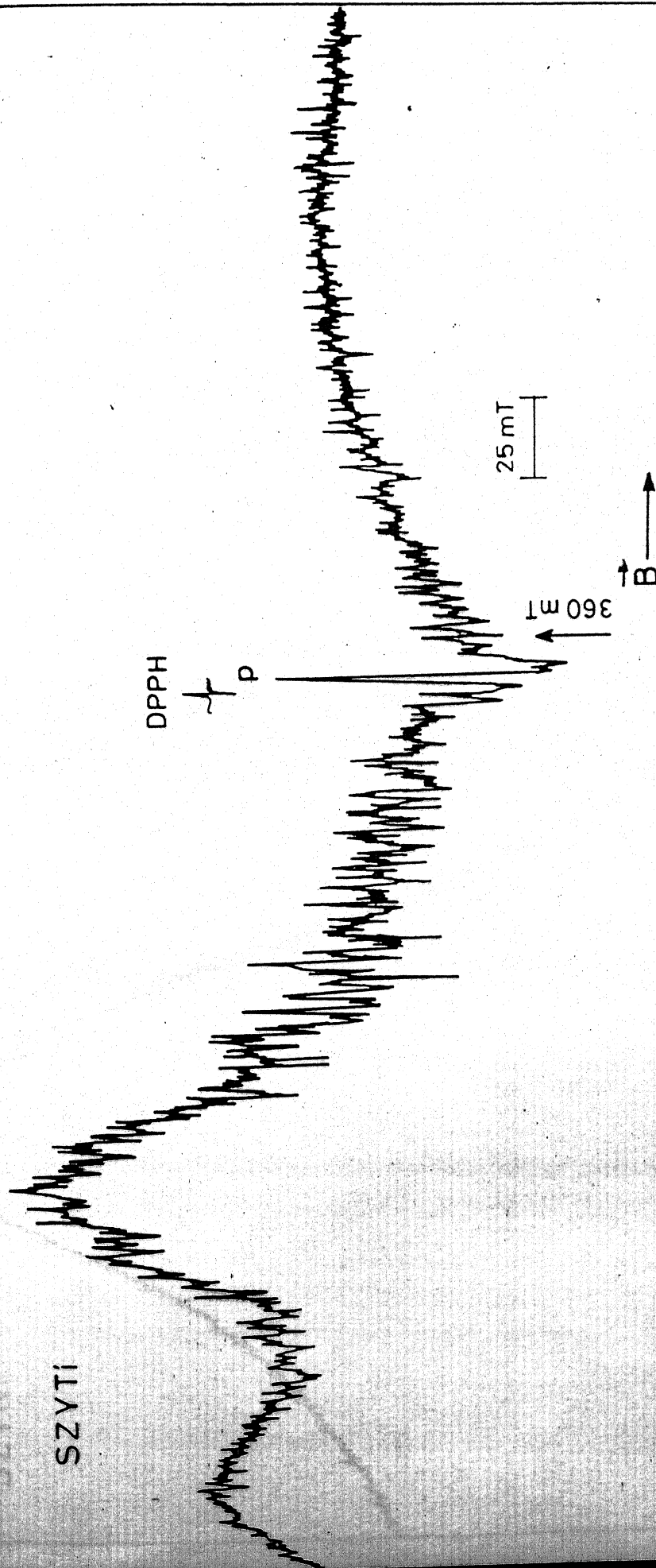


Fig 4.3 (b) ESR spectrum of sample SZYTi

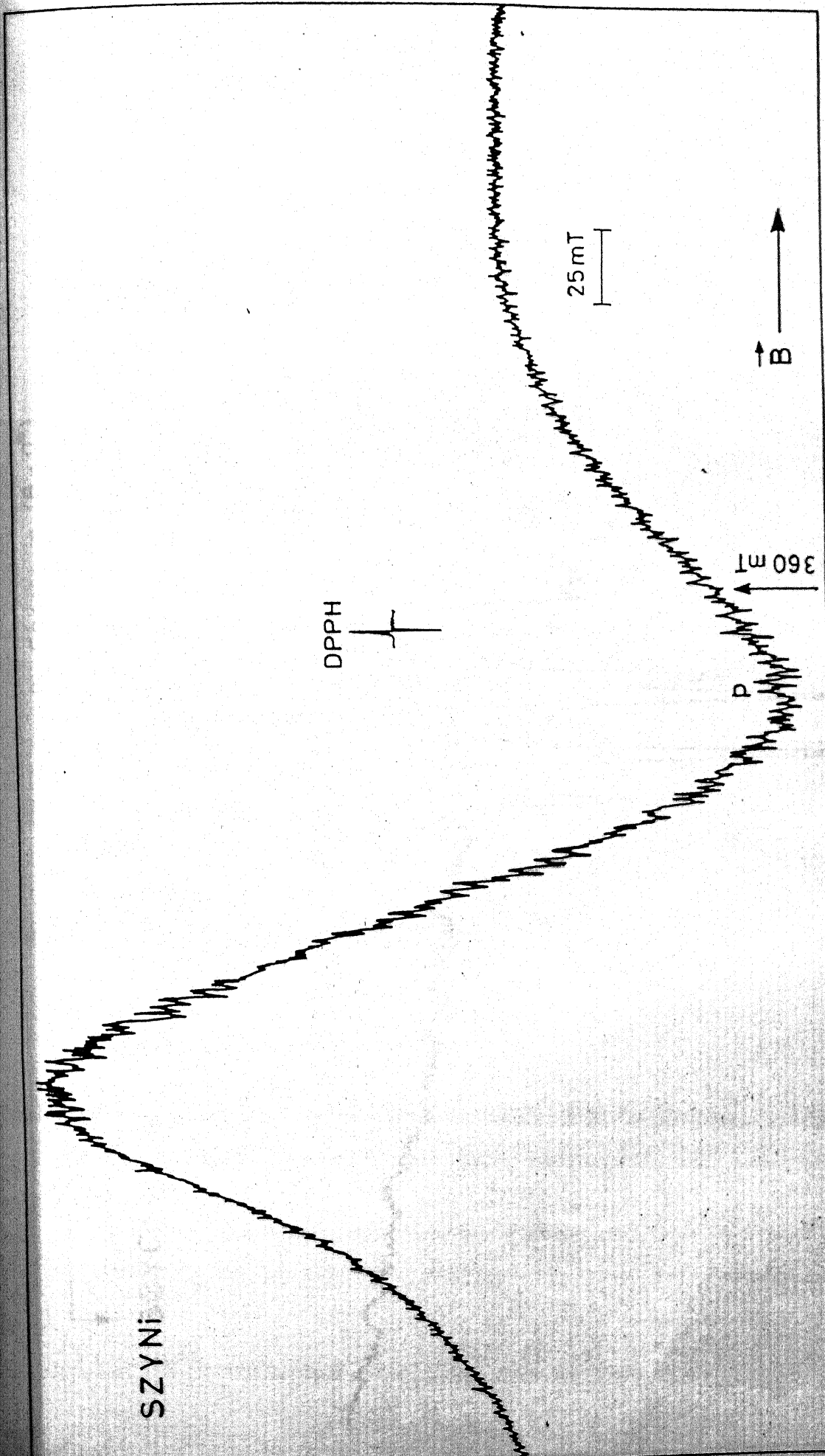


Fig 4.3 (c) ESR spectrum of sample SZYNi

II - Spectrum ($\theta = 0^\circ$)T - Spectrum ($\theta = 90^\circ$)

SZYCO

DPPH

P

362 mT

8 mT

B



References

1. R. Stevens "Zirconia Engineering Ceramics". Hand Book of Ceramics, Supplenent to interceram. 34, 1 (1985).
2. A. R. Burkin, H. Saricimen and B.C. Steel, Trans. J. Brit. Ceram. Soc. 79, 105 (1980).
3. N. M. Ghoneim and S. B. Hanna, J. Mater. Sci. 25, 5192 (1990).
4. N. R. Shankar, H. Herman, S. P. Singhal and C. C. Berndt, Thin Solid Films, 119, 159 (1984).
5. N. Iwamoto, N. Umesaki and S. Endo, Thin Solid Films 127, 129 (1985).
6. E. A. Zhilinskaya, V. N. Lazukin and I. V. Chepeleva, Magnetic Resonance and related phenomena 325, (1979).
7. R. A. Miller, J. L. Smaialek and R. J. Garlick, Adv. ceramic, 3, 241 (1981).
8. B. D. Cullity, Elements of X-ray diffraction, Addison Wesley Publishing company, Inc., California (1978).
9. J. E. Wertz and J. R. Bolton, Electron Spin Resonance : Elementary Theory and Practical Applications, McGraw Hill, chap. 11 (1972).
10. C. J. Ballhausen, Introduction to Ligand field theory, McGraw Hill Chap 10 (1962).

11. J. W. Orton, Electron paramagnetic resonance, Iliffe Books Ltd., London, Chap. 11 (1968).
12. A. Carrington and A. C. Mc Lachlan, Introduction to Magnetic resonance, Chapman & Hall Ltd., Chap. 10 (1979).
13. A. S. Marfunin, Spectroscopy, Luminescence and Radiation centers in minerals, Springer Verlag chap. 3 (1979).
14. Bleaney Phil. Mag. 42 441 (1951).
15. A. Abragam and B. Bleaney, Electron paramagnetic Resonance of transition Ions, Clarendon Press (1970).
16. P. Chand, V. K. Jain and G. C. Upreti, Magn. Resonance. Rev. 14. 49 (1988).
17. R. R. Tiwari, S. D. Pandey, and P. Chand, Solid State Commu, 69, 1109 (1989)
18. M. Stempí, H. Szymczak and A. A. Andreev, Acta Physica Pol. 63, A. 627 (1982).



CHAPTER -5

ESR study of

Copper Amino Acid

Complexes

CHAPTER - 5

5.1 INTRODUCTION :

Among the transition group elements, copper is one of the ideal ions for paramagnetic resonance study, because there is only one electronic transition and narrow lines are obtained at room temperature. When paramagnetic ion is placed in a solid, interactions take place between the paramagnetic ions themselves and with the diamagnetic neighbours. In order to draw quantitative information about the inter and intramolecular interactions with the spin of a paramagnetic ion, one must solve the spin-Hamiltonian of the paramagnetic ion in that surrounding. In most of the pure paramagnetic substances, ions are so close together that the information conveyed by them overlap and no inference can be drawn about the anisotropy of the spin-Hamiltonian parameters. As described earlier, the anisotropy study can be done easily and accurately by preparing single crystal of the paramagnetic substance diluted in a diamagnetic lattice. The diamagnetic substance for dilution should be isomorphic to the paramagnetic substance to be studied and the doped crystals are formed by replacing some of the crystal sites by paramagnetic ions. However, it is not always convenient to find an isomorphic substance and to prepare 'doped crystal' in every case. It has been found [1, 2] that a study of polycrystalline samples and on 'frozen solution' can also furnish an almost the same information.

In the present chapter a comprehensive ESR study on a few copper-

amino acid complexes has been undertaken. Complexes were studied in polycrystalline form and in aqueous solution at room temperature and also in frozen state i.e. a random and fixed distribution of paramagnetic ions. Information regarding the chemical bonding between the transition metal and the ligand atoms has been derived with the help of anisotropic parameters g_{\parallel} , g_{\perp} , A_{\parallel} , and A_{\perp} obtained from above studies [1]. Different theories of ESR linewidths have been used in order to know the contribution of dipolar width as well as exchange narrowing to the polycrystalline linewidths. Hyperfine structure linewidths in solution for all the four lines of the complexes have been calculated according to Kivelson's theory. Linewidth parameters both experimental and theoretical have been reported. The study done here, has been divided in to three sections.

I. Polycrystalline sample study

II. Glass study

III. Solution study

5.2 POLYCRYSTALLINE SAMPLE STUDY

The scope of the ESR studies of polycrystalline samples is limited by the fact that due to the random orientation of paramagnetic ions, important parameters like linewidth and g-value etc. are averaged out and the derivable informations are very much reduced. If g-value of

the substance is very close to 2.0023, the anisotropy would be small, it can be examined in powder without loss of resolution. If g is more, anisotropy increases, $g_{||}$ and g_{\perp} would be quite different and this gives rise to spreading out of the lines. Sometimes this spread out portions give important information about $g_{||}$ and g_{\perp} , as in case of many copper complexes studied here. ESR lineshape studies on powder copper complexes has been presented in the famous paper of Kneubuhl [2]. It was assumed that the paramagnetic molecules are differently distributed, the system gives rise to no hyperfine splitting and the broadening of lines occur due to only anisotropic g factor. He described a method of finding upto three principal g -values from an inspection of powder spectra of copper complexes with examples of $\text{CuCl}_2 \cdot 2\text{H}_2\text{O}$ and $\text{CuSO}_4 \cdot 5\text{H}_2\text{O}$. The assumptions lead to the following

Hamiltonian

$$\mathcal{H} = \beta [g_z H_z S_z + g_x H_x S_x + g_y H_y S_y] \quad (5.2.1)$$

Now two cases can be distinguished. For $g_x = g_y$, Sands [3] evaluated the normalized shape function $S(H_z)$ as

$$S(H_z) = H_{\perp}^2 H_{||} (H_{\perp}^2 - H_{||}^2)^{-\frac{1}{2}} H_z^{-\frac{1}{2}} (H_{\perp}^2 - H_z^2)^{-\frac{1}{2}} \quad (5.2.2)$$

If $g_z > g_y > g_x$, then for $H_z \leq H_2$:

$$S(H_z) = \frac{2}{\pi} \frac{H_1 H_2 H_3 H_z^{-2}}{(H_1^2 - H_z^2)^{1/2} (H_2^2 - H_z^2)^{1/2}} K(k) \quad (5.2.3)$$

$$\text{with } k^2 = \frac{(H_1^2 - H_2^2)(H_z^2 - H_3^2)}{(H_1^2 - H_z^2)(H_2^2 - H_z^2)}$$

and for $H_z \geq H_2$

$$S(H_z) = \frac{2}{\pi} \frac{H_1 H_2 H_3 H_z^{-2}}{(H_1^2 - H_z^2)^{1/2} (H_2^2 - H_z^2)^{1/2}} K(1/k) \quad (5.2.4)$$

$K(k)$ is the complete elliptic integral of the first kind.

$$K(k) = \int_0^{\pi/2} db / (1 - k^2 \sin^2 b)^{1/2} \quad (5.2.5)$$

$$K(0) = \pi/2, K(1) = \infty$$

From the fig. 5.1 drawn with the help of eqs. (5.2.2) and (5.2.4), one can distinguish the two cases of the derivative spectrum, one corresponding to two g -values ($g_{||}$ and g_{\perp}) which has five points of inflexion and the other of three g -values (g_x , g_y and g_z) which has seven points of inflexion.

Results and Discussion

The electron spin resonance spectra of all the polycrystalline samples have been taken at x-band and at room temperature. The spectra of polycrystalline samples along with their glass and solution spectra are shown in Figs. (5.3-5.10) The spectra of all the complexes are not similar in nature. Four of them have shown five points of inflexion and the other three been shown only three. The presence of five points of inflexion indicates two values of g , i.e. $g_{||}$ and g_{\perp} in them while three points of inflexion give only the average values of g . The values of g obtained here are quite close to the values obtained from glass study of the samples given in the next section. The

presence of two g-values in complexes also indicates that an axial crystalline field is acting at the Cu(II) due to the ligand surrounding the ion. Cu/ β -Alanine complex showed a bit strange behaviour. The spectra have shown seven points of inflexion and hence three values of g. All the three values have been measured see table 5.(I).

The lineshape of all the experimental curves has been tested and has been found to be Lorentzian. The lineshape graphs of a few samples are shown in fig. 5.2. The linewidth increases in all cases to the parent copper compound but the shape remains unchanged.

The change in linewidth is mainly due to change in spin-lattice, dipole-dipole and exchange interactions neglecting of course, the contribution of nuclear hyperfine interaction and saturation broadening [5]. In case of Cu salts, spins are loosely coupled to lattice vibration [6] and thus spin-lattice interaction does not affect the width to any marked extent. This means that only dipole-dipole and exchange interactions mainly control the width of the lines. The actual positions of copper ions inside the complexes are not known, but it seems from their molecular formulae that ions have been separated apart as compared to their positions in pure copper salts. Thus the dipolar interaction as well as exchange interaction has decreased, but the decrease in the latter is more than the former because of its exponential form [7] and hence finally the broadening is observed. It is obvious that after the complex is formed, the crystal structure changes, it is magnetically diluted and exchange coupling is also changed but it has been found

that all these factors could not bring any change in the Lorentzian shape of ESR lines obtained here, which indicates that still sufficient exchange is present in the complexes.

Different g-values for different samples, simply indicates that the factors which control the g-value viz. spin-orbit coupling constant λ , the energy separation between the ground level and the excited level Δ and nuclear and molecular magnetic field etc, might have changed in these complexes. The reduction in g-values as compared to parent salts [2] may be due to increase in Δ or a decrease in effective λ ($\lambda \times$ covalency factors α^2) or both. A small change in Δ does not effect g much, so $\alpha^2\lambda$ is mainly responsible for the reduction in g-values. This shows that covalency in the complexes have definitely increased.

In order to make the quantitative interpretation of the results obtained here, the computation of various ESR parameters has been done by using different theories [8-10]. According to Van Vleck [7] the half width ($\Delta H_{1/2}$)_{cal} due to dipole-dipole interaction is given by

$$\begin{aligned} (\Delta H_{1/2})_{\text{cal}} &= 2.35 [\langle \Delta H^2 \rangle]^{1/2} \\ &= 2.35 g\beta [3/5 S(S+1) \sum_k k r_{jk}^{-6}]^{1/2} \quad (5.2.6) \end{aligned}$$

where S is the spin quantum number of the ion, r_{jk} is the distance between the ions j and k and rest of the symbols have their usual significance. Since the crystal structure of all the complexes are not known and we want to study only the relative variation of exchange

frequency in these complexes, so for the sake of simplicity we have assumed that the systems have simple cubic structure, therefore

$$r_{jk}^{-3} = N\rho /M \quad (5.2.7)$$

where N is the Avogadro's number, ρ is the density and M is the molecular weight of the complex.

From the results given in table 5.(II), it appears that in all cases $(\Delta H_{\frac{1}{2} \text{ obs}})$ is smaller than $(\Delta H_{\frac{1}{2} \text{ cal}})$ due to the effect of exchange coupling. In some cases the difference between $(\Delta H_{\frac{1}{2} \text{ cal}})$ and $(\Delta H_{\frac{1}{2} \text{ obs}})$ is quite small which may be due to the fact that the actual position of the ions in the complexes are not known and we have taken a very rough approximation of simple cubic lattice structure. Moreover, the fine and hyperfine splittings which appear in dilute samples are not resolved in the case of concentrated specimens because of the strong exchange interaction. Timerov [11] has derived the relations for the contribution of the unresolved fine and hyperfine structure to the width of the line in magnetically concentrated solids by the method suggested by Kubo and Tomita [9]. The contribution of fine splitting of linewidth for copper complexes ($S = \frac{1}{2}$) is zero and that of hyperfine splitting can be calculated [10] if the values of their hyperfine splitting constant A are known. This will add to their dipolar broadening a contribution of the order of 40 gauss to the width of the line (The contribution is calculated by taking $A = 80 \times 10^{-4} \text{ cm}^{-1}$ for Cu^{2+}) and thus the difference between $(\Delta H_{\frac{1}{2} \text{ cal}})$ and $(\Delta H_{\frac{1}{2} \text{ obs}})$ increases more thereby indicating that strong exchange interaction is present in these

complexes.

Anderson and Wesis [8] developed the theory of paramagnetic resonance absorption lines in a more quantitative way than Van Vleck. The expressions for different parameters obtained from this theory are given below :

$$\text{Dipolar Width } \omega_p^2 = 15.2/3 (g^2 \beta^2 / \hbar)^2 n^2 S(S+1) \quad (5.2.8)$$

$$\text{Exchange frequency } \omega_e = \sqrt{8.48/3} J/\hbar \sqrt{S(S+1)} \quad (5.2.9)$$

Where n is the density of spins per cubic centimeter, J is exchange integral and the expression for half width at half power points is given by

$$\Delta\omega = \omega_p^2 / \omega_e \quad (5.2.10)$$

The computed values of ω_p^2 and ω_e are given in table 5.(II). For the sake of comparison, the values of these parameters have also been evaluated by using Kubo and Tomita Theory [9]. They developed the theory on a quantum mechanical basis instead of usual moment method as done by Van Vleck and Anderson and Weiss. The expression for different parameters given by Chirkov and Kokin [12] from Kubo and Tomita theory have been used here. The expressions are

$$\Delta\omega = 4.18 \omega_{10}^2 / \omega_{20} \quad (5.2.11)$$

$$\omega_{10}^2 = 3.79 g^4 \beta^4 \hbar^{-2} d^{-2} \quad (5.2.12)$$

$$\omega_{20} = 3.65 |J|/\hbar \quad (5.2.13)$$

and for simple cubic lattice structure

$$\sum_k r_{jk}^{-6} = 8.4 d^{-6} \quad (5.2.14)$$

where ω_{10}^2 , ω_{20} and d are the dipolar width, exchange frequency and lat-

tice constant respectively. The computed values of ω_{10}^2 and ω_{20} are given in table 5.(II).

From table 5.(II) , it appears that the computed values of dipolar width as well as narrowing due to exchange obtained from both theories [8,9] have decreased in all complexes as compared to the pure copper salt. The maximum decrease in these parameters has been observed in $\text{Cu}^{2+}/\text{DL-valine}$ complex.

The values of dipolar width and exchange frequency parameters computed with the help of Anderson and Weiss theory are different from that of Kubo and Tomita theory. Slight differences in the results obtained from these theories are simply because the method of approach of both the theories are different, but the relative variation of different parameters is the same. Since the rate of decrease of exchange interaction is higher than that of dipolar interaction, it can be concluded that the exchange is playing the main role in broadening the lines of these complexes.

Thus one can conclude from the theoretical computation of ESR parameters that the increase in linewidth in all these complexes is mainly due to the reduction in exchange interaction. The experimental linewidth are in general smaller than those expected by dipolar coupling alone because still sufficient exchange interaction is present in these complexes as evident from the Lorentzian shape of their ESR lines.

5.3 GLASS STUDY :

ESR study in polycrystalline sample was unable to provide information regarding the anisotropy of nuclear spin hyperfine coupling constant 'a' i.e. $A_{||}$, and A_{\perp} . Again the information regarding g-anisotropy was not accurately available in all cases, because in some cases, only three points of inflexion were observed. The peaks being very broad, the available information was not very reliable. The above informations were required in order to further study the nature of bonding between metal and ligands and the linewidths of hyperfine lines in solution. The required magnetic parameters $g_{||}$, g_{\perp} , $A_{||}$ and A_{\perp} can possibly be found from a study of glasses or highly viscous ligands containing paramagnetic ions. A glass is prepared by freezing a mixture of a paramagnetic substance and a diamagnetic or a nonmagnetic liquid. This become equivalent to a polycrystalline sample in which paramagnetic ions are diluted and fixed apart. This method has proved more useful in cases where it is difficult to prepare the single crystal of the substance doped in a suitable diamagnetic lattice, and has been followed by a large number of workers successfully [13-18].

Glasses in the present study were prepared by mixing an aqueous solution of the complex of known strength of glycerine of known volume so that glycerine to water ratio in the mixture becomes 60 : 40 by volume. This was cooled to -80°C to get frozen solution or glass. Pure water solution was not freezed for glass preparation in the light of the

complications of ice structure. $\text{NH}_4\text{OH}/\text{glycerine}$ glass was used for studies in case of Cu/DL-Methionine and Cu/L-Cystine. Cu/DL-Aspartic acid was dissolved in pyridine and freezed to -80°C for its glass study. Water/glycerine medium was used for all the remaining complexes.

The mixtures were taken in a quartz tube and were mounted in the cavity while the low temperature unit is on, otherwise the highly lossy mixture makes the tuning nearly impossible. The mixture, as soon as mounted freezes and the absorption falls to a convenient value. Low temperature was obtained by adjusting the temperature of dry N_2 gas which cools the sample after passing through liquid air.

Lineshape in 'Glasses' :

The spin-Hamiltonian for the present system of square planar Cu(II) complexes can be written as [19]

$$\mathcal{H} = \beta_0 [g_{\parallel} H_z \bar{S}_z + g_{\perp} (H_x \bar{S}_x + H_y \bar{S}_y)] + A_{\parallel} \bar{S}_z I_z + A_{\perp} (\bar{S}_x I_x + \bar{S}_y I_y) \quad (5.3.1)$$

where β_0 is Bohr magneton, g_{\parallel} and g_{\perp} are spectroscopic splitting factors parallel and perpendicular respectively to the symmetry axis. \bar{S} and \bar{I} are electron and nuclear spin operators. A_{\parallel} and A_{\perp} are hyperfine splitting constants for copper nucleus. ESR energy $h\nu_0$ for the above Hamiltonian is given as

$$h\nu_0 = g\beta_0 H + M_1 (A_{\parallel}^2 g_{\parallel}^2 \cos^2 \theta + A_{\perp}^2 g_{\perp}^2 \sin^2 \theta)^{1/2} \text{ g}^{-1} \quad (5.3.2)$$

where $g = (g_{\parallel}^2 \cos^2 \theta + g_{\perp}^2 \sin^2 \theta)^{1/2}$

$M_I = \pm 1/2, \pm 3/2$ for copper and θ is the angle between the symmetry axis of the molecule and the applied magnetic field H . In the case of a diluted single crystal, resonance value of

the field H for a frequency ν_0 depends upon θ , but in a polycrystalline sample, molecules are differently oriented and the resonance spectrum is the sum of the spectra of molecules in all possible orientations. In a polyorystalline sample, different orientations of the molecules are equally probable. The number of molecules dN , whose symmetry axes forms an angle between θ and $\theta + d\theta$ with respect to the applied magnetic field, is given by [3]

$$dN = \frac{N_0}{2\sin\theta} d\theta \quad (5.3.3)$$

where N_0 is the total number of molecules. The intensity of absorption in a range of magnetic field between H and $H + dH$ is given by $|dN/dH|$

$$\frac{dN}{dH} = (dH/d\theta) d\theta/dH \quad (5.3.4)$$

$dN/d\theta$ is given in Eq. (5.3.3). $d\theta/dH$ can be obtained from the following expression.

$$H = \frac{g_0 H_0}{g} - \frac{M_I K}{\beta_0 g^2} \quad (5.3.5)$$

where $K = (g_{\parallel}^2 A_{\parallel}^2 \cos\theta + g_{\perp}^2 A_{\perp}^2 \sin^2\theta)$

and the expression for dN/dH is given as

$$\frac{dN}{dH} = \frac{1}{2} N_0 \left\{ \frac{2 \cos \theta}{g^2} \left[\frac{(g_{\parallel}^2 - g_{\perp}^2) g_0 H_0}{2g} + \frac{M_I}{g} \left(\frac{g_{\parallel}^2}{2K} - \frac{A_{\parallel}^2 - g_{\perp}^2}{2K} - \frac{K(g_{\parallel}^2 - g_{\perp}^2)}{g^2} \right) \right] \right\}^{-1} \quad (5.3.6)$$

where $H_0 = h\nu_0 / g\beta_0$ and $g_0 = (g_{\parallel} + 2g_{\perp})/3$.

We are interested in the values of dN/dH for two values of θ
i.e. $\theta = 0$ and $\theta = \pi/2$.

For $\theta = 0$, $H = \frac{g_0 H_0}{g_{\parallel}} - \frac{M_I A_{\parallel}}{\beta_0 g_{\parallel}}$ and dN/dH is finite
and for $\theta = \pi/2$, $H = \frac{g_0 H_0}{g_{\perp}} - \frac{M_I A_{\perp}}{\beta_0 g_{\perp}}$
and $dN/dH \rightarrow \infty$

Thus when $\theta = 0$, the absorption starts suddenly and when $\theta = \pi/2$ it becomes theoretically infinite. Obviously the second derivative d^2/dH^2 (dN/dH) has singularity at both $\theta = 0$ and $\theta = \pi/2$ and the derivative spectrum has a weak line at $H(0)$ and a strong line at $H(\pi/2)$.

This theory predicts for copper ions for which $M_I = \pm 1/2, \pm 3/2$, that in the absence of any overlap, four weak derivative lines of different intensity separated by A_{\parallel} should be observed alongwith four strong derivative lines of different intensity separated by A_{\perp} . Thus in all eight lines are predicted.

Estimation of Magnetic Parameters:

Vanngard and Assa [20] discussed in detail the method, to determine different magnetic parameters from the "glass" spectrum of Cu/histidine complex at 77°K.

If four weak lines are obtained in a glass-spectra, g_{\parallel} is calculated corresponding to the magnetic field at the center of them. A_{\parallel} is proportional to the distance between the two consecutive lines in gauss. Thus

$$g_{\parallel} = \frac{2hv}{\beta_0(H_M + H_{-M})} \quad (5.3.8)$$

$$A_{\parallel} = \frac{g_{\parallel}\beta_0(H_M - H_{-M})}{2\hbar M} \text{ sec}^{-1}$$

where H_M is the magnetic field corresponding to line $M = 3/2$ or $1/2$ and H_{-M} is that corresponding to the line $M = -3/2$ or $-1/2$. v is given in Hz.

g_{\parallel} and A_{\parallel} can similarly be obtained from strong lines in higher magnetic field region. Often A_{\perp} is very small compared to the width of the strong lines and hence the spectra are not properly resolved. In such cases A_{\perp} is obtained by correlating glass with solution spectra from the relation

$$a = \frac{A_{\parallel} + 2A_{\perp}}{3} \quad (5.3.9)$$

where a is the average hyperfine splitting constant obtained from solution spectra. Most of the uncertainty in determining magnetic parameters from glass spectra lies in locating the maxima of the broad and weak hyperfine lines.

Estimation of Bonding Parameters :

As we confirm our complexes to be square-planar symmetric with the help of x-ray data for some of the complexes. In the solution or glass state, the structure may get distorted but the distortion from square-planar symmetry, if any is small and one can assume the complexes to be square-planar without sufficient error. This is also supported [21] by the difference of the values of g_{\parallel} and g_{\perp} .

Again the ground state of copper has been confirmed to be $d(x^2 - y^2)$ for our complexes. Thus the molecular orbital theory for a square-planar symmetric complex with a ground state $d_{x^2-y^2}$ can be utilized to calculate the bonding parameters here.

Now once the magnetic parameters g_{\parallel} , g_{\perp} , A_{\parallel} and A_{\perp} are known from glass spectra, one can calculate different bonding parameters α , α' , β_{\parallel} and β_{\perp} .

An approximate formula for α^2 can be obtained as given below.

$$\alpha^2 = \frac{-A_{\parallel}}{P} + g_{\parallel} - 2.0023 + \frac{3}{7}(g_{\perp} - 2.0023) + C \quad (5.3.10)$$

where the constant C lies in the range 0.01 to 0.04 and can be calculated from the expression

$$C = \frac{-8\lambda}{\Delta E_{xy}} (\alpha\alpha' \beta_1^2 S + \alpha\alpha' \beta_1 (1 - \beta_1^2)^{1/2} \frac{T(n)}{2} - \frac{6\lambda}{7\Delta E_{xz}} (\alpha\alpha' \beta^2 S + \alpha\alpha' \beta (1 - \beta^2)^{1/2} \frac{T(n)}{\sqrt{2}}) \quad (5.3.11)$$

Kivelson and Neiman [19] have calculated the values of the overlap integrals S for bonding parameter calculations for the complexes of copper, in which the nearest neighbours are nitrogen and oxygen. The values, for a ligand to metal distance of 1.9 Å are :

	S	π	T(n)
Oxygen	.076	.017	0.220
Nitrogen	.093	.038	0.333

K_0 , the isotropic contact term has been assigned a value 0.43 [23, 24]. ΔE_{xy} and ΔE_{xz} can be obtained from the Optical Absorption spectra for the complexes in aqueous solution. P has been found [19] of the order of $0.036 \text{ cm}^{-1} \cdot \text{Å}$ in the calculations was taken as -828 cm^{-1} .

α^2 calculated from (5.3.10) is further used for the calculation

of α' with the help of equations :

$$\alpha^2 + \alpha'^2 - 2\alpha\alpha' S = 1 \quad (5.3.12)$$

α , α' so calculated are used to obtain the parameters β_1 , and β . It was found [19] that an error of 2 percent in α^2 causes about 1 percent error in β_1^2 . The above method of calculation is well confirmed and has been applied successfully by a number of workers [16, 24-27].

Results and Discussion

The spectra of different samples taken in glass phase are shown in figs. (5.3 - 5.10). The parameters g_{\parallel} , g_{\perp} , A_{\parallel} , and A_{\perp} have been obtained from glass spectra as given below :

(1) ESR Parameters : The spectra of different samples in glass-state indicated that A_{\perp} in all the cases is quite small compared to the linewidth of $\theta = \pi/2$ lines. As a result, a single broad intense line was obtained in every case in place of 4 lines expected from theory. Cu/Glycine spectra showed four lines corresponding to $\theta = 0$ and one corresponding to $\theta = \pi/2$. g_{\parallel} was obtained from the center of these four lines. A_{\parallel} was calculated with the help of equation (5.3.8) in unit of sec^{-1} . Values of A_{\parallel} in cm^{-1} can be obtained by multiplying sec^{-1} values by 5.309×10^{-12} . g_{\perp} was taken at the position $\theta = \pi/2$ line whereas A_{\perp} was calculated with the help of the parameter 'a' from solution study and A_{\perp} found above as in Eq. (5.3.9). The spec-

tra of Cu/DL-Methionine is similar to above where four lines are obtained from $\theta = 0$ and one for $\theta = \pi/2$.

Thus in this case also five lines instead of eight are obtained. But in all the remaining cases except for Cu/DL-Aspartic acid, three lines are observed instead of four corresponding to $\theta = 0$. Interspaces between the lines show that the fourth line is merged with the strong line $\theta = \pi/2$. In this light, g_{\parallel} was calculated from the center of the central two lines and A_{\parallel} from the interspace between them. In Cu/DL-Aspartic acid spectrum, only two lines clearly resolved were obtained for $\theta = 0$. The spectrum was further supported by the same two strong lines observed in solution spectra at room temperature. The spectra for $\theta = 0$ appear more like dips than derivative lines. The minimum ratio of the intensities of $\theta = 0$ to $\theta = \pi/2$ lines has been found to be 1:8 in our spectra. The parameters g_{\parallel} , g_{\perp} , A_{\parallel} , and A_{\perp} thus obtained from glass spectra are given in table 5.(III).

(ii) Covalency : Comparing tables 5.(III) with 5.(I), one finds that g -values for the complexes in glass state are more than their corresponding values in polycrystalline state. The value of inplane-sigma bonding parameter α^2 and in-plane π bonding parameter β_i^2 , are directly proportional to g_{\parallel} and g_{\perp} and inversely to A_{\parallel} . Hence in-plane covalent bonding increases as g_{\parallel} and g_{\perp} decreases and A_{\parallel} increases. This is because, lesser the value of bonding parameters, more is the covalency. In other words, the covalency is directly proportional to $a = \frac{A_{\parallel} + 2A_{\perp}}{3}$ and inversely proportional to $g = \frac{g_{\parallel} + 2g_{\perp}}{3}$. Since the variation

in g_{\parallel} is large from sample to sample and is easily and accurately measurable parameter, it is expected to propagate important information regarding the covalency of the Cu to ligand bonds.

From the above discussion and tables 5.(I) and 5.(III), one infers that, covalency in a polycrystalline sample is more than that of its glass sample. X-ray crystallographic [28] data available on Cu/Glycine and a few others, also support the above inference.

In Cu/Glycine complex, copper is surrounded by four atoms O(1), O(3), N(1) and N(2) in a nearly co-planar arrangement. N(1) has two hydrogen bonds and N(2) has one hydrogen bond with the oxygens of the other molecule. These bonds act as a bridge between the one complex molecule and another. The hydrogen bonds between nitrogens and oxygens cause a change in the distribution of the electron density on the nitrogens in the neighbourhood of copper. In the presence of such a hydrogen bond a large proportion of electron density will be available for overlap of nitrogens of amino group with copper orbital and obviously the covalence would be more in this case than when no hydrogen bond is present. In an aqueous solution, hydrogen bonds do not operate effectively because in this case lattice structure breaks down. This suggests a large covalency in case of polycrystalline samples and hence lower values of g_{\parallel} as compared to g_{\perp} values of 'glass' samples. This is in harmony with the experimental observations made here.

(iii) Bonding parameters : Bonding parameters $\alpha^2, \alpha^2, \beta_1^2$ and β^2 calculated with the help of spin-Hamiltonian parameters and optical data for different complexes are shown in table 5.(IV) α represents inplane sigma bonding β_1 and β -values represent in-plane and out of plane π bonds respectively. Note that when α^2 or β_1^2 or β^2 is equal to 0.5, the respective bonding is covalent and as this value increases to 1, covalent nature tends to be ionic. Bonding is fairly covalent in most of the cases studied here. The values of the bonding coefficients are of the same order as given by many workers in case of copper complexes of similar nature [19]. In most of the cases β^2 is more than β_1^2 , and this suggests that the bonding of the central ion of the ligands is reasonably covalent and occurs principally in the molecular plane because out of plane π bonding is relatively ionic. Molecular weight of the complex and hence, the ligand atoms except for the nearest neighbours seem to be little affecting the bonding parameters. The fairly covalent nature of most of the compounds is also in agreement with the result from optical data. The ratio of excitation energies is slightly more than 1 and thus valency is fairly covalent according to Kivelson and Neiman [19].

5.4 SOLUTION STUDY OF THE SAMPLES

The electron spin resonance linewidth study on paramagnetic molecules in solution has been done extensively [29-34]. Very interesting developments in the theory were done by famous papers of

Kivelson et al. [35-37], followed by experimental papers, which helped the theory to prove its worth [38]. It was found that in the absence of paramagnetic impurities and oxygen, intermolecular paramagnetic interactions were negligible in dilute solutions. The linewidth was found to be due to the contributions of anisotropic g and nuclear hyperfine tensors as a result of motional modulation, but the experimental linewidth could only be explained after the idea of 'residual linewidth' was introduced i.e. the linewidth unexplained by above interactions. This 'residual linewidth' is independent of applied magnetic field and magnetic quantum number M. Again it is independent of dipole-dipole and exchange interactions as it does not depend significantly on concentrations. Out of many suggestions to explain, an idea analogous to electric field fluctuation mechanisms in solids [39-41] was applied in case of liquids so that the liquid fluctuations in solution replace the lattice vibrations in solids. The results proved negative, only one of the mechanisms viz. Orbach mechanism proved a bit useful.

The residual linewidth was further analyzed in terms of Hubbard Theory [42] of spin-rotational spin relaxation. This theory best applies to large molecules with strong intermolecular anisotropic interactions with their neighbouring solvent molecules. This was tried on two molecules vanadyl acetylacetone and copper acetylacetone in different solutions. It was found that the theory of anisotropic nuclear electronic magnetic dipolar and g tensor interactions along with the theory of spin-rotational relaxation are able to explain most of the

experimental results, the first two at lower temperatures and the latter at higher temperatures.

In order to see, to what extent these theories are able to explain the results of studies of copper complexes with amino acids in aqueous solutions, the present study was undertaken. These complexes have been found to have a square planar structure [43,44] similar to the acetylacetones, and therefore the theory as such can be applied in our complexes. The spin-Hamiltonian parameters needed for calculation were obtained from the glass-study of the complexes as described previously. Most of the complexes studied could not be dissolved in non-aqueous solvents.

The freshly prepared aqueous solutions in double distilled water were taken in sample tubes which in this case were specially prepared pyrex-capillary tubes, otherwise it was found nearly impossible to tune the cavity because of highly lossy nature of water. Aqueous solutions were properly degassed by heating in a tube before they were filled in capillary tubes as to avoid the possible broadening of ESR lines by dissolved oxygen gas. Solutions of Cu/DL-Methionine and Cu/DL-Aspartic acid were prepared in mild Ammonia solution and pyridine respectively. Since we are little interested in broadening caused because of spin-spin and exchange interactions, the concentration of the solutions were reduced till a further dilution does not affect the linewidths of the lines. A concentration well below this critical dilution was chosen for our studies. The order of dilu-

tion was kept .003 m/litre. Klystron was adjusted to a power much below the saturation stage. The magnetic field sweep was adjusted to give a slow variation of the field so as to get a true lineshape of the curve. The modulation amplitude was also adjusted for the same purpose. 1-1-diphenyl-2-picryl hydrazyl (DPPH) was used as a standard field marker which gave a sharp line at 3410 Gauss, measured with the help of varian F-8A flux meter.

Results :

The x-band derivative curves of the complexes in solution are shown in figs. (5.3 - 5.10). In most of the cases, four hyperfine lines corresponding to the nuclear spin $I = 3/2$ for copper were observed. Cu/DL-Aspartic acid gave two strong and two weak lines whereas for Cu/DL-valine and Cu/L-Asparagine solutions, five lines were observed in each case. The fifth line was a bit less resolved. This is proposed as an overlapping of three lines each of ^{63}Cu and ^{65}Cu paramagnetic ions. This is further supported by the fact that the first and the fifth lines in these spectra are much less intense than the central three lines.

The separation of the lines is found to be nearly equal. The individual hyperfine lines are not completely symmetric and are also not exactly Lorentzian. The spectral line is assumed to be represented by the following equation [35].

$$\omega_0 = g_0 \beta_0 H / \hbar + aM + \frac{1}{2} \hbar a^2 [I(I+1) - M^2] / g_0 \beta_0 H \quad (5.4.1)$$

where ω_0 is the microwave frequency in rad/sec., M is the Z-component of nuclear spin $I=3/2$, 'a' is the isotropic hyperfine splitting constant in radian sec⁻¹ and g_0 is the isotropic g-value. The parameters g_0 and a were obtained from solution spectra. The expressions are :

$$g_0 = g_D + 2g_D \frac{H_D - 1/2 (H_M + H_{-M})}{(H_M + H_{-M})} - \frac{2a^2 \hbar^2 (\frac{15}{4} - M^2)}{g_D \beta_0^2 (H_M + H_{-M})^2} \quad (5.4.2)$$

$$a = \frac{g_0 \beta_0}{2M\hbar} (H_M - H_{-M}) \quad (5.4.3)$$

where H_M is the magnetic field at the line corresponding to $+M$ and H_{-M} is the magnetic field at the line corresponding to $-M$. g_D and H_D are the g-value and magnetic field values corresponding to the standard substance, DPPH. Two values of g_0 and a are obtained from two pairs $(3/2, -3/2)$ and $(1/2, -1/2)$ and are averaged. Better results can be obtained by iterative procedure. The value of g_0 and a are an average of four runs of the spectra. The data so obtained on g_0 and a are given in table 5.(V).

The absolute sign of a , A_1 and A_1 was not determined from our data but the theoretical equation (5.4.1) suggests that if $M = -3/2$ line is supposed to be at a lower field than $M = 3/2$, 'a' should be

negative. The relative signs of all other parameters can then be determined. It was seen that a positive value of 'a' was quite convenient for our calculations and the error in interpretation and application of the theory caused due to this was insignificant. This is because the experimental values of the important linewidth parameter β comes out to be positive and the theoretical values of β can be positive only when a is positive. The peak to peak widths of first derivative of each hyperfine line of all the complexes have been measured and are given in table 5.(VII).

Linewidth Calculations

The linewidths calculated with the help of equations (5.4.4a - 5.4.4f), account for the contributions to linewidth due to the modulation of the anisotropic g-tensor and the hyperfine tensor only. But the calculations do not give results near to the experimental linewidths and a factor α' was introduced to the equation (5.4.4b) to account for the effects on linewidths caused due to unspecified mechanisms, out of which spin-rotational relaxation mechanism is most important in our case. The equation (5.4.4b) then changes to following eq.

$$\Delta H = (2/\sqrt{3}) T_2^{-1} (\hbar/g\beta_0) \quad (5.4.4a)$$

$$T_2^{-1} = \alpha + \beta M + \gamma M^2 + \delta M^3 \quad (5.4.4b)$$

$$\frac{\alpha}{\tau_R} = \frac{1}{45} [(\Delta\gamma H_0)^2 + 3(\delta r H_0)^2](4+3u) + \frac{1}{40} b^2 I(I+1)$$

$$(3+7u) + \frac{2}{15} C^2 I(I+1)(3+7u) - \frac{1}{8} b^2 I(I+1)$$

$$(a/\omega_0)u.f - \frac{1}{30} \Delta\gamma H_0 b I(I+1)(a/\omega_0)(1+u) \quad (5.4.4c)$$

$$\frac{\beta}{\tau_R} = \frac{1}{15} (b + \Delta\gamma H_0 + 4C\delta r H_0)(4+3u) - \frac{2}{45} (\Delta\gamma H_0)^2$$

$$(4+3u+3uf)(a/\omega_0) - \frac{1}{20} b^2 I(I+1)(a/\omega_0)(4+3u+7uf)$$

$$+ \frac{1}{40} b^2 (a/\omega_0)(3+2u)[2I(I+1)-1] \quad (5.4.4d)$$

$$\frac{\gamma}{\tau_R} = \frac{b^2}{40} (5-u) + \frac{2}{15} C^2 (5-u) + \frac{1}{8} b^2 (a/\omega_0) u.f$$

$$- \frac{1}{30} (\Delta\gamma b H_0)(a/\omega_0) (7+5u+12uf) \quad (5.4.4e)$$

$$\frac{\delta}{\tau_R} = \frac{1}{20} b^2 (a/\omega_0)(1+u+uf) \quad (5.4.4f)$$

$$\Delta H = (\alpha + \alpha') + \beta M + \gamma M^2 + \delta_M^3 \quad (5.4.4g)$$

The linewidth is obtained directly in terms of gauss if the parameters obtained from equations (5.4.4c - 5.4.4f) are changed from sec^{-1} to gauss after multiplying $2\hbar/\sqrt{3} g_0 \beta_0$, if the lines are assumed to be Lorentzian. The contribution to α' due to spin rotational relaxation mechanism can be calculated from the following expression [36] in gauss :

$$\alpha_{RS} = \frac{2\hbar}{\sqrt{3} g_0 \beta_0} \frac{1}{12\pi r^3} \frac{(\Delta g_{||}^2 + 2\Delta g_{\perp}^2)kT}{\eta} \quad (5.4.5)$$

Where $\Delta g_{||} = g_{||} - 2.0023$

$$\Delta g_{\perp} = g_{\perp} - 2.0023$$

The calculated values are shown in table 5.(VI). Experimental values of $(\alpha + \alpha')$, β , γ and δ were found by solving simultaneously, four equations for each complex after substituting the linewidth of each hyperfine line. The experimental value of α' is then obtained by subtracting the calculated α from the experimental $(\alpha + \alpha')$. The linewidth parameters $\alpha, \alpha', \beta, \gamma$ and δ both calculated theoretically as well as obtained from experimental data are shown in table 5.(VI).

The various magnetic parameters required for above calculations were obtained from the combination of glass and solution spectra in each case. $A_{||}$ was obtained from glass spectra, 'a' from solution spectra and A_{\perp} from the formula

$$3a = A_{||} + 2A_{\perp} \quad (5.4.6)$$

The combination of the solution parameter with glass parameter has been done with the assumption that a negligible variation of the parameters take place with temperature, and this is apparent from a small difference in g-values obtained from studies of solutions at two temperatures -80 °C and 27°C. Different required magnetic pa-

rameters used for calculation are given in table 5.(III). The viscosity data for water was obtained from literature [45].

The only adjustable parameter in the calculations is r , the molecular hydrodynamical radius and was adjusted so as to get best agreement between experimental and calculated values of parameters β and γ . The values of r thus adjusted in each case are shown in table 5.(VII). It varies from 2.1 \AA^0 to 2.9 \AA^0 in our complexes. The moment of inertia of Cu/Glycine complex along the symmetry axis and passing through the copper-nucleus has been calculated [26] equal to $1103.56 \times 10^{-16} \text{ a.m.u. cm}^2$ by taking the bond distance from crystal structure data [46]. The value of moment of inertia thus obtained gives the radius of an equivalent sphere to be 3.334 \AA^0 . The value 2.508 \AA^0 used here for this complex then does not seem to be too low, in the light of the uncertainties associated with the determination of magnetic parameters, from glass and the approximations in applying equation (5.4.4b)

The value of r was found to be 3.357 \AA^0 in Cu-acetylacetone in toluene [38]. Acetylacetone molecule being much bigger than Glycine, and thus a smaller value of r for Cu/Glycine is reasonable. Further it is noticed that the value of r roughly increases with the increase in molecular weight of the complex.

The unexact variation of r with molecular weight might be due to the variation of covalency in-the compounds which results in contracting the bond distances. Thus the moment of inertia does not remain proportional

to the increase in mass and consequently gives a smaller value of the radius of the equivalent sphere. The peak to peak width of each hyperfine line derivative of all the complexes have been calculated with the help of expression 5.4.4.g.linewidth parameters $\alpha, \alpha', \beta, \gamma$ and δ given in table 5.(VI). The theoretically computed values of linewidth alongwith experimentally measured are given in table 5.(VII)

Kivelson [37] gave expressions for three important mechanisms which contribute to experimental linewidths. The molecular parameters required for the estimation of these contributions have not been determined very accurately. Upto first decimal accuracy, the parameters found in our complexes are nearly the same as given by Kivelson for $\text{Cu}(\text{H}_2\text{O})_6^{++}$, as mentioned below

$$\frac{\lambda}{\Delta} = 0.1, \frac{\phi' q_0}{\Delta r_0} = 0.2, \frac{\delta_{on}}{\Delta} = 0.1 \quad (5.4.7)$$

and

$$\frac{\hbar \delta_{on}}{kT} = 4$$

where λ/Δ is obtained roughly from the expression $g - 2.0023 \approx \lambda/\Delta$. The order of $\phi' q_0 / \Delta r_0$ has been obtained from solvent induced shifts in the visible spectra.

$$\text{Also } \phi' = \sum_i |(\partial V_{\text{crys}} / \partial q_i) / r_0| \quad (5.4.8)$$

q_0 = the root mean square values of q_i , which is the amplitude of intemolecular oscillations.

r_0 = intermolecular distance

τ_c = correlation time, different from the reorientation correlation time τ_R .

$\frac{\delta_{\text{on}}}{\Delta}$ was estimated from absorption spectra.

For $\tau_c \approx 10^{-12} \text{ sec}$ and $\omega_e \approx 6 \times 10^{10} \text{ sec}^{-1}$

The contributions from different mechanisms to the linewidth in terms of Gauss are

Van Vleck direct = 3

Van Vleck-Raman = 27

Orbach = 526

Unexplained experi-

mental hyperfin extreme

linewidth in case

of Cu/ β -Alamine = 222

The above results show that these processes are inadequate to account for the experimental linewidth unexplained by other mechanisms. Only Orbach process gives some hopeful results in the cases where it is applicable.

Discussion

It is seen from table 5.(VII) that the linewidths of the 4 lines in each case vary with $M = \pm 3/2, \pm 1/2$. In most cases the $\pm 3/2$ lines are found to be broader than $\pm 1/2$ lines. Linewidth parameter calculation from these lines give positive β values and for β to be positive, a positive nuclear-hyperfine splitting constant 'a' was considered. It is seen in table 5.(VI) that the magnitudes of calculated parameters α and β are quite comparable and a large residual linewidth α' is left unexplained. This is because, the first terms in the expression of α and β are quite significant for their magnitudes and come out nearly of the same order in our complexes. Fortunately the linewidth contribution α_{RS} due to spin-rotational relaxation mechanism is not less than α' but is sufficiently more. This might be, because the Hubbard theory which is the basis of calculation of α_{RS} best applies to bigger molecules where intermolecular anisotropic interactions are more with solvent molecules. Deviation of calculated linewidths from the experiment is more in extreme lines and rather in one of the extreme lines. One of the reasons can be that the theory does not give β and γ of different signs. Both could be positive or negative depending upon the sign of 'a'.

The hydrodynamical radius r is found to be very important in adjusting the magnitudes of the linewidth parameters, but does not significantly affect their ratio. This is because the cube power of r is involved in τ_R , which multiplies the right hand side of the expressions (5.4.4C - 5.4.4f)

In two of cases, e.g. Cu/DL-valine and Cu/L-Asparagine, five hyperfine lines have been observed. The fifth line is not very clearly resolved. The calculations were done for the first four lines in each case.

From above, it can be said that the agreement between theory and experiment is not as good as was found in case of Vanadyl and Copper acetylacetones in chloroform by Kivelson [38]. This is also because the theory holds best for small values of $|b/\omega_0|$ and $|\frac{\Delta\gamma}{\gamma}|$. Our value of $|b/\omega_0|$ is 0.03 compared to 0.007 for Vanadyl acetylacetone and 0.01 for copper acetylacetone and similarly for $|\frac{\Delta\gamma}{\gamma}|$ values.

From the present knowledge, one can say that the unexplained linewidths can be ascribed to spin-rotational relaxation mechanism or Orbach process. The Van Vleck direct and Van Vleck -Raman processes can be overlooked. But for complete explanation of linewidth an exhaustive study of the subject is still needed

5.5 CONCLUSION

It can be concluded from a study of powder samples that even when the points of inflexion on the derivative curves of copper complexes are not five, a rough estimation of g_1 and g_1 . can be made from positions of the peaks at a lower and higher magnetic field sides respectively. The absence of at least two points of inflexion out of

five may be assumed to be submerged with the derivative peak. This argument gets justification from a look at tables 5.(I) and 5.(III) for g_{\parallel} and g_{\perp} of Cu/L-Cystine and Cu/DL-Aspartic acid Lineshape of all the lines is Lorentzian. An increase in linewidth of all the complexes compared to parent compound has been ascribed to a decrease in exchange due to complexation. In plane bonding in these complexes are fairly covalent as compared to the out of plane π bonding which has been found to be more ionic. Linewidth calculations show that a better fit with the experimental results can be obtained by accepting the contributions of the significant mechanisms like spin-rotational relaxation, Orbach and Van Vleck-Raman relaxations.

TABLE 5.1 ESR Parameters obtained from polycrystalline sample study.

Sample	g_{\parallel}	g_{\perp}	Δg	g	Line with ΔH_{pp} cersted
Cu/Glycine	2.2153	2.0641	.01512	2.1145	223.68
Cu/ β -Alanine	$g_3 =$ 2.2203	$g_2 = 2.1015$	$g_1 =$ 2.0637	2.1285	230.26
Cu/DL-Methionine	2.1972	2.456	0.1516	2.0961	230.13
Cu/DL-Valine	2.1969	2.0415	0.1554	2.0933	245.90
Cu/L-Cystine	2.1689	2.0662	0.1027	2.1004	152.32
Cu/L-Glutamic acid	2.2028	2.0904	0.1124	2.1279	136.56
Cu/DL-Aspartic acid	2.1793	2.1143	0.0650	2.1360	90.16
Cu/L-Asparagine	2.2636	2.0538	0.2098	2.1237	308.34

TABLE 5.(II) Computed values of linewidth, dipolar width and exchange frequencies by using different theories of ESR linewidth.

Sample	Van Vleck's Theory		Anderson Theory		Kubo and Tomita Theory	
	$(\Delta H_{1/2})^*_{\text{exp}}$ (Gauss)	$(\Delta H_{1/2})_{\text{cal}}$ (Gauss)	$\omega_p^2 \times 10^{-8}$ (rad ² . sec ⁻²)	$\omega_e \times 10^{-9}$ (rad. sec ⁻¹)	$\omega_{10}^2 \times 10^{-18}$ (rad ² . sec ⁻²)	$\omega_{20} \times 10^{-9}$ (rad. sec ⁻¹)
CuCl ₂ .2H ₂ O	74.65	696.17	44.85	34.18	31.95	101.77
Cu/Glycine	193.71	347.48	10.77	3.16	7.67	9.42
Cu/β-Alanine	199.41	252.90	5.81	1.66	4.14	4.94
Cu/DL-Methionine	199.29	327.36	9.62	2.25	6.86	8.18
Cu/DL-Valine	212.95	220.96	4.26	1.14	3.04	3.39
Cu/L-Cystine	131.91	172.24	2.62	1.13	1.86	3.36
Cu/L-Glutamic acid	118.26	396.30	13.92	6.70	9.92	19.95
Cu/DL-Aspartic acid	78.08	333.68	10.03	7.31	7.14	21.75
Cu/L-Asparagine	267.02	286.22	7.36	1.57	5.24	4.67

* $\Delta H_{1/2}$ = Half width at half power points = $\sqrt{2} \Delta H_{pp} / 2$ (For Lorentzian shape).

TABLE 5.(III) The parameters obtained from glass and solution studies ($\eta = 0.01002$ poise,
 $T = 300^{\circ}\text{K}$, $\nu = 9.5$ KHz) used for the linewidth calculation studies.

Sample	g_{\parallel}	g_{\perp}	Δg	g	^a (10^9 sec $^{-1}$)	A_{\parallel} (10^9 sec $^{-1}$)	A_{\perp} (10^9 sec $^{-1}$)	^b (10^9 sec $^{-1}$)
Cu/Glycine	2.289	2.079	0.210	2.1490	1.224	3.133	0.2694	1.9091
Cu/ β -Alanine	2.344	2.115	0.229	2.1913	0.932	2.870	0.0358	1.9392
Cu/DL-Methionine	2.233	2.059	0.174	2.1170	1.322	3.402	0.2826	2.0796
Cu/DL-Valine	2.316	2.065	0.251	2.1487	1.251	3.007	0.3842	1.7484
Cu/L-Cystine	2.232	2.042	0.190	2.1053	-	3.300	-	-
Cu/L-Glutamic acid	2.327	2.092	0.235	2.1703	1.063	3.103	0.0414	2.0411
Cu/DL-Aspartic acid	2.384	2.107	0.277	2.1993	1.418	3.684	0.2850	2.2660
Cu/L-Asparagine	2.305	2.076	0.229	2.1523	1.260	2.906	0.3975	1.6723

TABLE 5.(IV) Chemical Bonding parameters from glass studies.

Complex	α^2	α'	β_1^2	β^2
Cu/Glycine	0.8250	0.2428	0.6866	0.9114
Cu/ β -Alanine	0.8533	0.2111	~1	~1
Cu/DL-Methionine	0.7967	0.2743	0.7909	0.8708
Cu/DL-Valine	0.8240	0.2440	0.9300	0.8433
Cu/L-Cystine	0.7733	0.2999	0.8072	0.6691
Cu/L-Glutamic acid	0.8608	0.2027	0.8688	~1
Cu/DL-Aspartic acid	~1	0.0231	0.9453	~1
Cu/L-Asparagine	0.8028	0.2675	0.8943	0.9707

TABLE 5.(V) g and a Parameters from solution study.

Sample	g_o	a (10^2 cm^{-1})
Cu/Glycine	2.1236	0.650
Cu/ β -Alanine	2.1259	0.495
Cu/DL-Methionine	2.1155	0.702
Cu/DL-Valine	2.1133	0.668
Cu/L-Cystine	2.1482	-
Cu/L-Glutamic acid	2.1485	0.564
Cu/DL-Aspartic acid	2.1210	0.803
Cu/L-Asparagine	2.1216	0.655

TABLE 5.(VI) ESR Line width parameters for different complexes.

Samples	Experimental Parameters						Calculated Parameters			τ_R 10^{-11} Sec	α_{RS} gauss
	Gauss			Gauss							
α	β	γ	δ	α	α'	β	γ	δ			
Cu/Glycine	33.610	3.517	2.820	-1.866	5.447	28.133	3.289	0.266	0.0056	1.600	39.88
Cu/ β -Alanine	29.504	3.350	2.845	-1.200	5.979	23.524	3.598	0.291	0.0044	1.628	58.13
Cu/DL-Methionine	38.038	3.672	3.586	1.707	5.720	32.317	3.770	0.472	0.0089	2.127	19.33
Cu/DL-Valine	33.810	5.329	-0.820	-1.640	9.161	24.649	5.048	0.367	0.0066	2.591	27.86
Cu/L-Glutamic acid	33.456	2.032	1.523	0.274	4.405	29.051	2.560	1.666	0.0035	0.929	88.00
Cu/DL-Aspartic acid	33.656	3.106	1.799	-1.866	6.047	27.608	3.414	0.195	0.0061	1.007	110.00
Cu/L-Asparagine	30.087	4.680	-0.479	-1.932	7.321	22.765	4.126	0.306	0.0058	2.377	29.20

TABLE 5.(VII) Experimental and calculated linewidths of hyperfine lines.

Sample	M	He experimental Linewidth Gauss	Hc calculated Linewidth Gauss	He-Hc	r Hydro- dynamical radius
Cu/Glycine	3/2	38.93	38.60	0.33	2.508 Å
	1/2	35.84	34.76	1.08	
	-1/2	32.79	31.47	1.32	
	-3/2	40.98	28.69	12.29	
Cu/β-Alanine	3/2	36.88	35.57	1.31	2.523 Å
	1/2	31.74	31.38	0.36	
	-1/2	28.69	27.78	0.91	
	-3/2	34.93	24.75	10.18	
Cu/DL-Methionine	3/2	57.38	44.79	12.59	2.758 Å
	1/2	40.98	40.04	0.94	
	-1/2	36.88	36.27	0.61	
	-3/2	34.84	33.15	1.69	
Cu/DL-Valine	3/2	34.43	42.23	-7.80	2.945 Å
	1/2	36.07	36.43	-0.36	
	-1/2	31.15	31.38	-0.23	
	-3/2	29.51	27.04	2.47	
Cu/L-Glutamic acid	3/2	37.71	37.68	0.03	2.092 Å
	1/2	34.89	34.78	0.11	
	-1/2	32.79	32.22	0.57	
	-3/2	36.06	30.00	6.06	
Cu/DL-Aspartic acid	3/2	36.07	39.24	-3.17	2.150 Å
	1/2	35.43	35.41	0.02	
	-1/2	32.79	32.00	0.79	
	-3/2	39.34	28.95	10.39	
Cu/L-Asparagine	3/2	29.51	36.98	-7.47	2.863 Å
	1/2	32.07	32.23	-0.16	
	-1/2	27.87	28.10	-0.23	
	-3/2	28.51	24.57	3.94	

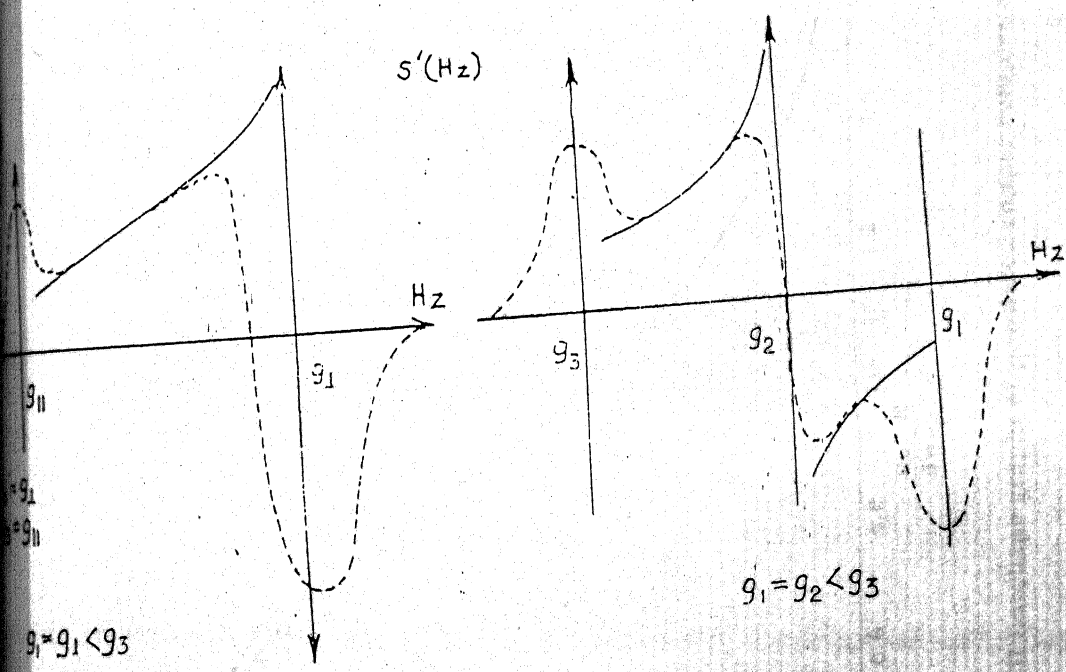


Fig 5.1 The derivative of the shape function $S(Hz)$ Vs Magnetic field Hz .
The continuous lines represent ideal curves and the broken ones are an approach to the real shape.

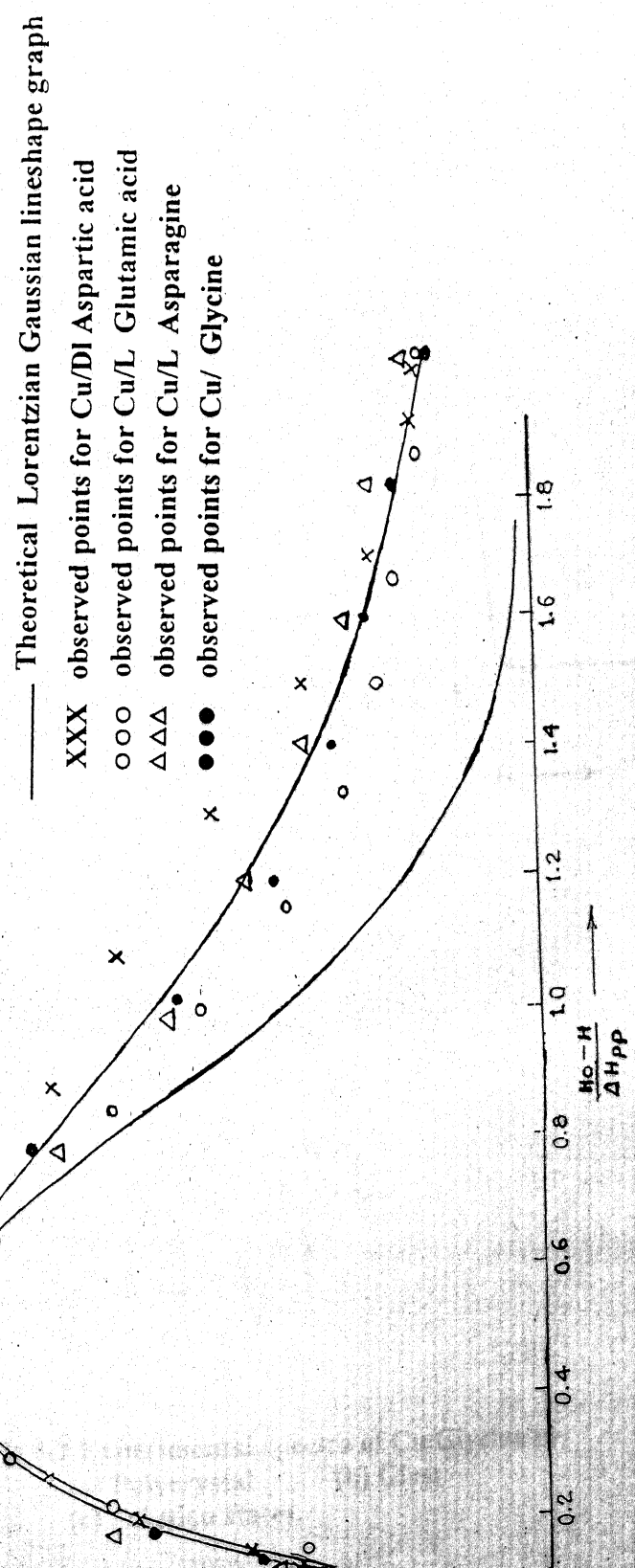


Fig 5.2 ESR lineshape graphs of powdered copper complex at room temperature.

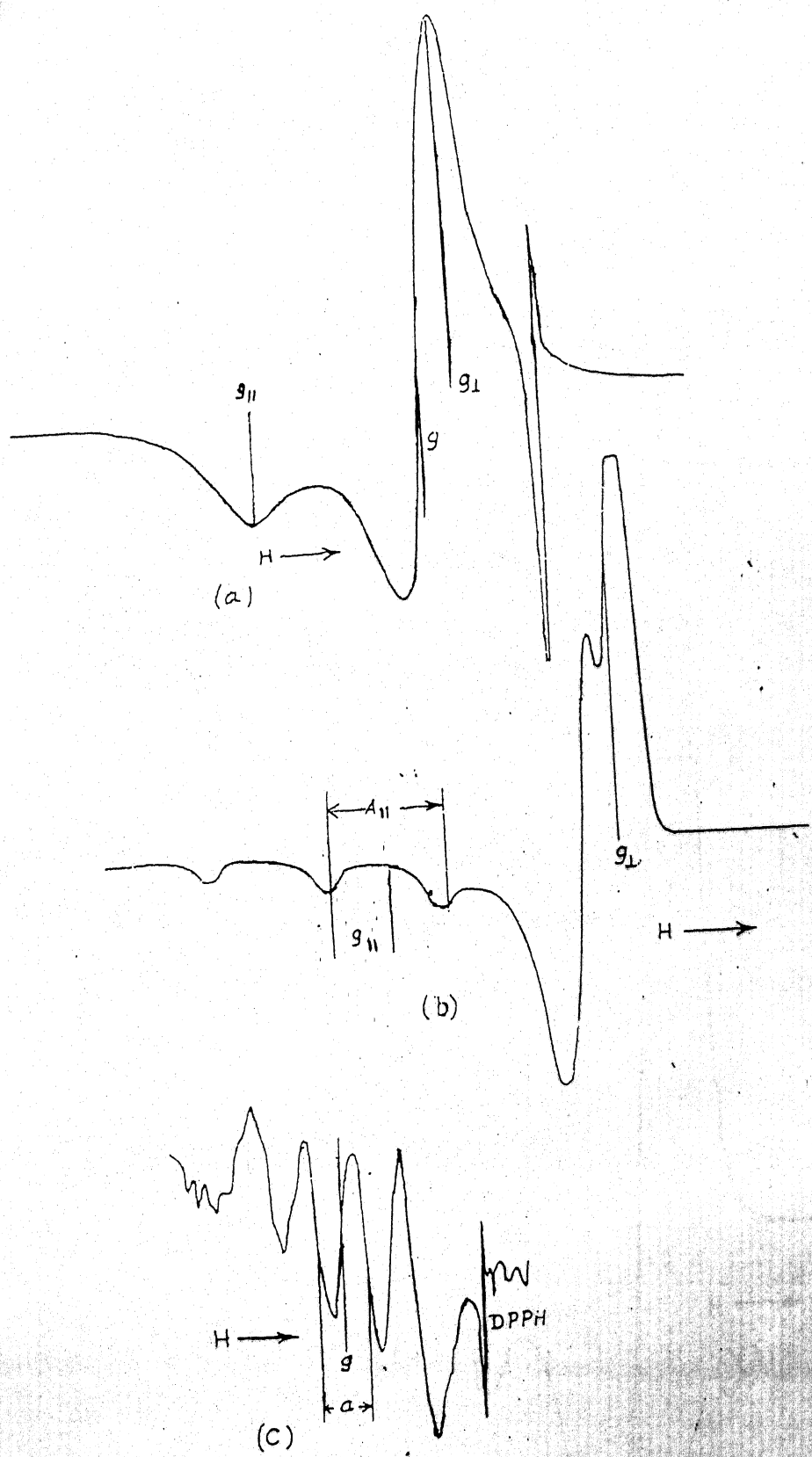
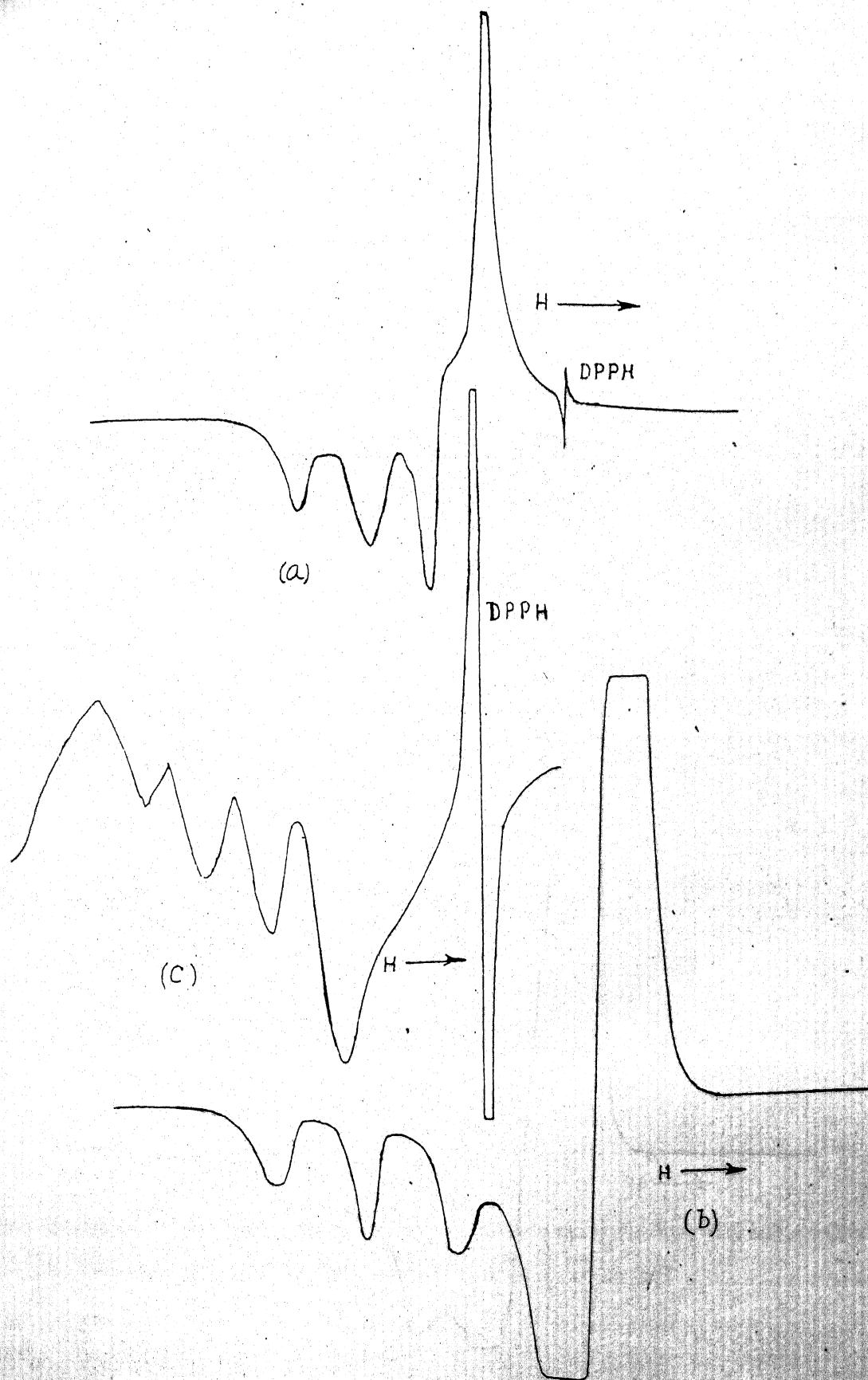


Fig 5.3 Experimental spectra of Cu/Glycine in
 (a) Polycrystal (b) Glass
 (c) Solution states.



**Fig 5.4 Experimental ESR of Cu/ β -Alanine in
(a) Polycrystalline (b) Glass (c) Solution states.**

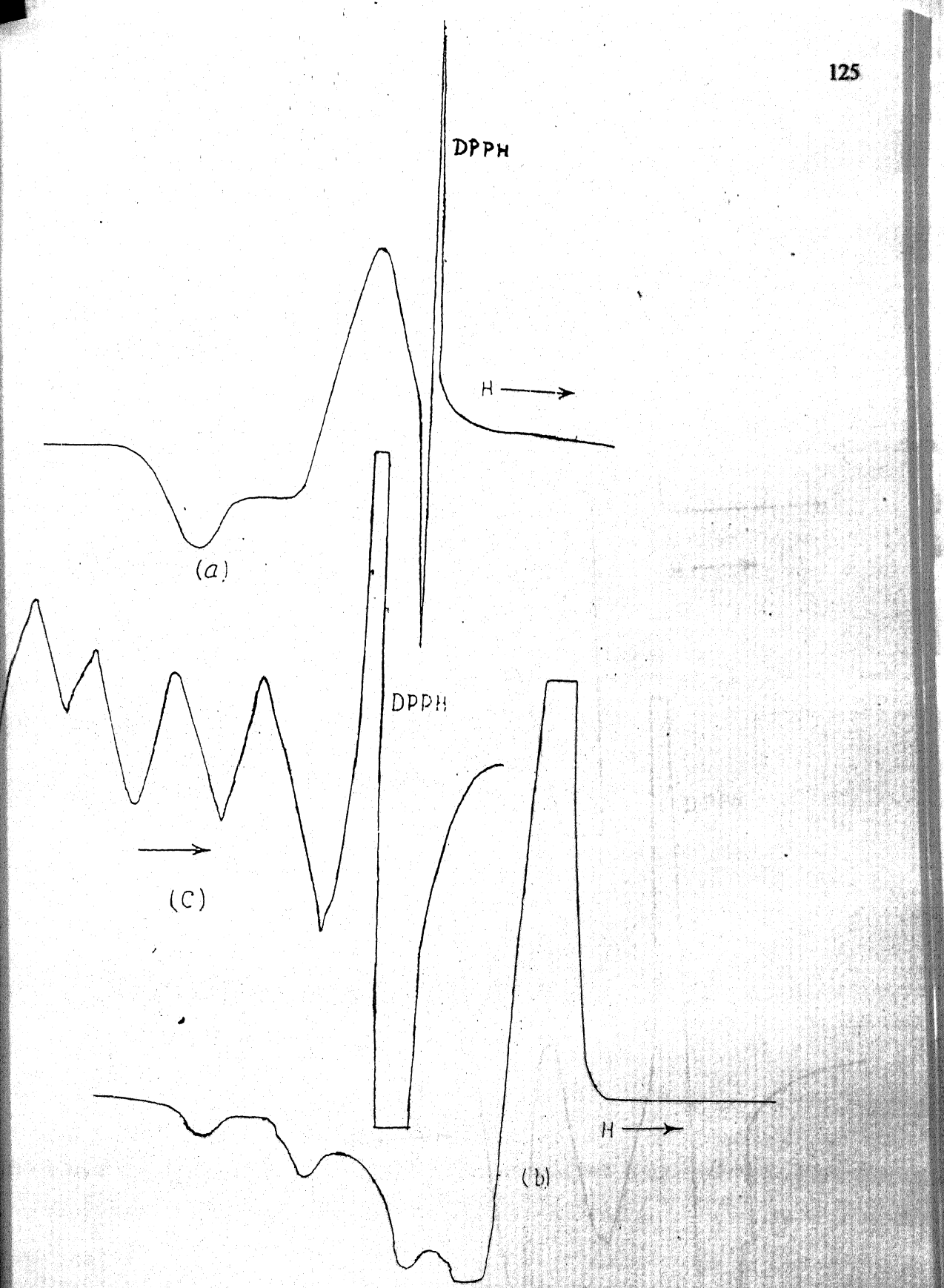


Fig 5.5 Experimental ESR spectra of Cu/DL- Methionine in
(a) Polycrystalline (b) Glass states (c) Solution states.

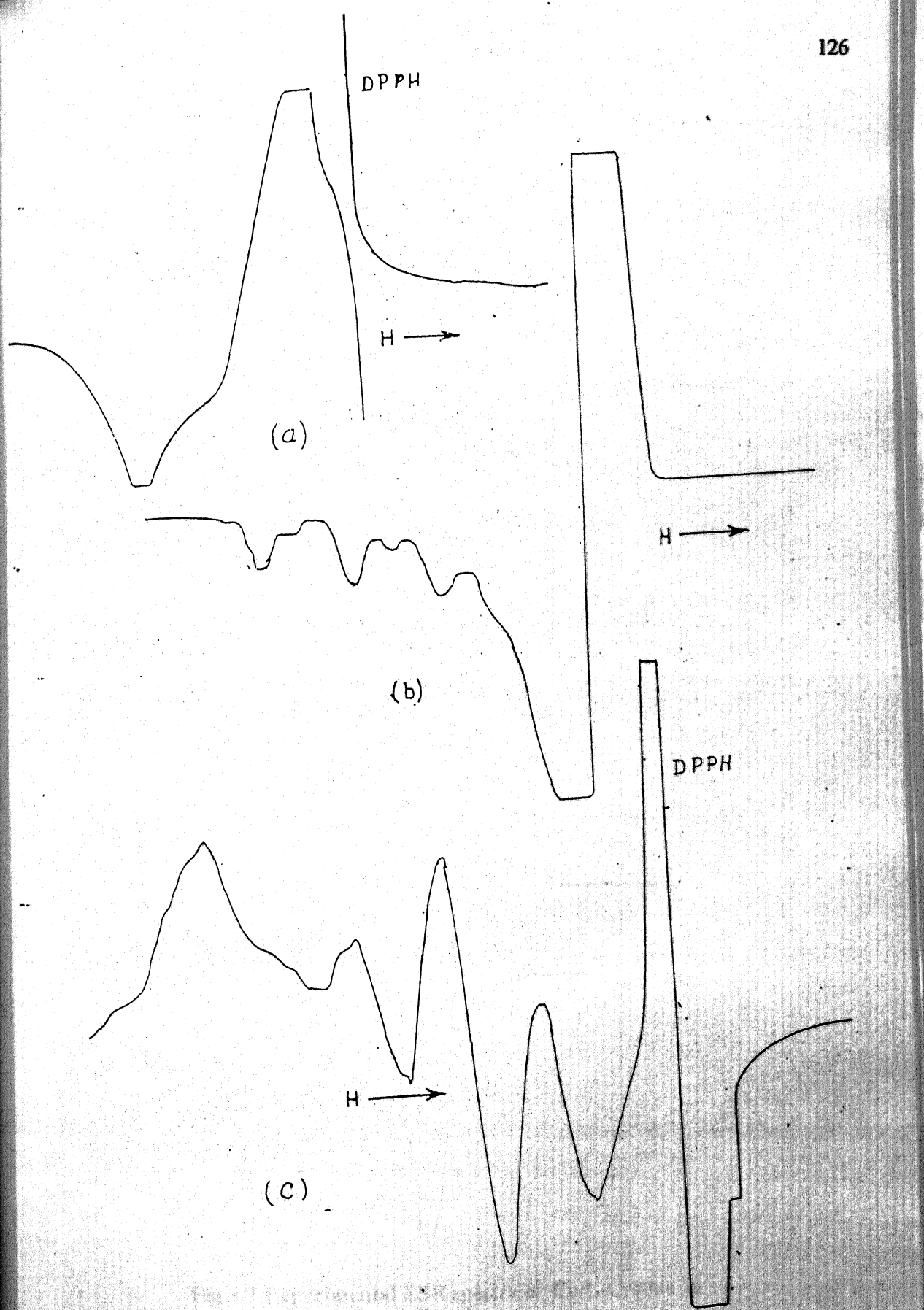


Fig 5.6 Experimental ESR spectra of Cu/DL-Valine in
(a) Polycrystalline (b) Glass states (c) Solution states.

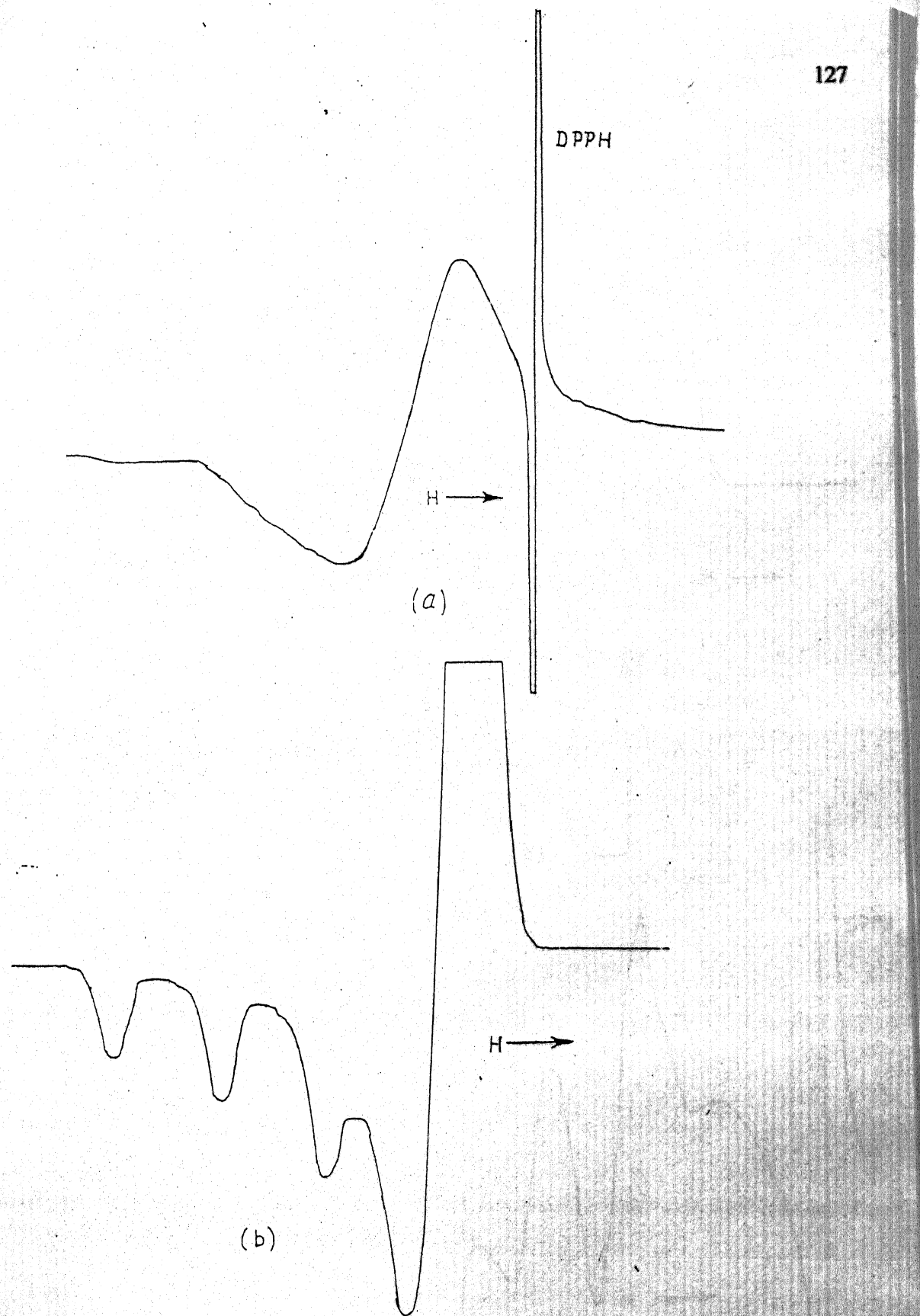


Fig 5.7 Experimental ESR spectra of Cu/L-Cystine in
(a) Polycrystalline (b) Glass states

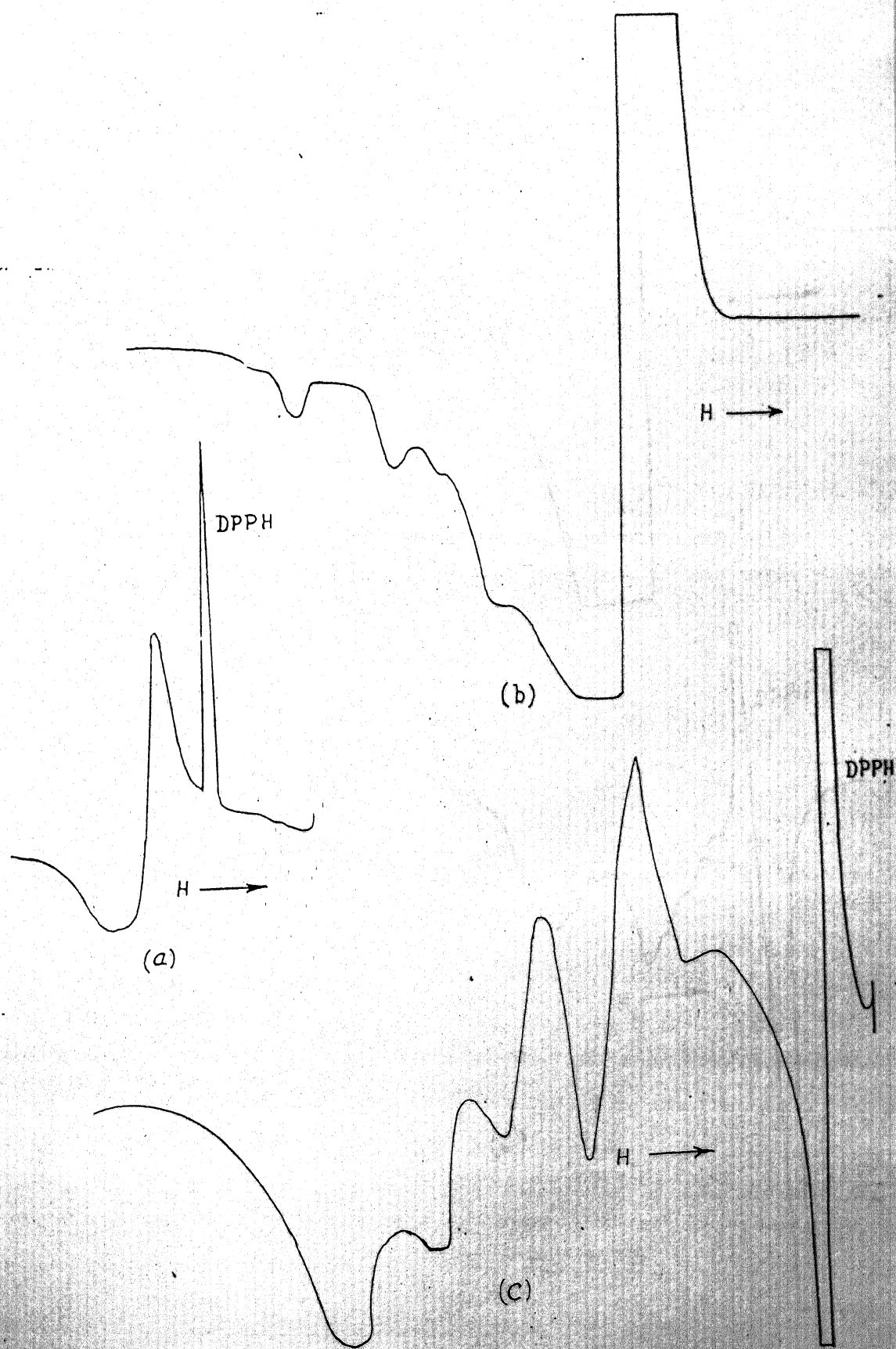


Fig 5.8 Experimental ESR spectra of Cu/L-Glutamic acid in
(a) Polycrystalline (b) Glass states (c) Solution states.

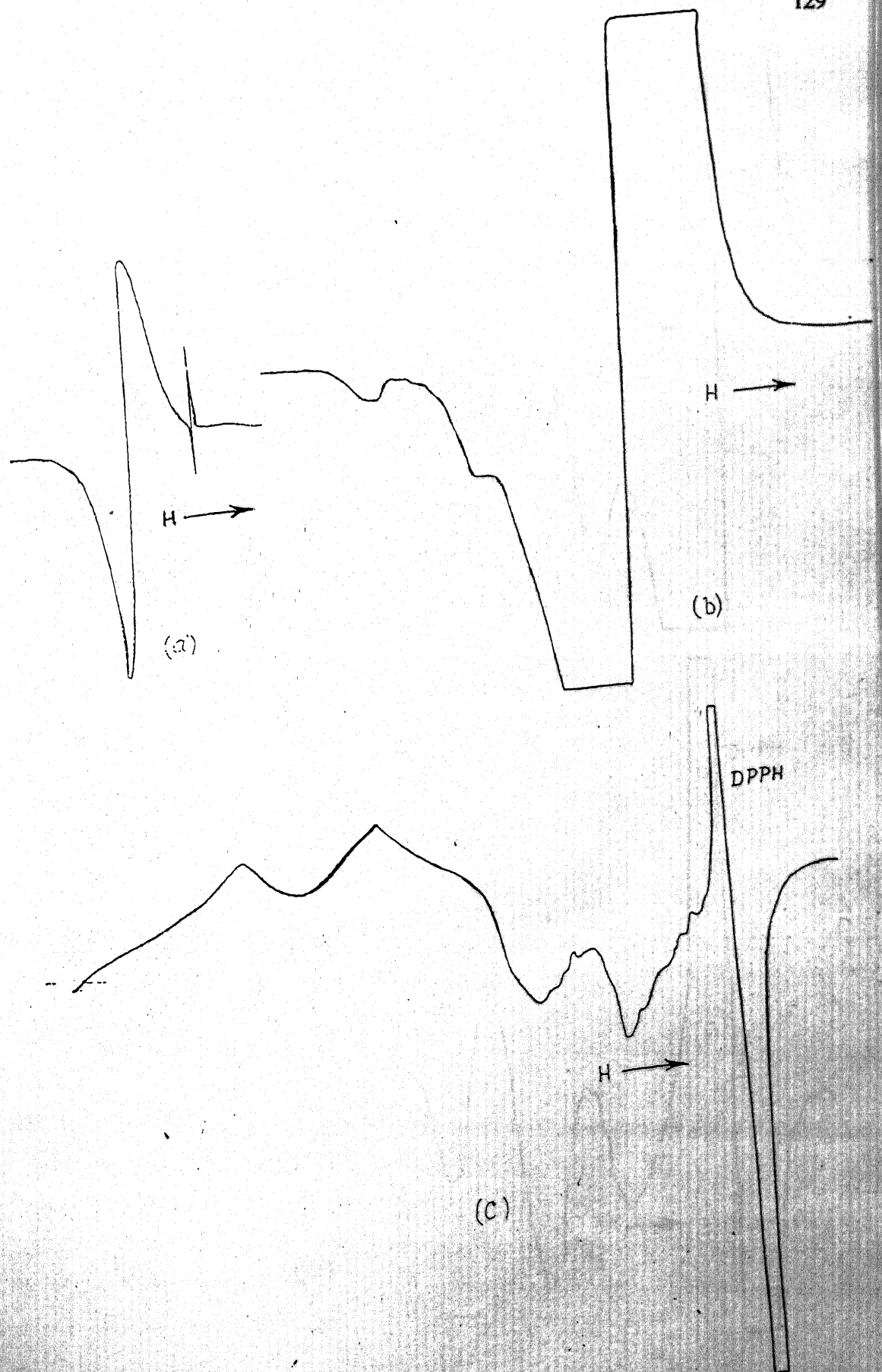


Fig 5.9 Experimental ESR spectra of Cu/DL-Aspartic acid in
(a) Polycrystalline (b) Glass states (c) Solution states.

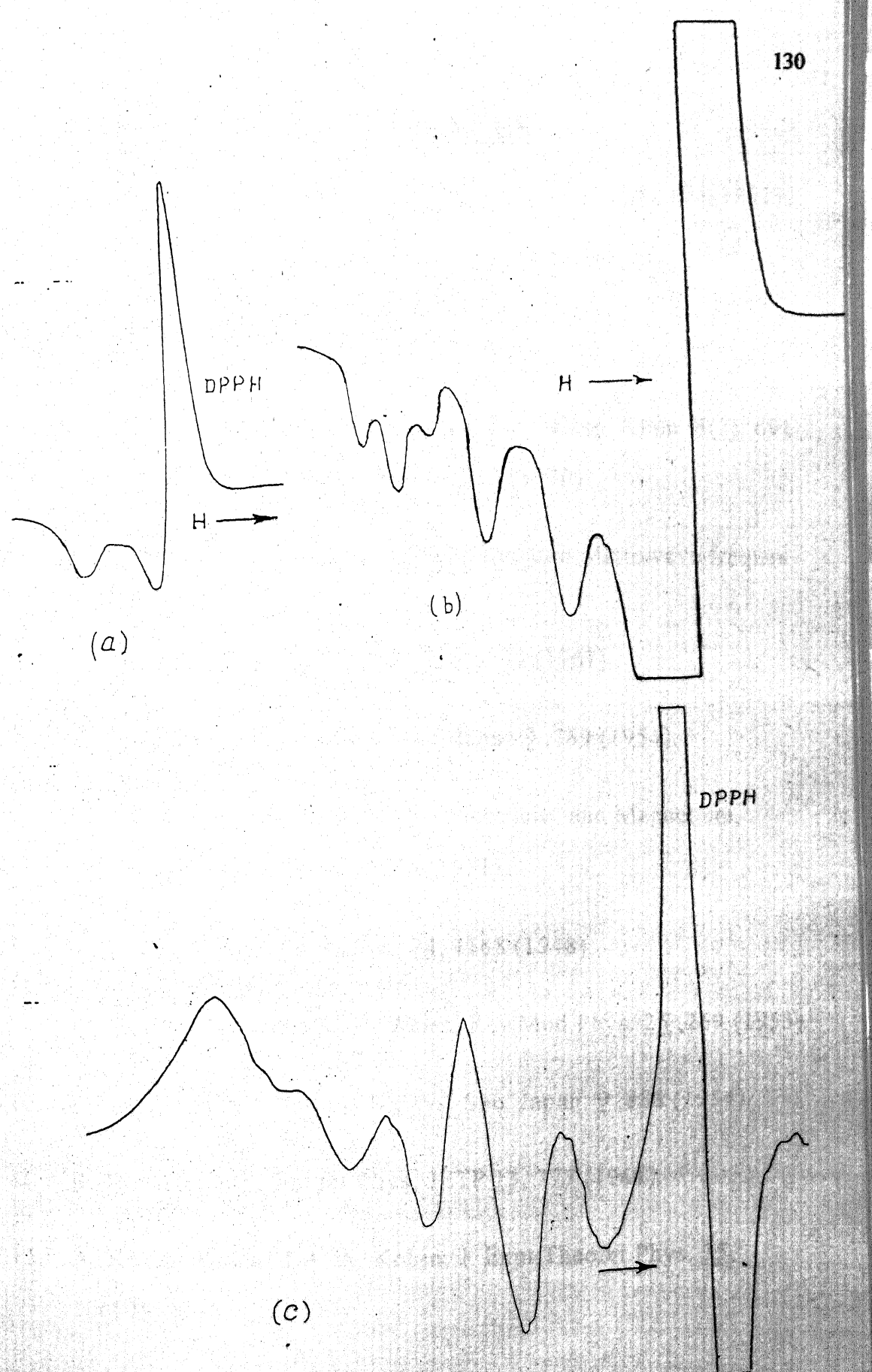


Fig 5.10 Experimental ESR spectra of Cu/L-Asparagine in
(a) Polyacryllic acid (b) G1

REFERENCES

1. R. Neiman and D. Kivelson, J. Chem. Phys. 35, 156 (1961).
2. F. K. Kneubuhl, J. Chem. Phys. 33, 1074 (1960).
3. R. H. Sands, Phys. Rev. 99, 1222 (1955).
4. L. N. Grigor'eva, T. A. Shurupova, Teor. Eksp. Khim. 6(5), 691 (1970). Zh. Strukt. Khim. 11(6), 1013 (1970).
5. D. J. E. Ingram, Spectroscopy at Radio and Microwave frequencies, Butter worths Publications, London, 89 (1967).
6. H. Kumagai et al., J. Phys. Soc. Japan 9, 369 (1954).
7. B. A. Bleaney and B. Bleaney., Electricity and Magnetism, Clarendon Press, London 576 (1951).
8. J. H. Van Vleck, Phys. Rev. 74, 1168 (1948).
9. P. W. Anderson and R. R. Weiss, Rev. Mod. Phys. 25, 269 (1953).
10. R. Kubo and K. Tomita, J. Phys. Soc. Japan. 9, 888 (1954).
11. R. Kh. Timerov, Soviet Phys. JETP 13, 777 (1961).
12. A. K. Chirkov and A. A. Kokin, J. Expt. Theoret. Phys. 35, 50 (1958).

13. D. E. O'Reilly, J. Chem. Phys. 29, 1188 (1958).
14. B. G. Malmstrom and T. Vanngard, J. Mol. Biol. 2, 118 (1960).
15. E. M. Roberts and W. S. Koski, J. Am. Chem. Soc. 82, 3006 (1960).
16. Y. Hsu, Mol. Phys. 21, 1087 (1971).
17. R. Kirmse, S. Wartewig, W. Windsch and E. Hoyer, J. Chem. Phys. 56, 5273 (1972).
18. A. D. Semenov, V. G. Zaletov and I. M. Semenova, Teor. Eksp. Khim. 5(4), 523 (1969).
19. (a) D. Kivelson and R. Neiman, J. Chem. Phys. 35, 149 (1961).
(b) R. Srinivasan and C. K. Subramanian, Ind. J. Pure and Appl. Phys. 8, 817 (1970).
20. T. Vanngard and R. Assa, Proc. 1st Int. Conf. on E.S.R., Jerusalem, Israel, 1961, Vol. II (1962).
21. C. J. Ballhausen, Introduction to Ligand Field Theory, McGraw Hill (1962).
22. G. F. Bryce, J. Phys. Chem. 70, 3549 (1966).
23. A. H. Maki and B. R. McGarvey, J. Chem. Phys. 29, 35 (1958).
24. H. R. Gersmann and J. D. Swalen, J. Chem. Phys. 36, 3221

(1962).

25. H. G. Hecht, J. Inorg. Nucl. Chem. 31, 2639 (1969).
26. P. V. Bakore, Thesis 1967, University of Rajasthan, Jaipur.
27. E. Buluggiu, Dascola, Gennaro, Giori, Camillo, Veracca, Villorio, A. Vera, Phys. Status Solidi 42(2), 693 (1970).
28. H. C. Freeman, M. R. Snow, I. Nitta and K. Tomita, Acta Crystallographica 17, 1563 (1964).
29. H. M. McConnell, J. Chem. Phys. 25, 709 (1956).
30. B. R. McGarvey, J. Phys. Chem. 60, 71 (1956); 61, 1232 (1957).
31. D. Kivelson, J. Chem. Phys. 33, 1094 (1960).
32. R. Rogers and G. Pake, J. Chem. Phys. 33, 1107 (1960).
33. M. J. Stephen and G. K. Fraenkel, J. Chem. Phys. 32, 1440 (1960).
34. J. H. Freed and & G.K. Fraenkel, J. Chem. Phys. 39, 326 (1963).
35. R. Wilson and D. Kivelson, J. Chem. Phys. 44, 154 (1966).
36. P. W. Atkins and D. Kivelson, J. Chem. Phys. 44, 169 (1966).
37. D. Kivelson, J. Chem. Phys. 45, 1324 (1966).
38. R. Wilson and D. Kivelson, J. Chem. Phys. 44, 4440, 4445 (1966).

39. J. H. Van Vleck, Phys. Rev. 57, 426 (1940).
40. R. Orbach, Proc. Phys. Soc. (London), A77, 821 (1961).
41. R. Mattuck and M. W. P. Strandberg, Phys. Rev. 119, 204 (1960).
42. P. S. Hubbard, Phys. Rev. 131, 1155 (1963).
43. J. G. Forrest, C. K. Prout and F. J. C. Rossotti, Chemical Communications 18, 658 (1966).
44. A. J. Stosick, J. Chem. Soc. 67, 362 (1945).
45. International Critical Tables, McGraw Hill, N. Y. (1930).
46. D. P. Graddon and L. Munday, J. Inorg. Nucl. Chem. 23, 231 (1961).



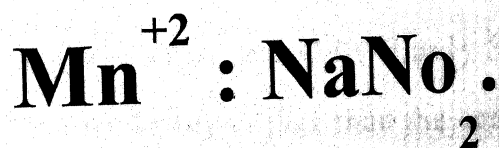
CHAPTER- 6

The angular variation and

temperature variation of line

widths and temperature variation

of Spin- Hamiltonian parameters in



CHAPTER -6

6.1 EXPERIMENTAL OBSERVATIONS

The temperature measurement accuracy was $\pm 0.4^{\circ}\text{C}$. The temperature stability at the sample was $\pm 0.2^{\circ}\text{C}$ over ~ 30 minutes. The minimum possible step of temperature increment was 1.0°C .

The measurements (recording of spectra) at a particular temperature were done after heating the sample at that temperature for about 20 to 30 minutes. While measuring the line widths, the contribution due to the temperature gradient along the sample, was taken into account. All measurements were done on heat treated crystals which had negligible intensity of spectrum-II at $\sim 30^{\circ}\text{C}$.

While studying temperature variation of S-I and S-II, various difficulties were encountered due to poor intensity and anisotropic line widths. The general features, for different orientations of \vec{H} , are given below.

$\vec{H} \parallel [100]$:

With increasing temperature, above $\sim 60^{\circ}\text{C}$ the S-I starts getting converted into S-II and above $\sim 150^{\circ}\text{C}$ only S-II is present. Above $\sim 230^{\circ}\text{C}$ the fine structure groups other than the central group ($+\frac{1}{2} \leftrightarrow -\frac{1}{2}$) are lost in the noise partly due to excessive broadening and partly due to fast expulsion of Mn^{+2} from the volume of the crystal to its surface. The various spectra are not recorded at the same gain ; the gain in general had to be increased with increasing temperature.

$\vec{H} \text{ // } [010]$:

The ESR spectra for $\vec{H} \text{ // } [010]$ at various temperatures in the range $\sim 30^\circ\text{C}$ to 150°C are shown in Figures 5.6 and 5.7. The extreme fine structure sextets ($\pm \frac{5}{2} \leftrightarrow \pm \frac{3}{2}$), both for S-I and S-II, are completely broadened out above $\sim 100^\circ\text{C}$ and the sextets ($\pm \frac{3}{2} \leftrightarrow \pm \frac{1}{2}$) above $\sim 150^\circ\text{C}$.

$\vec{H} \text{ // } [001]$:

At $\sim 30^\circ\text{C}$ itself the spectrum for $\vec{H} \text{ // } [001]$ is quite complicated. As the temperature was raised above $\sim 30^\circ\text{C}$, the lines got broadened and mixed with each other, further complicating the spectrum. Above $\sim 140^\circ\text{C}$ only the central sextets ($-\frac{1}{2} \leftrightarrow +\frac{1}{2}$) of S-I and S-II could be observed. Above $\sim 230^\circ\text{C}$ the central sextet was also lost into the noise, partly due to excessive line broadening and partly due to the expulsion of Mn^{+2} .

Temperature Variation of the Parameters D and E.

As below $\sim 100^\circ\text{C}$ the data regarding all the five fine-structure sextets along all the three principal axes and the intermediate angles was available, the accuracy of the calculated parameters D and E is high. Above $\sim 100^\circ\text{C}$, all the five fine structure transitions field positions could only be measured along [100], for both S-I-and S-II, as even on going off [100] by 5° or more, the lines got nearly lost into noise (except those of the central sextet). Hence parameters are calculated from the experimental data for all 30 lines for $\vec{H} \text{ // } [100]$ and the data for only central fine structure sextet for $\vec{H} \text{ // } [010]$ &

[001]. This causes some what large errors in calculation of the parameters D and E. Above 100°C, the parameters D and E of S-I could be accurately calculated only upto $\sim 138^\circ\text{C}$. Further, above $\sim 138^\circ\text{C}$ some lines of S-I got mixed with those of S-II (for $\bar{H} // [100]$). Due to increasing widths, the error in measurement of the line positions increased with increasing temperature. The experiments were, therefore, carried out several times using several crystals, and only the results which could be repeated are presented here. For the calculation of the parameters the modified Uhrin's method was used.

For S-I the principal axis X is parallel to [100]. The X component of the diagonal D-tensor of S-I, i.e. $3/2 D_{xx}$ is plotted vs. temperature in the range $\sim -170^\circ\text{C}$ to $\sim 138^\circ\text{C}$ and the plot is shown in Figure 6.1.

The Z -axis of S-II is parallel to [100]. The $D = 3/2 D_{zz}$, where D_{zz} is the principal value of the D-tensor of S-II, is plotted versus temperature in the range of $\sim 30^\circ\text{C}$ to $\sim 220^\circ\text{C}$ and is shown in Figure 6.2. The plot of D of S-II and $(3/2 D_{xx})$ of S-I in the temperature range 30°C to 138°C is shown for comparison in Figure 6.3. In this figure the broken straight line corresponds to the straight line fitting of the Figure 6.1. The temperature variation of the parameter $E = 1/2(D_{xx} - D_{yy})$ of S-II in the range $\sim 30^\circ\text{C}$ to $\sim 220^\circ\text{C}$ is shown in Figure 6.4. In this figure, the points between 30°C and 60°C are obtained using a crystal having S-II present at $\sim 30^\circ\text{C}$.

Temperature Variation of Linewidths

The peak to peak derivative linewidths (hereafter to be referred as line widths only) were measured for S-I and S-II in the temperature range

~-170°C to ~220°C for \vec{H} along the principal axes. Because of the ratio of signal height to noise amplitude being very low, the (100 KHz) modulation signal amplitude had to be kept large to improve the signal to noise ratio. At the temperatures above ~-10°C for $\vec{H} // [010]$ and above ~60°C for $\vec{H} // [100]$, the modulation amplitude used was large enough to cause distortions of the line shape, and therefore errors involved in line shapes determination and line widths are large, specially for the extreme sextets ($\pm \frac{5}{2} \leftrightarrow \pm \frac{3}{2}$). These errors were reduced by taking into account the line shape distortion due to modulation [1].

The line widths of S-I for $\vec{H} // [100]$, [010], [001], Z_I , and Y_I at the temperatures ~30°C, and ~-100°C are given in Table 6.(I) As is evident from these tables, the linewidths are M_S dependent and at ~30°C the widths are asymmetric about the central fine structure sextet i.e. the widths of $(+M_S \leftrightarrow M_S - 1)$ are not the same as those of $(-M_S \leftrightarrow -M_S + 1)$. This asymmetry of line widths along with M_S dependence exists for S-I upto its disappearance at ~150°C. Further the widths of S-I for $\vec{H} // [100]$ are far sharper compared to those for $\vec{H} // [010]$ and for $\vec{H} // [001]$. The asymmetry of widths is most prominent for $\vec{H} // [001]$ and $\vec{H} // Y_I$.

The temperature variation of widths of the fine structure sextet $-5/2 \leftrightarrow -3/2$ of S-I for $\vec{H} // [010]$ from ~-170°C to ~30°C is shown in Figure 6.5. The line widths for this orientation could not be determined with reasonable accuracy above ~40°C. The temperature variation of line width of the fine structure sextet $+5/2 \leftrightarrow +3/2$ of S-I for $\vec{H} // [100]$, from -170°C to 140°C

is shown in Figure 6.6. Even upto $\sim 140^{\circ}\text{C}$ the lines of S-I for $\vec{H} \parallel [100]$ are far sharper compared to those for $\vec{H} \parallel [010]$ and [001].

The linewidths of S-II at $\sim 30^{\circ}\text{C}$ are given in Table 6(II). The widths of S-II have similar line width anisotropy as those for S-I i.e. the lines are sharpest for $\vec{H} \parallel [100]$. Temperature variation of the widths of S-II for different orientations of \vec{H} , in the range $\sim 170^{\circ}\text{C}$ to $\sim 150^{\circ}\text{C}$ is similar to that for S-I. The temperature variation of the line widths, in the range $\sim 30^{\circ}\text{C}$ to $\sim 220^{\circ}\text{C}$, of the sextet $+5/2 \leftrightarrow +3/2$ of S-II for $\vec{H} \parallel [100]$ is shown in Figure 6.7. The temperature variation of line widths of the $+3/2 \leftrightarrow +1/2$ sextet of S-II for $\vec{H} \parallel [100]$ is shown in Figure 6.8.

For S-II, the M_s dependence of line widths is present even upto $\sim 250^{\circ}\text{C}$. For S-II, the lines are much sharper for if $\vec{H} \parallel [100]$ compared to those for $\vec{H} \parallel [010]$ and for $\vec{H} \parallel [001]$ in the complete temperature range $\sim 30^{\circ}\text{C}$ to $\sim 250^{\circ}\text{C}$. The asymmetry in the line widths about the central sextet is present for S-II, for $\vec{H} \parallel [100]$, from $\sim 100^{\circ}\text{C}$ to $\sim 220^{\circ}\text{C}$. Above $\sim 150^{\circ}\text{C}$ a M_s dependence of the widths of S-II is also observed.

The angular variation of the line widths of the $-5/2 \leftrightarrow -3/2$ sextet of S-I in the (001) plane at $\sim 35^{\circ}\text{C}$ is shown in Figure 6.9.

The temperature variation of the line widths of S-III for $\vec{H} \parallel [100]$ in the range $\sim 170^{\circ}\text{C}$ to $\sim 30^{\circ}\text{C}$ is nearly the same as that for S-I. The line widths of S-III for different orientations are given in Table 6.(III). The lines of S-III are sharpest along [100], and broadest along [010]. The angular varia-

tion of the widths of $-5/2 \leftrightarrow -3/2$ sextet of S-III at $\sim 30^\circ\text{C}$ in the plane (001) is shown in Figure 6.10.

Line Shapes

The line shape of all the five sextets of S-I at $\sim 130^\circ\text{C}$ for $\vec{H} \parallel [100]$ is Gaussian, while for $\vec{H} \parallel [010]$ and $\vec{H} \parallel Z$, it is very slightly different from Gaussian. As the temperature is raised, above $\sim 10^\circ\text{C}$, the deviation of line shape from Gaussian towards Lorentzian takes place. In the temperature range $\sim 10^\circ\text{C}$ to $\sim 30^\circ\text{C}$ the line shape of S-I for $\vec{H} \parallel [100]$ is intermediate to Gaussian and Lorentzian, and for $\vec{H} \parallel [010]$ though it could not be determined accurately, it seems to be nearer to Lorentzian rather than Gaussian.

6.2 DISCUSSION

6.2.1 TEMPERATURE VARIATION OF D & E AND PHASE TRANSITIONS.:

Theoretical Considerations :

The case of axial symmetry, the D-tensor has only one independent component, namely the axial field parameter $D = 3/2 D_{zz}$. For orthorhombic symmetry, there are two independent parameters namely D_{zz} and the orthorhombic parameter $E = 1/2 (D_{xx} - D_{yy})$. But all the three components, D_{zz} , D_{xx} and D_{yy} can be considered as axial field parameters, depending on the choice of the axis of quantization of spin. As no unique definition of the axial field parameter for orthorhombic symmetry is available in literature, hence in

the following analysis, for orthorhombic symmetry, the temperature variation of all the three principal components D_{xx} , D_{yy} & D_{zz} is assumed to be similar, except for the systems where the phase transitions are involved.

The origin of the axial field splitting parameter D for S-state ions like Mn^{+2} is explained on the basis of the models which consider the interactions between the ground state and excited states, and has been considered in detail by Sharma, Das and Orbach [2-4] Wybourne [5] and Van Heuvelen [6]. Large discrepancies were observed between theory and experiments, for D-values of Mn^{+2} in the various systems. Much useful qualitative knowledge of the change in crystalline environment can not be deduced from the SH parameters, because of the complexity of the processes relating them to the crystal field parameters [2-4].

The two major effects, found to contribute to the temperature dependence of axial field parameter D, [7-23] are as follows.

1. Due to thermal lattice expansion the distances between the atoms in the crystal are changed, leading to changes in the crystal field. This is termed as temperature dependence of the static distortion [18] and its contribution D_s to the axial field parameter D is expressed

$$\text{as } D_s = D_s^o (1 + \alpha T + \beta T^2) \quad (6.2.1)$$

2. Thermally excited phonons modulate the crystal field and change the population of the electronic states of the paramagnetic ion. This is termed as lattice vibrational contribution D_v expressed as [18] ;

$$D_V = D_V^0 \operatorname{Cot} h(\hbar\nu/2kT) \quad (6.2.2)$$

where ν is the frequency of the exciting vibration. The total D is written as

$$D = D_s^0 (1 + \alpha T + \beta T^2) + D_V^0 \operatorname{Cot} h(\hbar\nu/2kT) \quad (6.2.3)$$

Above $\sim 100^\circ\text{K}$ (-173°C), various authors [12,13,19-21] found the D vs. temperature curves to be linear and could be fitted to hyperbolic cotangent. Manooigian and Leclerc [18,22] have attempted to explain the linear behavior by equation (6.2.3) consisting of both the static and the vibrational contributions.

When the structural phase transitions occur in a system, the temperature variation of the D-tensor components becomes a complicated problem. Near the phase transition temperatures, the equation (6.2.3) is no more valid.

The study of structural phase transitions by ESR can be divided into two parts.

(i) The systems where phase transition is from cubic phase ($D = 0, E = 0$) to the tetragonal or trigonal phase ($D \neq 0, E = 0$). Also included are the systems where phase transition is from tetragonal or trigonal phase to orthorhombic or lower symmetry phase ($D \neq 0, E \neq 0$). In such phase transitions the SH parameter D or E can be considered as a sort of order parameter. Some examples of such phase transitions studied by ESR are $\text{LaAlO}_3 : \text{Fe}^{3+}$ [24], $\text{SrTiO}_3 : \text{Fe}^{3+}, \text{Gd}^{3+}$ [24], $\text{BaTiO}_3 : \text{Fe}^{3+}, \text{Gd}^{3+}$ [25,26], and Cr^{3+} in hexaurea aluminium per chlorate [27]. Further a new order parameter observed in LaAlO_3 and SrTiO_3 [24] is the angle of rotation ϕ of the principal axes of

the D-tensor related to distortions of the molecular groups. In such systems [24] D is found to behave as

$$D = D_0 / (T_c - T) / T_c J^{2\beta} \quad (6.2.4)$$

and $D \propto \phi^2$

where β is the critical exponent which according to Landau theory has the value $1/2$, but is found to have the value $1/3$ in the critical region [24]. An expression for E, similar to (6.2.4) can be written when E is the order parameter [27]. In these systems total D can be written as

$$D = D_s + D_v + D_{st} \quad (6.2.5)$$

where D_{st} is similar to D of equation (6.2.4) and is the contribution due to the changes associated with the structural phase transition. Then following the results of [24-27], it can be seen that near the phase transition, contribution of D_{st} to the temperature variation part of D is so large, that it alone determines the changes in D according to the equation (6.2.4). In fact near the phase transition temperature both D_s and D_v will contribute through D_{st} . In such a situation, in no way the three parts of equation (6.2.5) can be separated, and the variation of total D will be given by (6.2.4). Far away from the phase transition temperature, the three parts of equation (6.2.5) can be considered separately, but they may still be related to each other. Far away from the phase transition temperature the contribution due to D_{st} will be linear in temperature (as the order parameter is nearly constant) and if that of D_s and D_v is also linear, the temperature variation of total D will also be linear.

(ii) The systems in which the phase transition is from orthorhombic or lower symmetry ($D \neq 0, E \neq 0$) to orthorhombic or lower symmetry ($D \neq 0, E \neq 0$). In this case neither D nor E can be considered as an order parameter, and therefore the temperature variation of D_s in (6.2.5) cannot be expressed in a simple form, as was possible in case (i) above. However, the temperature variation of total D can be expected to be linear, well away from the phase transition temperature (provided the temperature variation of D_s and D_v is also linear).

In the case of ferroelectric phase transitions, there are additional contributions to D , from the Pseudo-Stark effect of spontaneous polarization \vec{P}_s . In the ferroelectric phase, the paramagnetic ion is generally situated at a site which lacks centre of inversion. The local electric field due to \vec{P}_s is generally very-large and therefore, causes large shifts in the ESR spectral lines. Further \vec{P}_s may also cause rotation of principal axes of D -tensor. In some systems, this results in splitting of the lines. The shifts, the rotation angle and the splittings are directly related to \vec{P}_s and may be taken as order parameters, as these vanish as the P_s becomes zero at $T=T_c$. Let the contribution to D due to such effect of \vec{P}_s be denoted by D_{FE} . Such shifts and rotation angles in various ferroelectrics have already been observed [28-32].

In addition to these splittings and rotations, which are purely due to Pseudo-Stark effect, one observes the rotation of molecular ions due to structural changes in the ferroelectric phase resulting in rotation of D -tensor axes and splittings of ESR lines [28]. As the rotating molecular ions, have net

dipole moment, the rotation angle of these molecules and hence of D-tensor axes, is related to P_s . This was observed by Windsch et al. in TSCC:Mn⁺² [28]. The contribution to temperature dependence of D due to this, can be included in the D_{st} of equation (6.2.5). Thus, in the ferroelectric phase, the total D can be expressed as.

$$D = D_s + D_v + D_{st} + D_{FE} \quad (6.2.6)$$

here $D_{st} \rightarrow 0$ and $D_{FE} \rightarrow 0$ as $T \rightarrow T_c$.

In the ferroelectric phase transitions, even if there are no structural rotations of molecules, the D_{st} will be still related to P_s . Thus in equation (6.2.6), the terms D_{st} and D_{FE} both are related to P_s .

In the literature [29-32], the two parts D_{st} and D_{FE} have not been studied separately. As for these systems [29-32] temperature variation of D could be related to temperature variation of P_s , one can conclude that near the phase transition temperature, only the terms D_{st} and D_{FE} of (6.2.6) are significant contributors to the temperature variation of total D, and the terms D_s and D_v need not be explicitly considered.

Temperature Variation of Spectrum- I

As we know that the principal axes Y and Z of D of S-I are rotated about [100] by angles $\pm\alpha$ off the crystallographic axes, due to \bar{E}_{loc} of \bar{P}_s . For small values of angle α one gets,

$$\alpha = K P_s \quad (6.2.7)$$

where K is a constant. Further the D'_{zz} is proportional to E_{loc} i.e. P_s and leads to

$$D_{FE} = E_x R_{113}$$

If near the phase transition temperature, the contribution of D_{FE} to the temperature variation of D_{xx} is far larger compare to that of other terms of (6.2.6), a linear relationship between P_x and D_{xx} should be expected. Such a linear relationship between D and P_s , near the phase transition temperature was experimentally observed in many ferroelectrics [28, 30, 33]. Away from the phase transition temperature, the temperature variation of P_s is nearly linear, and if those of terms D_s and D_v is also linear, the temperature variation of D_{xx} will be linear.

The temperature variation of $3/2 D_{xx}$ of S-I is shown in figure 6.1, from which it is evident that below $\sim 30^\circ\text{C}$, the D_{xx} is nearly linear upto $\sim 160^\circ\text{C}$. Hamano [34] measured the temperature dependence of P_s in NaNO_2 crystals. He observed an increase by ~ 2 percent in P_s , on decreasing the temperature from $\sim 24^\circ\text{C}$ to $\sim 100^\circ\text{C}$. Hence below $\sim 30^\circ\text{C}$, the D_{st} and D_{FE} will be nearly temperature independent, and the temperature dependence of total D_{xx} can be accounted by the static and vibrational parts (i.e. D_s and D_v). In various systems, the contribution of D_s and D_v is found to be linear with temperature [12, 13, 19-21]. Hence the linear behaviour of D_{xx} of S-I can be satisfactorily explained.

Above $\sim 24^\circ\text{C}$, P_s decreases slowly and above $\sim 140^\circ\text{C}$, it decreases very fast [34]. Hence above $\sim 30^\circ\text{C}$ the contribution of D_{st}

and D_{FE} cannot be neglected. Further it has been shown that the thermal expansion of pure NaNO_2 starts deviating from the linear behaviour (i.e. the anomaly associated with the phase transition at T_c starts appearing) above $\sim 50^\circ\text{C}$ [35-37]. This will lead to significant changes in the contribution of D_s and D_{st} to temperature variation of D_{xx} , above $\sim 50^\circ\text{C}$. Experimentally (see Figure 6.1), deviation from straight line behaviour of D_{xx} versus temperature starts above $\sim 30^\circ\text{C}$. It can then be understood as due to combined effect of changes in D_{st} , D_{FE} and D_s . As above $\sim 140^\circ\text{C}$, where large changes in P_s take place, the S-I could not be observed, we could not derive a relationship between P_s and D_{xx} .

The angle α given by equation (6.2.7) will become zero as $T \rightarrow T_c$. But as the S-I could not be observed above 150°C and α could not be determined above $\sim 70^\circ\text{C}$, it was not of any help in interpreting the phase transition at T_c .

Temperature Variation of S-II

As S-II was concluded to be either due to metastable clusters or due to isolated Mn^{2+} , the former being more probable. The changes in the SH parameters D and E with temperature, near the phase transition are interpreted, considering both models for S-II.

The metastable clusters are small regions around the Mn^{2+} vacancy complexes, which are surrounded by the ordered ferroelectric

region. Though the spontaneous polarization \vec{P}_s was concluded to be approximately zero in the metastable regions, there still may be some sort of ordering existing in metastable regions, which will be related to the ordering of the ferroelectric phase. Though it is difficult to predict the nature of changes inside the metastable clusters, near the phase transition temperature, it is certain that the changes (and thus the structure) inside the metastable clusters will be very sensitive towards the changes in the surrounding ordered ferroelectric regions. Therefore one can expect the changes in the SH parameters of S-II to be related to the changes in the order parameter and thus to \vec{P}_s .

As in the paraelectric phase, the Na^+ and NO_2^- ions are flipping rapidly, metastable cluster formation will be least probable. Thus the metastable clusters may also undergo a transition to the paraelectric phase at T_c .

In the sinusoidal anti-ferroelectric phase, there is a short range ordering of the parallel and antiparallel domains [38,39]. The spectra due to parallel and antiparallel domains will be same, irrespective of whether Mn^{+2} is associated with a vacancy or not. As the temperature range of this phase is very narrow ($\sim 2^\circ\text{C}$) [38,39], and the error in calculated D and E parameters is quite large (see Figures 6.2 and 6.4) in the neighbourhood of T_c , nothing could be concluded regarding this phase. Thus the T_c will be considered as the temperature of phase transition from ferroelectric to paraelectric phase, and antiferroelectric phase will be overlooked.

In the paraelectric phase the unit cell of NaNO_2 has centre of inversion macroscopically. But, from a microscopic point of view, the unit cells at a particular instant are polarized and have same symmetry as in the ferroelectric phase

If one assumes that the substituted Mn^{+2} ion along with associated vacancy is also jumping between the two equivalent positions, with the same frequency, as that of the Na^+ ion, then as both the parallel and antiparallel polarized states give the same spectrum, the spectrum in the paraelectric phase should be quite similar to the spectrum S-I, in the ferroelectric phase. But it is difficult to imagine such a motion of Mn^{+2} and vacancy together. If it were so, then at the transition temperature the changes in S-II should be prominent, which is contrary to the small changes experimentally observed. Further it is possible that Mn^{+2} in the paraelectric phase does not jump between two equivalent positions or it is jumping with a rate slower than of Na^+ . In such a situation, a time averaging of the crystal field will take place, which can result in no major changes in the spectrum of the paraelectric and ferroelectric phases. In any case, as the microscopic symmetry does not change on phase transition and anomalies in the lattice constants (unit cell dimensions) are reported to be very small [35-37], only small changes in crystalline field leading to small anomalies in the SH parameters are anticipated.

In case, the S-II is due to isolated Mn^{+2} in the ordered ferroelectric region, the D-tensor components associated with S-II will

be appreciably influenced by \bar{E}_{loc} due to \bar{P}_s . In such a situation, the temperature variation and magnitude of anomalies at T_c will be determined by the contribution of the term D_{FE} (and to some extent D_{st}) to the temperature variation of D , relative to those of other terms in equation (6.2.6).

Temperature variation of D of S-II shown in the Figure 6.3, is quite similar to that of $(3/2 D_{xx})$ of S-I. This may be fortuitous. But if S-II is due to isolated Mn^{+2} , then this similar variation may very well be due to similar contribution of the term D_{FE} (which is purely due to temperature variation of \bar{P}_s) for the S-I and S-II. Temperature variation of D of S-II in the temperature range $\sim 30^\circ C$ to $220^\circ C$ is shown in Figure 6.2. It is evident from the figure that the anomaly at T_c is very small. The temperature variation curve in the range $\sim 130^\circ C$ to T_c is quite different from that of P_s given in [34]. It is evident that, none of the different constituent processes of equation (6.2.6) is dominant. The contribution of all the terms seems to be significant.

Above T_c , one can see two slopes in the D vs temperature curve, with an anomaly at $175 \pm 3^\circ C$. The anomaly is more prominent for the cooling cycle compared to the heating cycle. The anomaly at $175 \pm 3^\circ C$ is related to the already reported phase transition at $\sim 178^\circ C$ in the pure $NaNO_2$ crystals [40,41]. Takagi and Gesi [40] interpreted it as due to some sort of short range order existing upto $\sim 178^\circ C$, above which Curie-Weiss law holds nicely.

From Figure 6.1, it can be seen that no anomaly exists in the temperature range 30°C to $\sim -120^{\circ}\text{C}$. The reported phase transition at $\sim -95^{\circ}\text{C}$ in the pure crystals, thus could not be detected.

The temperature variation of the parameter E of S-II is shown in Figure 6.4. The temperature variation of E is quite similar to that of P_s given in [34]. The anomaly observed near T_c is rather large compared to that for the parameter D . The E vs. temperature curve could be fitted to an expression of the form

$$E(T_c) - E(T) = \Delta E = (T_c - T)^{\beta} \quad (6.2.8)$$

with $\beta \approx 0.21$ and $T_c = 159^{\circ}\text{C}$ in the temperature range $\sim 130^{\circ}\text{C}$ to 154°C . It could not be fitted for the range 154°C to 159°C where the error in measurement of E is quite large. A variation of P_s reported by Hamano [34] is of the form

$$P_s = B (T_0 - T)^{\beta}, \quad \beta = 0.2, \quad T_0 = 165.15^{\circ}\text{C}$$

for the temperature range $\sim 128^{\circ}\text{C}$ to T_c . There is a striking similarity between temperature variations of E and P_s . If S-II is assumed to be due to isolated Mn^{+2} , then for the effect of \bar{E}_{loc} , (and symmetry C_{2v}), it can easily be shown that

$$(D_{xx} - D_{yy}) \propto E_{\text{loc}} \\ \propto P_s$$

and if the contribution of D_{FE} (i.e. E_{FE}) to the temperature variation of the total D (i.e. E in this case) of equation (6.2.6) is far large

compared to those of other terms, one can write,

$$E \propto P_s$$

and $E = E(T_c) + KP_s$

where K is a constant. Thus the temperature variation of E near the phase transition temperature can be explained assuming S-II to be due to isolated Mn^{2+} . But as the origin of S-II is not confirmed, this may again be fortuitous.

Due to large errors in measurement of E above T_c , the phase transition at $175^\circ C \pm 3^\circ C$ could not be detected. The temperature variation of E above T_c seems to be linear.

The phase transition temperature determined from ESR experiments is $T_c = 159 \pm 2^\circ C$. For pure crystals the temperature of phase transition from ferroelectric to sinusoidal antiferroelectric phase (T_c) is reported to be between $\sim 163^\circ C$ and $\sim 165^\circ C$. The shift in T_c in Mn^{2+} doped crystals is the effect of Mn^{2+} impurity. Such shift of phase transitions due to impurities is well established for ferroelectric crystals. The shift in phase transition temperature has also been observed for γ -ray irradiated $NaNO_2$ crystals [42,43].

6.2.2 LINE WIDTHS

The various line broadening mechanisms considered are;

- (i) The spin-lattice relaxation [44-46], (ii) the spin-spin interaction [44-46] (iii) the mosaic structure in a nearly perfect crystal [47,48]

(iv) the inbuilt stresses (strain broadening) [49,50] (v) the charged point defects and impurities which are capable of creating strong electric field at the site of paramagnetic ion [51] (vi) the vacancy jumps (hopping) [52-54] (vii) the broadening due to fluctuations in spontaneous polarization [33,55].

The broadening due to mechanisms (i) and (ii) are in general isotropic (independent of field orientation) and M_s independent [44-46]. The line widths due to mechanism (i) for Mn^{2+} paramagnetic ion in a lattice are found to vary little with temperature. As the crystals of $NaNO_2 : Mn^{2+}$, have very small concentration of Mn^{2+} , the broadening due to mechanism (ii) will be negligible over the complete temperature range of interest. As the broadening mechanisms (i) to (v) have been considered in detail in literature, only mechanisms (vi) and (vii) will be considered in detail.

Broadening due to Vacancy Hopping

Above a certain temperature the Mn^{2+} cation vacancy pairs are continually changing their orientation as a result of vacancy jumps under thermal activation [56]. The vacancy jumps are mainly of two types, the one which only changes the orientation of the pair and leaves the distance R between vacancy and Mn^{2+} unchanged, and the other which changes the orientation and distance R both (or changes only distance R). Each time a vacancy moves the ESR spectrum of the complex may change completely and if hopping is taking place,

it will result in a life time broadening of the ESR spectral lines. Watkins [52] was the first to report that the ESR line under such vacancy jumps assume a Lorontzian shape which can be associated with a finite life time, τ , for the vacancy at the site associated with the spectrum. Tucker [53] derived the following expression for τ

$$\frac{1}{\tau} = \frac{1}{\tau_0} \exp \left(-\frac{E}{kT} \right) \quad (6.2.9)$$

where E is the activation energy for the process. τ is then directly related to the excess line width. This was later experimentally confirmed [54].

For S-I in $\text{NaNO}_2 : \text{Mn}^{2+}$, there are two complexes $\text{Mn}^{2+}-\text{V}001$ and $\text{Mn}^{2+}-\text{V}00\bar{1}$. These two complexes give inequivalent (distinguishable) spectra for \vec{H} off the [010] and [001] in the (100) plane. An exchange of vacancy and Mn^{2+} will cause the broadening of the lines only for \vec{H} in the (100) plane and off the [010] and [001]. As the two complexes give identical spectrum (indistinguishable) for any other orientation of \vec{H} , no line broadening should be observed in the (010) and (001) planes, including the crystallographic axis [100].

If the vacancy jump is from 001 or $00\bar{1}$ site to some other site which causes formation of a new complex giving a different spectrum, the broadening of the lines of S-I for any orientation of \vec{H} including [100] should be observed.

Similarly for S-III, which is due to $\text{Mn}^{2+}-\text{V}100$ and $\text{Mn}^{2+}-\text{V}\bar{1}00$

complexes, if Mn^{2+} -vacancy exchange takes place, excess broadening should be observed only for \vec{H} in the plane (001) and off the axes [100] and [010].

Broadening Due to Fluctuations in the Spontaneous Polarization

Torsional oscillations of NO_2^- will cause fluctuations in the dipolar field contribution to the crystalline field and in the spontaneous polarization \vec{P}_s . The dipolar contribution due to NO_2^- dipoles to the crystalline field was not considered earlier, but its effect was in a way incorporated in the SH by considering the effect of local field due to \vec{P}_s . In addition to torsional oscillations of NO_2^- , thermal oscillations of Na^+ ions will also contribute to the fluctuations of P_s . With the rising temperature, the amplitudes of torsional oscillations of NO_2^- increase, and above $\sim 30^\circ C$ these are very large [57-60]. This will result in large fluctuations of P_s . The estimates of the different mean square amplitudes at $27^\circ C$ from NQR studies [57] are

$$\langle \theta_a^2 \rangle = 0.768 \times 10^{-2} \text{ rad}^2, \langle \theta_b^2 \rangle = 1.43 \times 10^{-2} \text{ rad}^2, \langle \theta_c^2 \rangle = 4.79 \times 10^{-2} \text{ rad}^2$$

As we know, the fine structure tensor for all the spectra has significant contribution from \vec{P}_s . Therefore the fine structure tensor components will be time dependent due to the mean square fluctuations ($\langle P_s^2 \rangle - \langle P_s \rangle^2$) of the polarization. If the fluctuations are sufficiently fast, there will be time dependent spread in the D-tensor principal values which will result in the broadening of the ESR lines of the spectra in the ferroelectric phase. Another effect of fluctuations in P_s will be to cause the time dependent changes in the orientation of the principal axes of D-tensor resulting in a spread of principal

axes over a small angle which may cause significant contribution to line widths. Though in NaNO_2 , the contribution of the NO_2^- dipoles to spontaneous polarization is only 15 percent [34,61], the main contribution to the fluctuations in P_s will be from the torsional oscillations of NO_2^- .

We assume that the mean square fluctuations in D_{xx} are much smaller than those in D_{yy} and D_{zz} and fluctuations in D_{yy} are smaller than those in D_{zz} , i.e.

$$(\langle D_{xx}^2 \rangle - \langle D_{xx} \rangle^2) \ll (\langle D_{yy}^2 \rangle - \langle D_{yy} \rangle^2) \ll (\langle D_{zz}^2 \rangle - \langle D_{zz} \rangle^2) \quad (6.2.10)$$

Because of the fluctuations in fine structure tensor components, both spin-lattice relaxation and T_2 -like relaxation or the transverse relaxation (called as 'secular broadening' by Slichter [44]) will get enhanced. In fact the contribution to the spin lattice relaxation will result in far lesser broadening compared to that due to the T_2 -like relaxation [55]. The transverse relaxation time T_2 for \vec{H} parallel to a principal axis, can be expressed as

$$T_2^{-1} = M [\langle D^2 \rangle - \langle D \rangle^2] \tau_c \quad (6.2.11)$$

where τ_c is the correlation time of the quantity D , and M is constant whose value will depend on the M_s i.e. the fine structure group being considered. Because of such dependence on D , the anisotropy and M_s dependence of the broadening of the lines will be observed. The effect of E , will be in second order, and hence small. For $\vec{H} \parallel X_I \parallel [100]$, the line positions of S-I are linearly dependent on D_{xx} while $E_x = 1/2 (D_{yy} - D_{zz})$ affects line positions in second order only [46]. Hence line broadening of S-I for $\vec{H} \parallel [100]$ will be mainly determined

by the fluctuations of D_{xx} , which, if small, will give small broadening of lines. As the fluctuations in D_{xx} , D_{yy} and D_{zz} are in phase, the asymmetry of line widths (i.e. widths of $+M_s \leftrightarrow +M_s - 1$ and $-M_s \leftrightarrow -M_s + 1$ fine structure groups not being equal) will result from the second order contributions of E_x [$E_x = 1/2 (D_{yy} - D_{zz})$] and D_{xx} as this contribution is not the same for the sextets corresponding to fine structure transitions $+M_s \leftrightarrow +M_s - 1$ and $-M_s \leftrightarrow -M_s + 1$.

For $\vec{H} // Z_I$ axis of S-I, if fluctuations in D_{zz} are large, large broadening of the lines with little asymmetry about central fine structure transition will be observed. As [010] is only 4.5° off the Z_I axis, the line widths will be nearly same for the two orientations. For $\vec{H} // Y_I$ axis of S-I, if fluctuations of D_{yy} are intermediate to those of D_{xx} and D_{zz} , the line broadening will be intermediate to those for Z and X axes. As the fluctuations of the parameter $E_y = 1/2 (D_{xx} - D_{zz})$, are quite large, the asymmetry about the central fine structure transition will be quite significant. As [001] is only 4.5° off Y_I , the line widths will be nearly same for the two orientations.

Thus the observed M_s dependence of the widths and asymmetry of widths of S-I for $\vec{H} // X_I // [100]$, $\vec{H} // Y_I // [001]$, Z_I and [010] can be explained satisfactorily, if one assumes equation (6.10). A similar analysis will be developed for S-III.

Temperature Variation of Line Widths of Spectrum -I

(a) Line Widths Below $\sim 100^{\circ}\text{C}$:

As is evident from Figures 6.5 and 6.6, the line widths of S-I are nearly temperature independent in the temperature range $\sim 100^{\circ}\text{C}$ to $\sim 170^{\circ}\text{C}$. The slight variation may be due to spin-lattice relaxation. The line widths are anisotropic and are smallest for $\vec{H} \parallel [100]$ and largest for $\vec{H} \parallel [010]$ [see Table 6.(I)]. The amplitudes of torsional oscillations of NO_2^- are extremely small below $\sim 95^{\circ}\text{C}$ [61] and hence the contribution due to fluctuations in P_s will also be very small. The line width anisotropy below $\sim 100^{\circ}\text{C}$ can then be explained due to the mosaic structure or due to inbuilt stress (strain broadening), as both the mechanisms are static in nature, in general causing an anisotropic broadening of lines which is temperature independent. As the mosaicity causes $\sin 2\theta$ dependence of the width [47,48] and experimentally this was not observed, it can be ruled out as possible mechanism. The strain broadening can satisfactorily explain the anisotropy and temperature independence of widths following the discussion of [49]. The main sources of stress are randomly distributed impurities and point defects. In $\text{NaNO}_2 : \text{Mn}^{2+}$, additional sources of strains are aggregates of Mn^{2+} vacancy dipoles, and the strains developed near the domain walls. As the line widths for \vec{H} in (100) plane are much larger compared to those for other orientations of \vec{H} , it appears that the imbuilt stresses preserve the point symmetry of Mn^{2+} -vacancy complexes. This may probably be related to the domain structure in

NaNO_2 . The domain walls in NaNO_2 are parallel to (100) planes, and slight misorientations of domains about [100] axis may result in such symmetric behaviour. The observed line width $\Delta H'$ can be written as :

$$\Delta H' = (\Delta H_s^2 + \Delta H_i^2)^{1/2} \quad (6.2.12)$$

where ΔH_s is broadening due to the random strains and ΔH_i is the intrinsic broadening mainly due to spin-lattice and spin-spin relaxation.

If the line broadening below $\sim -100^\circ\text{C}$ is due to the reasons given above, one should observe variation in line widths from sample to sample as crystals grown under different conditions will have different strains. This was experimentally confirmed. The line widths observed in different crystals (samples) at $\sim -100^\circ\text{C}$, varied from 3.2 to 3.8 Gauss for $\vec{H} \parallel [100]$ and from 5.0 to 8.5 Gauss for $\vec{H} \parallel Z_I$ and $\vec{H} \parallel [010]$.

(b) Line widths Above $\sim -100^\circ\text{C}$.

Line widths of S-I for $\vec{H} \parallel [100]$ and $\vec{H} \parallel Z_I$ start increasing slowly above $\sim -100^\circ\text{C}$ (see Figures 6.5 and 6.6), and very fast above $\sim -10^\circ\text{C}$. The line broadening for $\vec{H} \parallel Z_I$ is much larger and faster compared to that for $\vec{H} \parallel [100]$. From Figure 6.5 it is evident that for $\vec{H} \parallel Z_I$, the plot of $\log (\Delta H_{\text{excess}})$ versus $1/T$ can be fitted to a straight line above $\sim -10^\circ\text{C}$ which corresponds to an activation energy of $E_2 \approx 0.24 \text{ e.V.}$ ΔH_{excess} is equal to $(\Delta H_{\text{observed}} - \Delta H')$ where $\Delta H'$ is width at $\sim -100^\circ\text{C}$. In the temperature range -100°C to -10°C

10°C it can be fitted very approximately to a straight line with activation energy of $E_1 \approx 0.06$ e.V.

The $\log(\Delta H_{excess})$ vs. $1/T$ curve for $\vec{H} // [100]$ can not be fitted to a straight line in the temperature range -100^0C to $\sim -20^0\text{C}$ but in the temperature range $\sim -20^0\text{C}$ to $\sim 80^0\text{C}$ it can be nicely fitted to a straight line with activation energy of $E'_2 \approx 0.34$ e.V.

Gesi [62] reported a phase transition at $\sim -95^0\text{C}$ which he interpreted as due to the small anomaly in the amplitudes of torsional oscillations of NO_2^- . He further concluded that the torsional oscillation amplitude starts increasing faster above $\sim -95^0\text{C}$ compared to that below -95^0C . The observed slow increase in line widths above $-100^0 \pm 8^0\text{C}$ can then be due to the faster increase in the amplitude of oscillations of NO_2^- resulting in the increase in the fluctuations of P_s . The sudden increase in widths above $\sim 10^0\text{C}$ (corresponding to activation energy E_2) should then be due to another anomaly in the torsional oscillation amplitudes of NO_2^- . But no such anomaly for $NaNO_2$ in the temperature range -95^0C to 30^0C is reported in literature [35,62,63]. The anomalous increase above $\sim 10^0\text{C}$ can then be due to the vacancy hopping. As the lines for $\vec{H} // [100]$ broaden much lesser compared to those for $\vec{H} // Z_I$ and Y_I , only the vacancy and Mn^{2+} exchange seems to be taking place. The activation energy for this process, according to equation (6.2.9) comes out to be $E_2 \approx 0.24$ eV from $\vec{H} // Z_I$ plot (see Figure 6.5). This will not be true value as the contribution due to fluctuations in P_s has not been separated. The difference between the values of E_2 and E'_2 may be due to the fact that the

contribution due to vacancy hopping, if Mn^{2+} -vacancy exchange is taking place, will be very small for $\vec{H} \parallel [100]$ and will not be given by equation (6.2.9). Again as the widths for $\vec{H} \parallel [100]$ are much sharper compared to those for $\vec{H} \parallel Z_1$ and Y_1 , even upto $\sim 150^\circ C$, the identity (6.2.10) will be true, for S-I. The increase in the widths above $-100 \pm 8^\circ C$, then confirms the phase transition at $\sim -95^\circ C$ reported for pure $NaNO_2$ crystals by other studies [35, 62, 63].

The widths for $\vec{H} \parallel [100]$, above $\sim 80^\circ C$ can be fitted to a straight line with activation energy $E_3 \approx 0.34$ eV, which is larger than E_2' for the range $-10^\circ C$ to $\sim 80^\circ C$. This anomalous increase above $\sim 80^\circ C$, seems to be due to fluctuations in P_s becoming very large, thus increasing its contribution to the widths compared to the contribution from vacancy hopping.

Our line width experiments, thus suggest a combined contribution due to both vacancy hopping and torsional oscillations of NO_2^- i.e. fluctuations in P_s . It will be extremely difficult to separate the two contributions.

In the whole temperature range $\sim -10^\circ C$ to $150^\circ C$, only the vacancy Mn^{2+} exchange seems to be taking place. From Figures 3.2(a), (b), (c) it can be visualized that the diffusion of Na^+ from any site other than those lying along [100] and [001], is difficult due to the large volume of NO_2^- ion and resulting gaps being very small. Further the \vec{E}_{loc} of \vec{P}_s is very strong and will put constraints on the vacancy jumps. All this seems to make, only the Mn^{2+} vacancy (at 001 or $00\bar{1}$ for S-I) exchange feasible. The angular variation of linewidths of S-I for \vec{H} in (001) plane shown in Figure 6.9 supports this model.

The fast broadening of lines is observed for all other spectra S-III, S-IV etc above $\sim 10^{\circ}\text{C}$. The broadening due to fluctuations in P_s will have nearly similar temperature dependence and anisotropy for all the spectra. The fast broadening above approximately same temperature ($\sim 10^{\circ}\text{C}$) for all the spectra suggests that the activation energies for vacancy hopping (jumps) for various complexes is nearly same. The angular variation of line width of S-III, at $\sim 35^{\circ}\text{C}$ is shown in Figure 6.10. It is evident that the width is smallest for $\vec{H} // [100]$ [also see Table 6(III)] and largest near $[010]$. Such an anisotropy is expected from both vacancy Mn^{2+} exchange and fluctuations in P_s .

Line Widths of Spectrum-II

As S-II was concluded to be most probably due to the metastable clusters, but the possibility of its being due to isolated Mn^{2+} was not ruled out. If S-II is due to two complexes $\text{Mn}^{2+}\text{-V } 001$ and $\text{Mn}^{2+}\text{-V } 00\bar{1}$ in metastable clusters, then the Mn^{2+} -vacancy exchange will not cause broadening of the lines, as the two complexes give only one spectrum for any orientation of \vec{H} . If S-II is due to isolated Mn^{2+} , the question of vacancy hopping does not arise.

The spontaneous polarization in the metastable clusters was concluded to be nearly zero. But the NO_2^- ions in the metastable phase may be undergoing torsional oscillations, and their oscillations will cause fluctuations in the dipolar field at the Mn^{2+} site. If the Mn^{2+} complex lacks the centre of inversion (which it will, because of association with vacancy) these fluctuations may cause significant broadening of the ESR lines of S-II, which may give anisotropy and temperature

dependence of line widths similar to those for S-I. If S-II is due to isolated Mn^{2+} then fluctuations in P_s will cause the broadening and this will be very much similar to that for S-I.

The linewidths for S-II in the range $\sim 30^\circ C$ to $\sim 150^\circ C$ are nearly similar, to those of S-I, in anisotropy and temperature dependence both. The line widths for S-I had significant contribution from the vacancy hopping and such contribution for S-II is not expected. Then the similarity of widths of S-I and S-II, can be explained only by assuming that the fluctuations due to P_s give major contribution to line widths of S-I as well as S-II, in the complete temperature range.

There is marked M_s dependence and asymmetry about central transition of line widths of S-II, above $\sim 100^\circ C$. The asymmetry of line widths can be only explained on the basis of fluctuations in the components of D-tensor.

In Figures 6.7 and 6.8, the temperature variation of widths of S-II in the range $\sim 30^\circ C$ to $\sim 220^\circ C$ is shown. The $\log (\Delta H)$ versus $1/T$ curve corresponding to Figure 6.7 shows the following behaviour. In the temperature range $\sim 30^\circ C$ to $\sim 85^\circ C$ it can be fitted to a straight line with activation energy of ~ 0.10 eV. in the range $\sim 100^\circ C$ to $\sim 140^\circ C$ with activation energy of ~ 0.24 eV. and in the range $\sim 150^\circ C$ to $\sim 159^\circ C$ with activation energy of ~ 0.8 eV. Above $\sim 150^\circ C$, a very fast increase in line widths is observed which is related to the anomaly in torsional oscillations of NO_2^- at the phase transition.

These changing slopes show the increase in the fluctuation of P_s due to increase in amplitudes of torsional motion. Above $\sim 150^\circ\text{C}$, there will be substantial number of NO_2^- ions flipping between parallel and antiparallel polarized states. This will account for the sudden increase in widths above this temperature. Due to large errors in width measurements, the phase transition temperature could not be determined accurately (rough estimate is $161 \pm 2^\circ\text{C}$). But from the E vs temperature curve of Figure 6.4, T_c was determined to be $159 \pm 2^\circ\text{C}$.

In the sinusoidal antiferroelectric phase, there is a short range ordering of ferroelectric domains (~ 8 unit cells [38]). Such an ordering will cause substantial decrease in line widths, compared to those just below T_c . But we could not observe such behaviour even after repeated attempts with various crystals. This may be due to either the temperature range of antiferroelectric phase becoming very narrow or vanishing due to presence of Mn^{+2} ions.

Above T_c the increase in widths is slower compared to that before phase transition. It can be easily seen that despite large errors a marked difference exists between heating and cooling cycles (above T_c). On cooling the crystal from 220°C , the width decreases faster compared to the increase during the heating cycle, upto $175 \pm 3^\circ\text{C}$. Below this temperature the width increases upto $163 \pm 2^\circ\text{C}$. Below this, the widths decreases and below $\sim 160^\circ\text{C}$, the behaviour is nearly identical with that for heating cycle. This anomalous behaviour on cooling seems

to be related to the phase transition reported at $\sim 178^{\circ}\text{C}$ [40, 41] which has been identified at $\sim 175 \pm 3^{\circ}\text{C}$ from the temperature variation of D of S-II (fig. 6.3).

TABLE 6.(I) Peak to peak derivative widths (ΔH) of Spectrum-I.

Temperature	Field Orientation	Fine Structure Transition Groups					
		-5/2 <-->-3/2	-3/2 <-->-1/2	-1/2 <-->+1/2	+1/2 <-->+3/2	+3/2 <-->+5/2	+1/2 <-->+5/2
30°C	$\vec{H}/[100]$	6.5 \pm 0.2	5.5 \pm 0.2	5.1 \pm 0.1	6.0 \pm 0.2	6.2 \pm 0.2	6.2 \pm 0.2
	$\vec{H}/[001]$	-	11.0 \pm 1.5	5.1 \pm 0.2	6.8 \pm 0.5	14.0 \pm 2.5	
	$\vec{H}/[010]$	25.0 \pm 2.5	17.0 \pm 2.0	6.5 \pm 0.2	19.0 \pm 2.0	23.0 \pm 2.5	
	\vec{H}/Z_1	25.0 \pm 3.5	18.0 \pm 2.5	6.5 \pm 0.2	19.0 \pm 2.5	25.0 \pm 3.0	
	\vec{H}/Y_1	-	10.0 \pm 2.0	5.0 \pm 0.2	6.6 \pm 0.5	14.0 \pm 2.5	
	$\vec{H}/[100]$	3.0 \pm 0.2	2.7 \pm 0.2	2.7 \pm 0.2	2.7 \pm 0.2	3.3 \pm 0.2	3.3 \pm 0.2
-100°C	$\vec{H}/[001]$	-	4.5 \pm 0.5	2.7 \pm 0.2	3.0 \pm 0.3	5.0 \pm 0.3	
	$\vec{H}/[010]$	6.0 \pm 0.2	4.8 \pm 0.2	3.0 \pm 0.2	-4.8 \pm 0.2	5.8 \pm 0.2	
	\vec{H}/Z_1	6.2 \pm 0.2	4.7 \pm 0.2	3.0 \pm 0.2	4.8 \pm 0.2	5.8 \pm 0.2	
	\vec{H}/Y_1	-	4.3 \pm 0.5	2.7 \pm 0.2	3.3 \pm 0.3	4.8 \pm 0.3	

All values are in Gauss.

TABLE 6.(II) Peak to peak derivative widths (ΔH) of Spectrum-II.

Temperature	Field Orientation	$-5/2 <-->-3/2$	$-3/2 <-->-1/2$	$-1/2 <-->+1/2$	$+1/2 <-->+3/2$	$+3/2 <-->+5/2$
30°C	$\vec{H}/[100]$	7.6 ± 0.4	5.5 ± 0.4	5.1 ± 0.2	5.4 ± 0.4	7.6 ± 0.4
	$\vec{H}/[001]$	-	-	5.1 ± 0.3	7.0 ± 0.5	16.0 ± 3.0
	$\vec{H}/[010]$	30.0 ± 5.0	20.0 ± 5.0	5.4 ± 0.3	20.0 ± 5.0	30.0 ± 5.0
-140°C	$\vec{H}/[100]$	30 ± 3.0	27.0 ± 3.0	10.0 ± 2.0	22.0 ± 2.0	30.0 ± 3.0

All values are in Gauss.

TABLE 6.(III) Peak to peak derivative line widths (ΔH) of Spectrum- III.

Temperature	Field Oriantation	-5/2 <-->-3/2	-3/2<-->-1/2	-1/2<-->+1/2	1/2<-->+3/2	+3/2<-->+5/2
30°C	$\vec{H}/[100]$	8.0 \pm 1.5	-	-	5.0 \pm 1.0	-
	$\vec{H}/[001]$	-	-	5.5 \pm 1.0	6.5 \pm 1.0	8.5 \pm 2.0
	$\vec{H}/[010]$	27.5 \pm 3.0	16.0 \pm 3.0	-	-	27.5 \pm 3.0
	$\vec{H}/\langle X_m \rangle$	18.0 \pm 2.0	12.0 \pm 2.0	10.0 \pm 2.0	12.0 \pm 2.0	18.0 \pm 2.0
	$\vec{H}/\langle Z_m \rangle$	28.0 \pm 3.0	20.0 \pm 3.0	12.0 \pm 2.0	20.0 \pm 3.0	28.0 \pm 3.0
	$\vec{H}/[100]$	3.5 \pm 0.2	-	-	3.3 \pm 0.2	-
-100°C	$\vec{H}/[001]$	4.5 \pm 0.2	4.0 \pm 0.3	3.5 \pm 0.3	4.0 \pm 0.2	4.5 \pm 0.2
	$\vec{H}/[010]$	-	5.0 \pm 0.5	-	-	6.0 \pm 0.5
	$\vec{H}/\langle X_m \rangle$	4.0 \pm 0.2	3.5 \pm 0.2	3.0 \pm 0.3	3.5 \pm 0.2	4.0 \pm 0.3
	$\vec{H}/\langle Z_m \rangle$	5.5 \pm 0.3	4.6 \pm 0.3	3.3 \pm 0.3	4.06 \pm 0.3	5.5 \pm 0.5
	$\vec{H}/[100]$	-	-	-	-	-

All values are in Gauss.

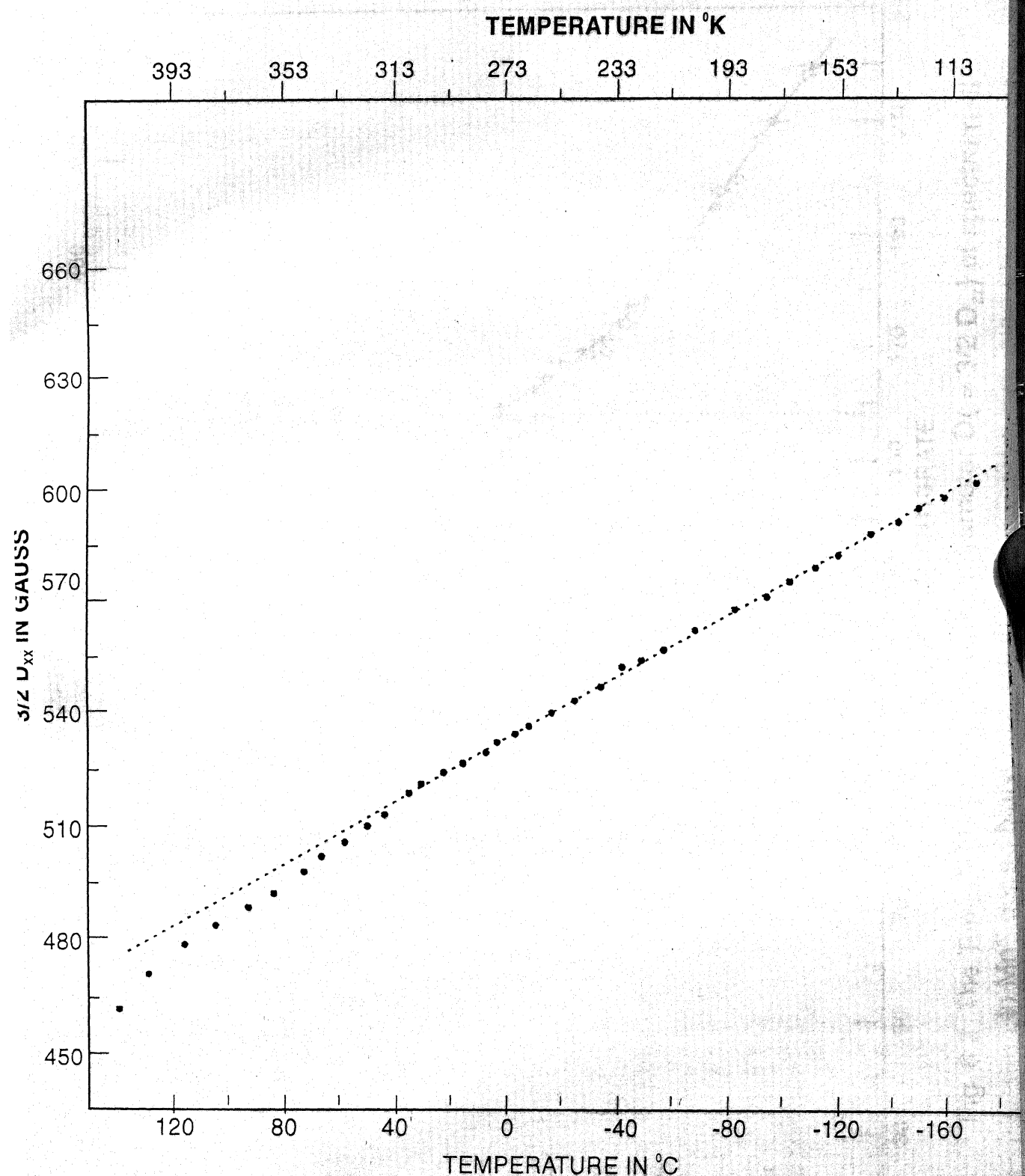


Fig. 6.1 The Temperature Variation of the Parameter
 $\frac{3}{2} D_{xx}$ of Spectrum I in Mn^{+2} Doped NaNO_2 Single crystal.

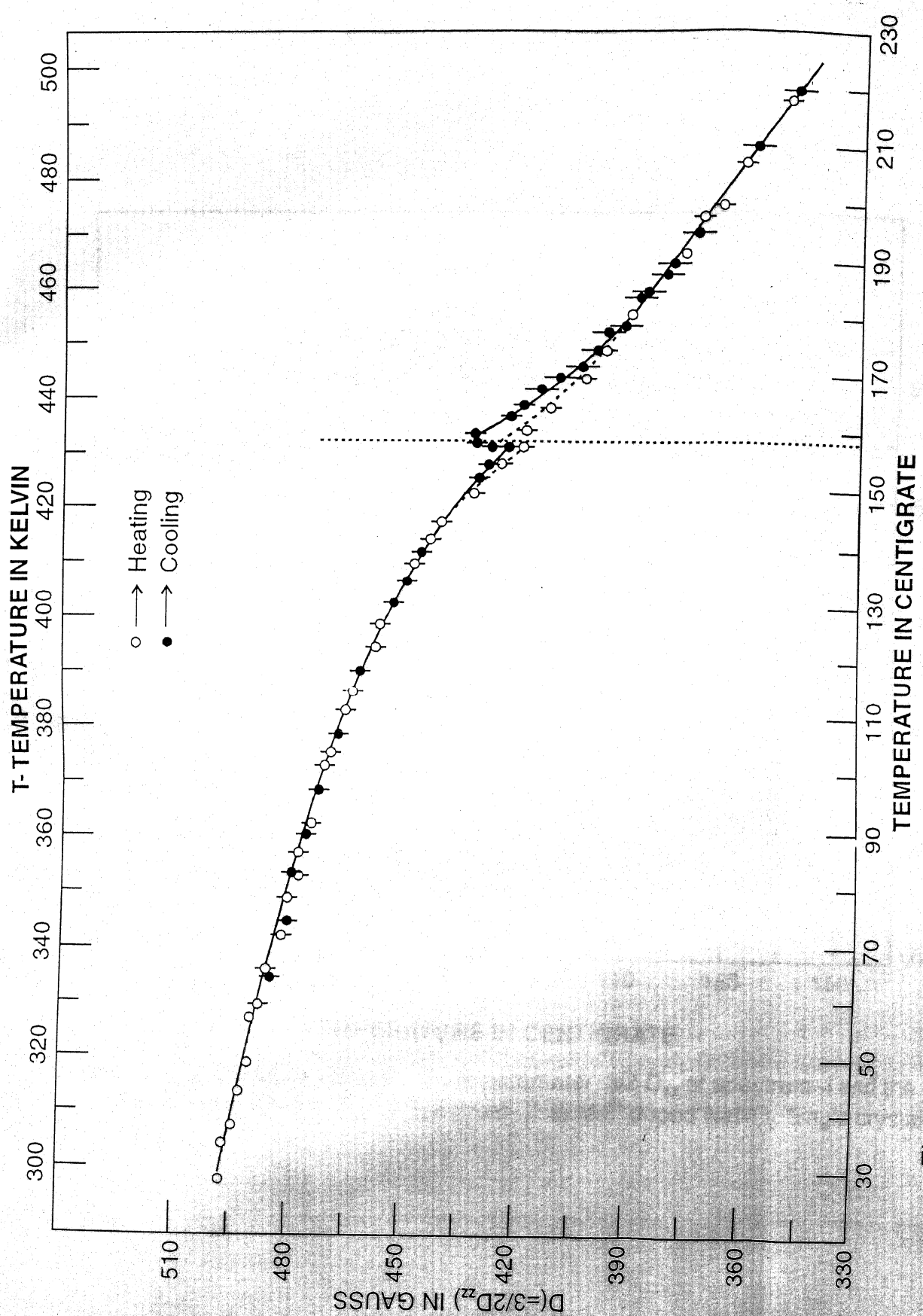


Fig. 6.2 The Temperature Variation of the parameter $D (= 3/2 D_{zz})$ of spectrum -II in Mn^{2+} doped NaNO_3 Single crystal

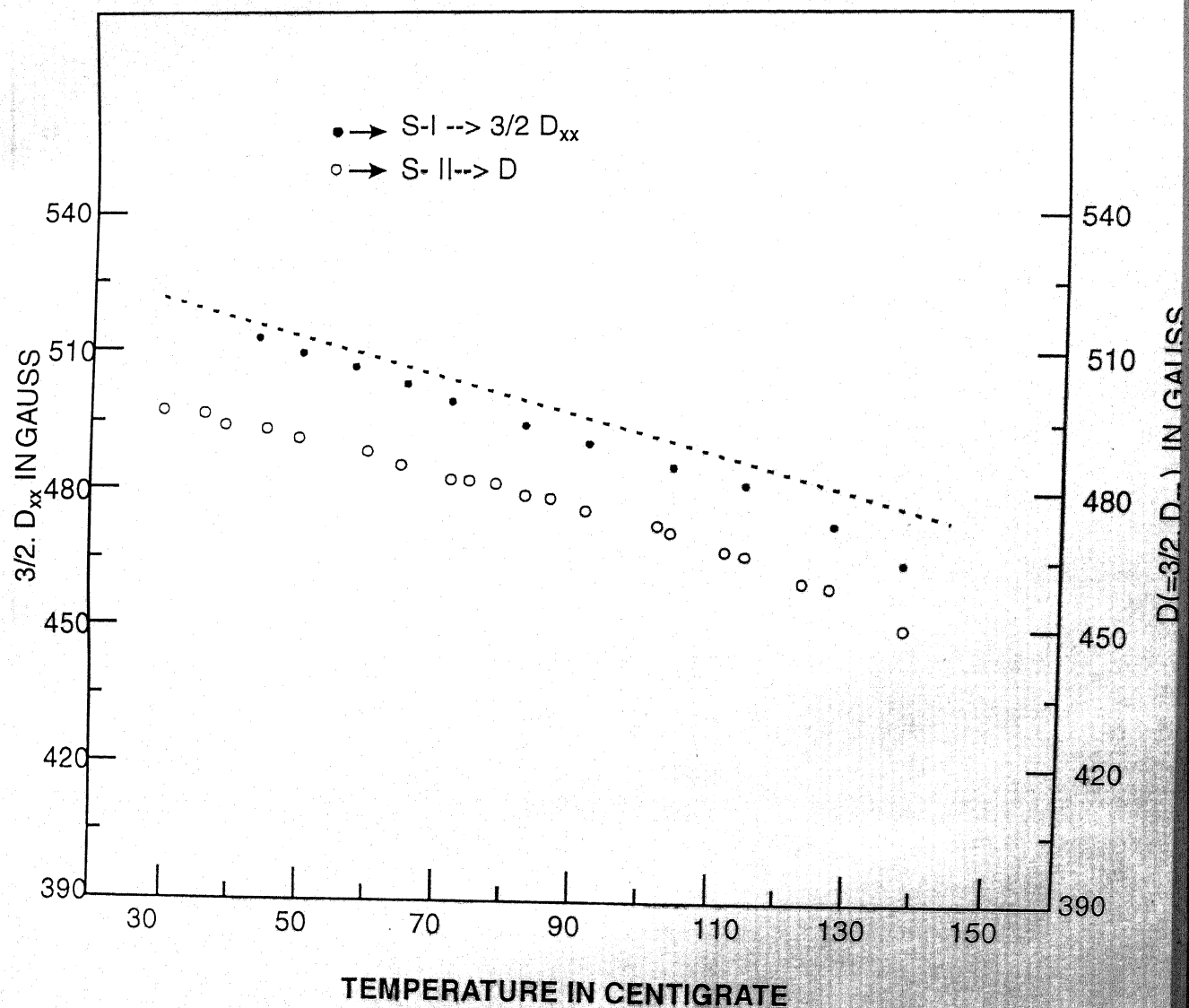


Fig. 6.3 The Temperature Variation of the parameter $3/2 D_{xx}$ of spectrum -I and the parameter $D(=3/2 D_{zz})$ of Spectrum- II in Mn^{2+} doped $NaNO_2$ Single crystal.

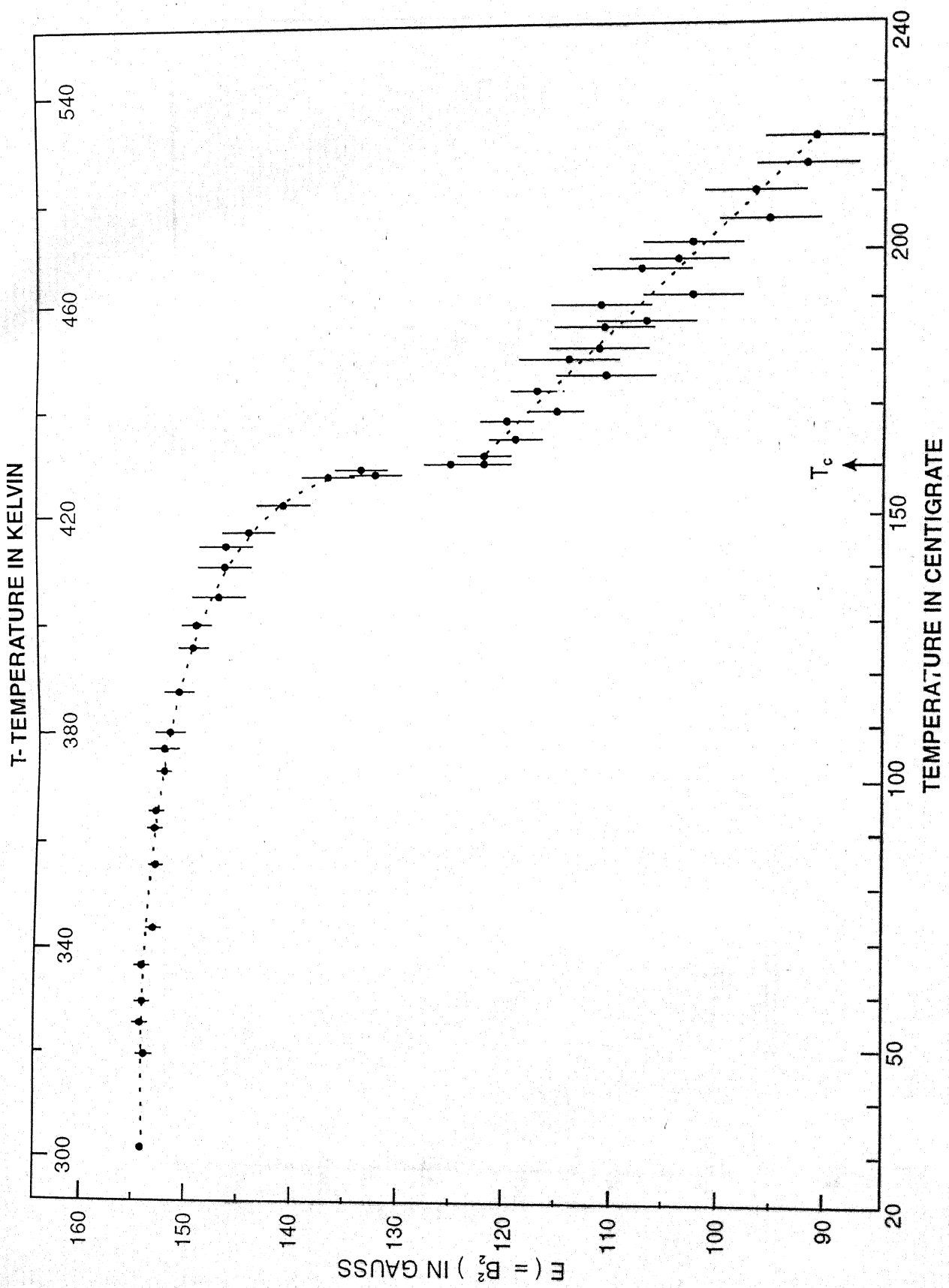


Fig. 6.4 The Temperature Variation of the parameter $E (= B_z^2 = 1/2 (D_{xx} - D_{yy}))$ of spectrum -II in Mn^{2+} doped $NaNO_2$. T_c is the Phase Transition temperature.

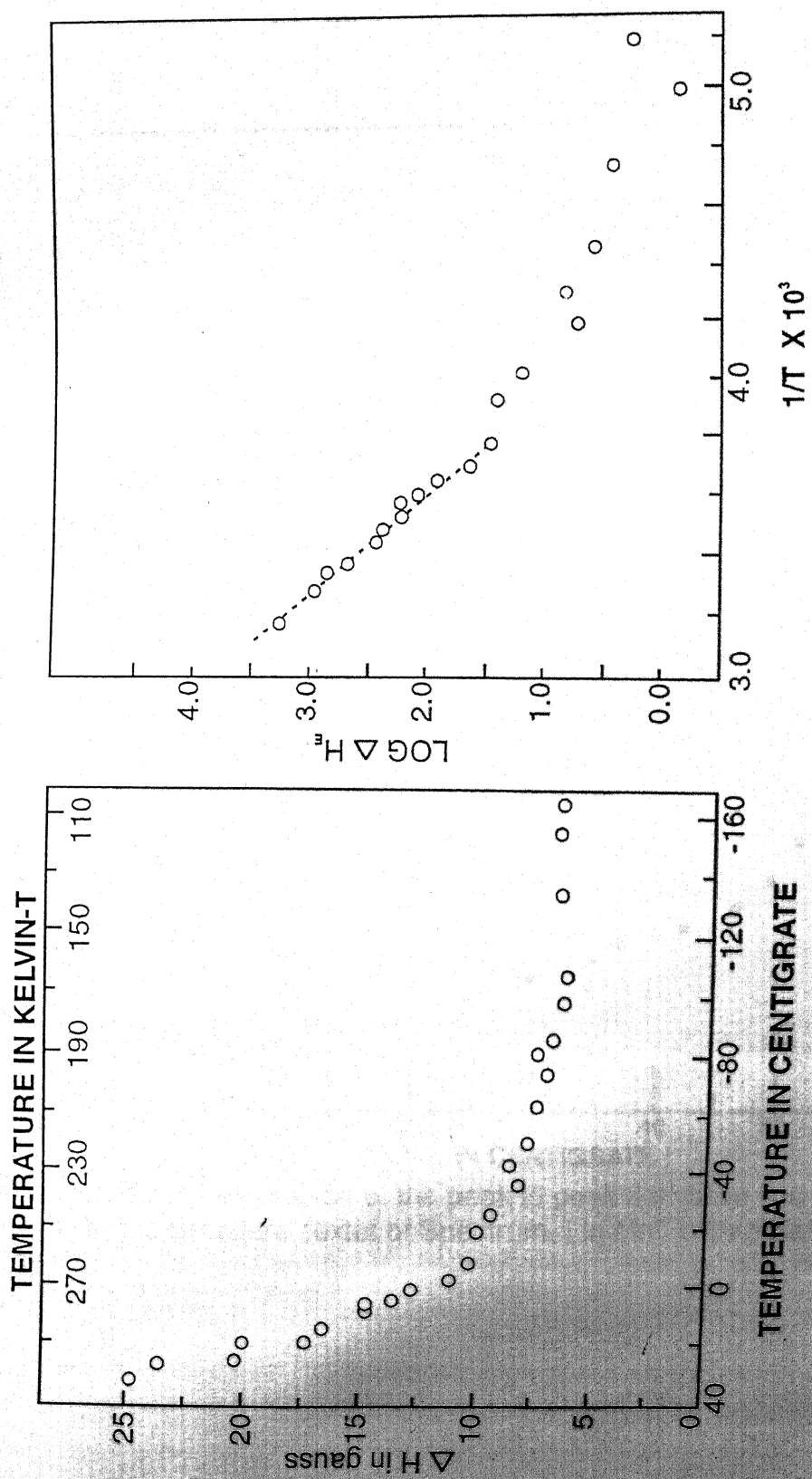


Fig. 6.5(a) The Temperature Variation of the peak to peak derivative line width (ΔH) of $(-5/2 \leftrightarrow -3/2)$ Fine Structure sextet of S-I in Mn^{2+} doped $NaNO_2$. For H/Z_1
 (b) Log of Excess linewidth (ΔH_E) is plotted versus $10^3/T$.

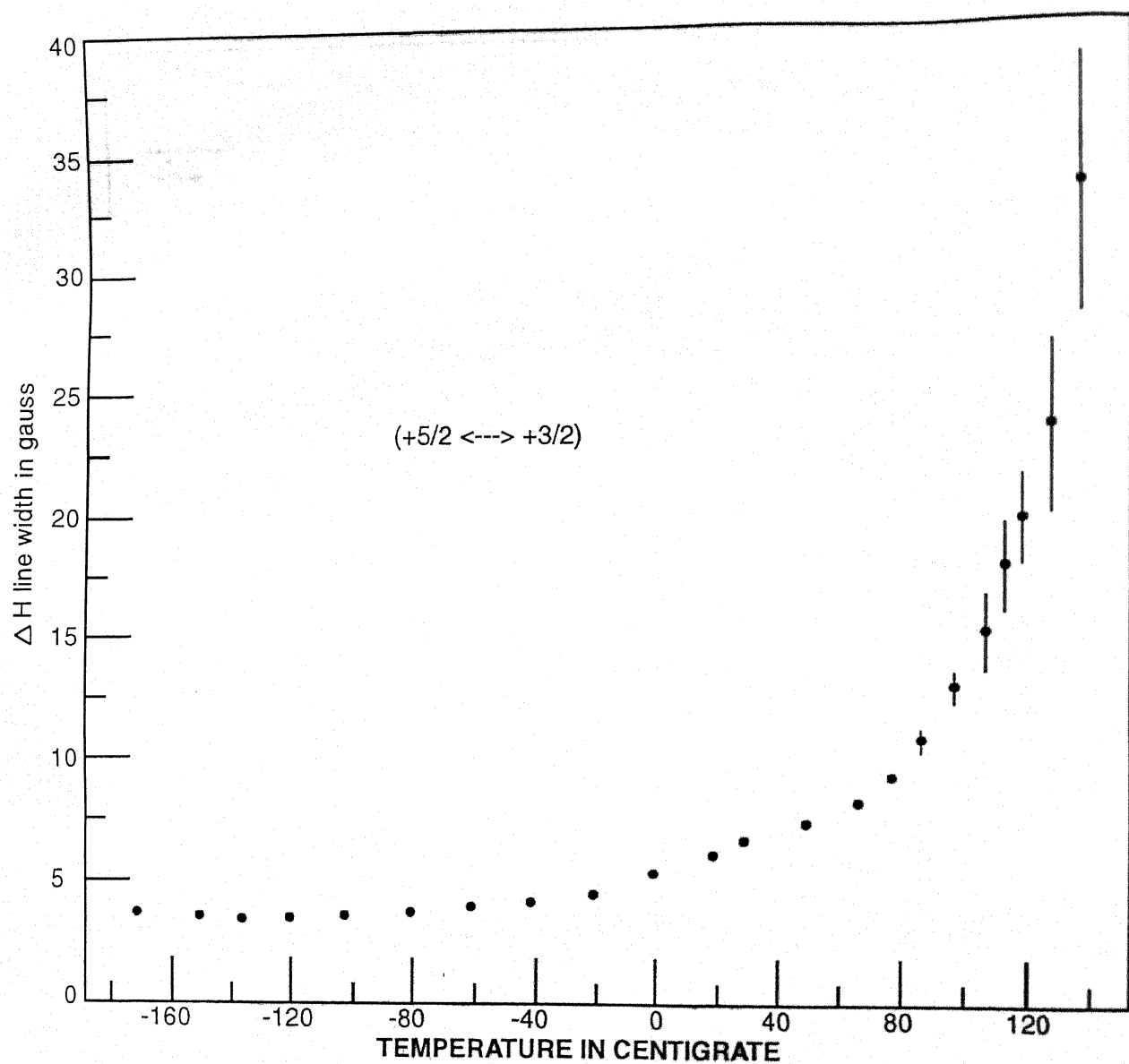


Fig. 6.6 The Temperature Variation of the peak to peak derivative line width (ΔH) of $(+5/2 \leftrightarrow +3/2)$ Fine Structure sextet of Spectrum- I in Mn^{2+} doped $NaNO_2$ Single crystal for $H \parallel [100]$.

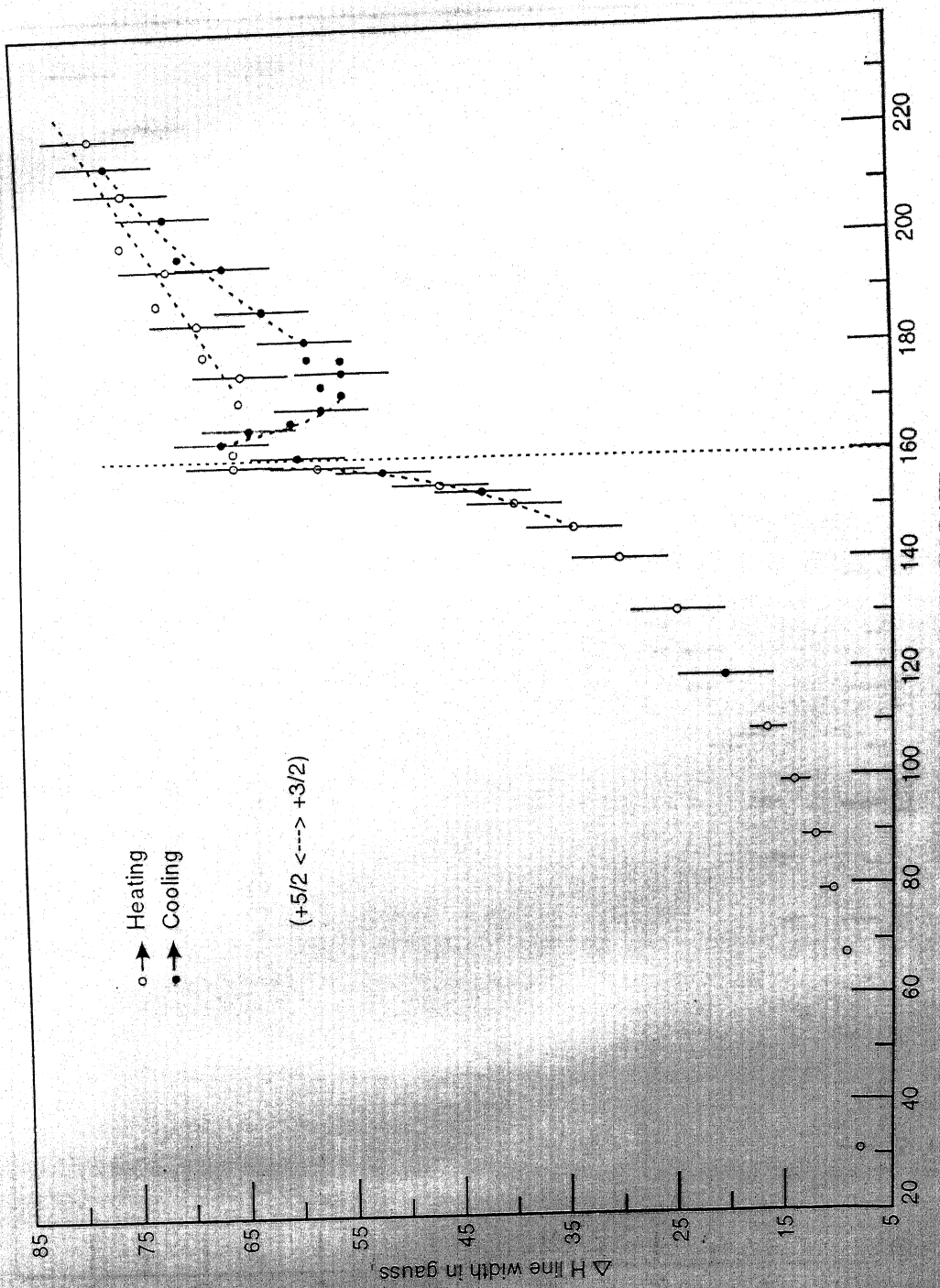


Fig 6.7 The Temperature Variation of the peak to peak derivation line width (ΔH) of $(+5/2 \leftrightarrow +3/2)$ Fine Structure sextet of S-II in Mn^{2+} doped $NaNO_2$ Single crystal for $H \parallel [100]$.

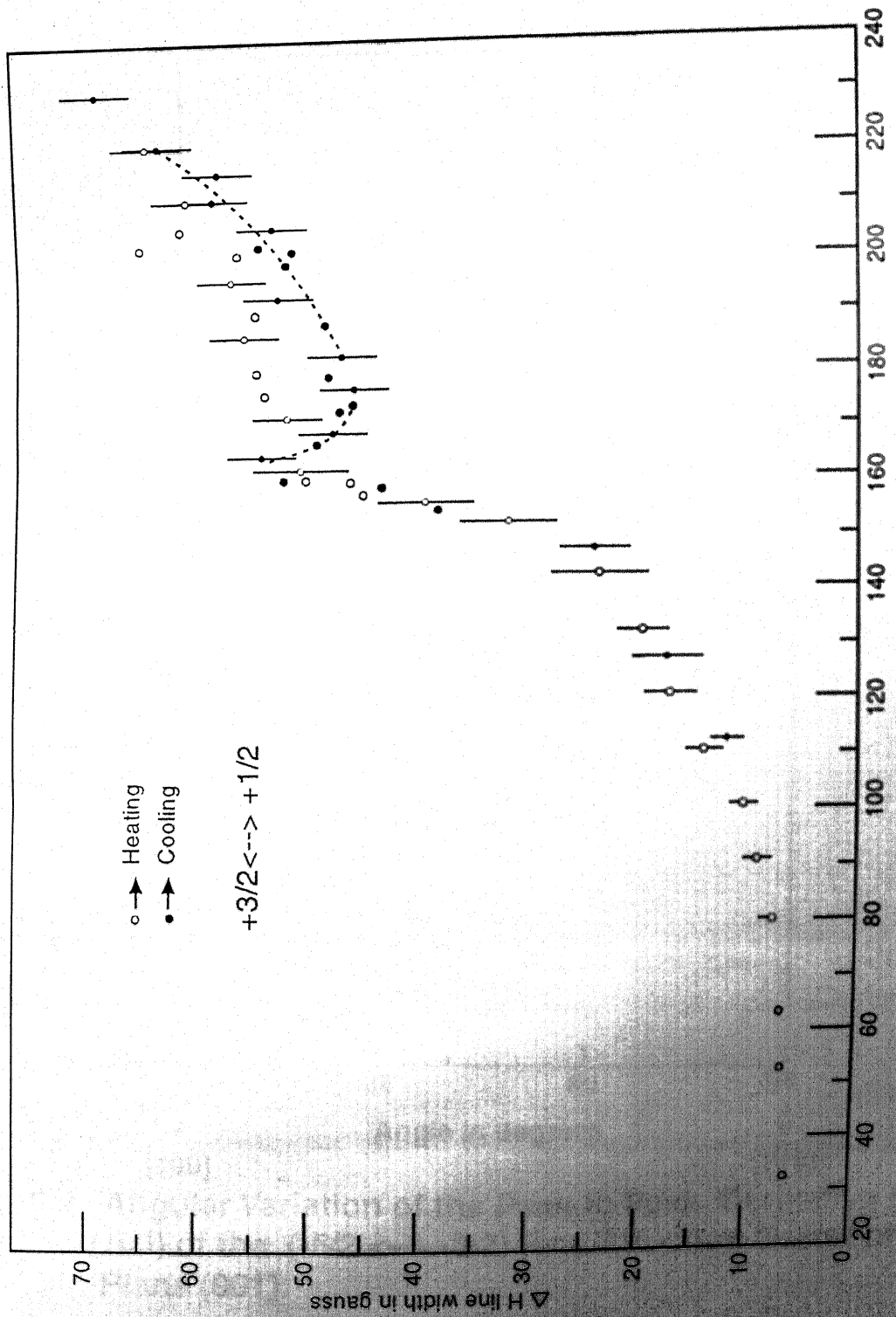


Fig 6.8 The Temperature Variation of the peak to peak derivative line width (ΔH) of $(+3/2<-->+1/2)$ Fine Structure sextet of S-II in Mn^{2+} doped Single crystal for $\mathbf{H}/[100]$.

TEMPERATURE IN CENTIGRATE

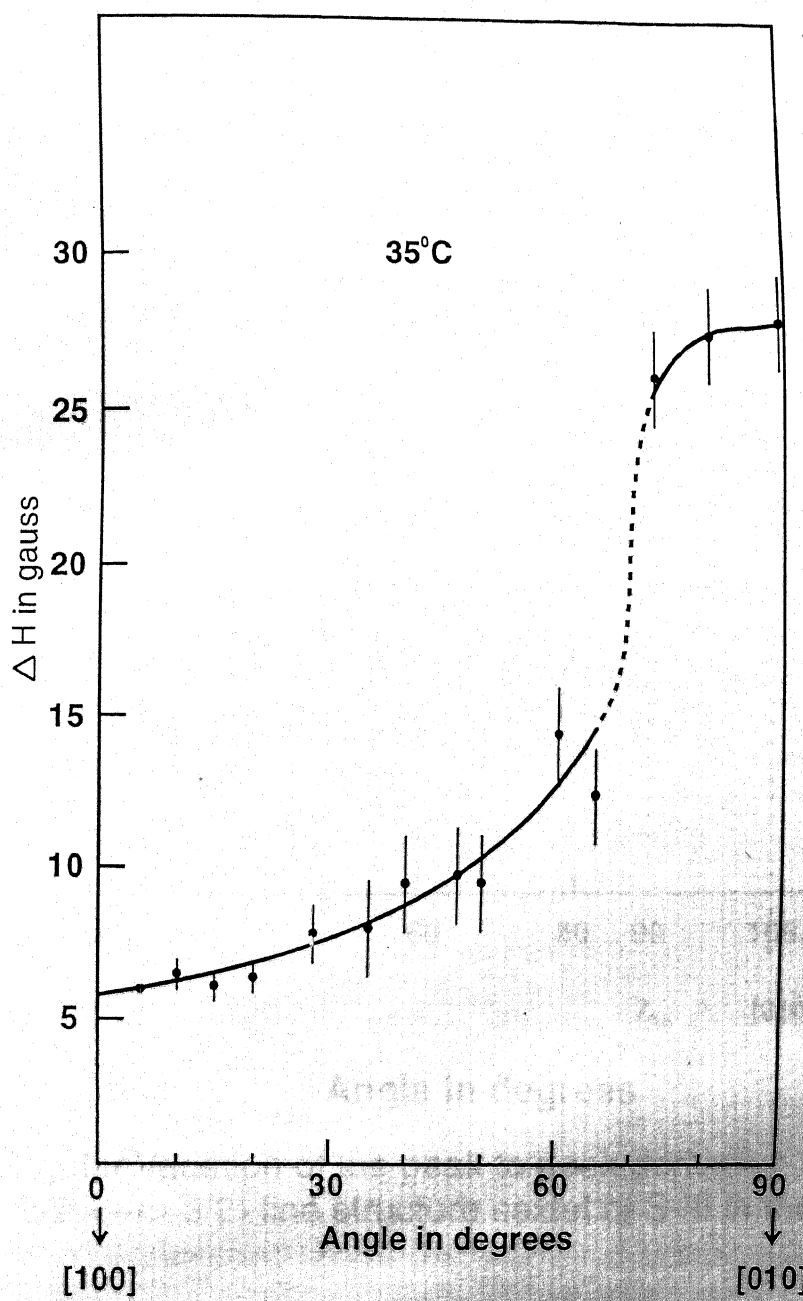


Fig. 6.9 : Angular Variation of the Peak to Peak Derivative Line Width (ΔH) of the $(-5/2 \leftrightarrow -3/2)$ Fine Structure Sextet of S-I In this Plans (001).

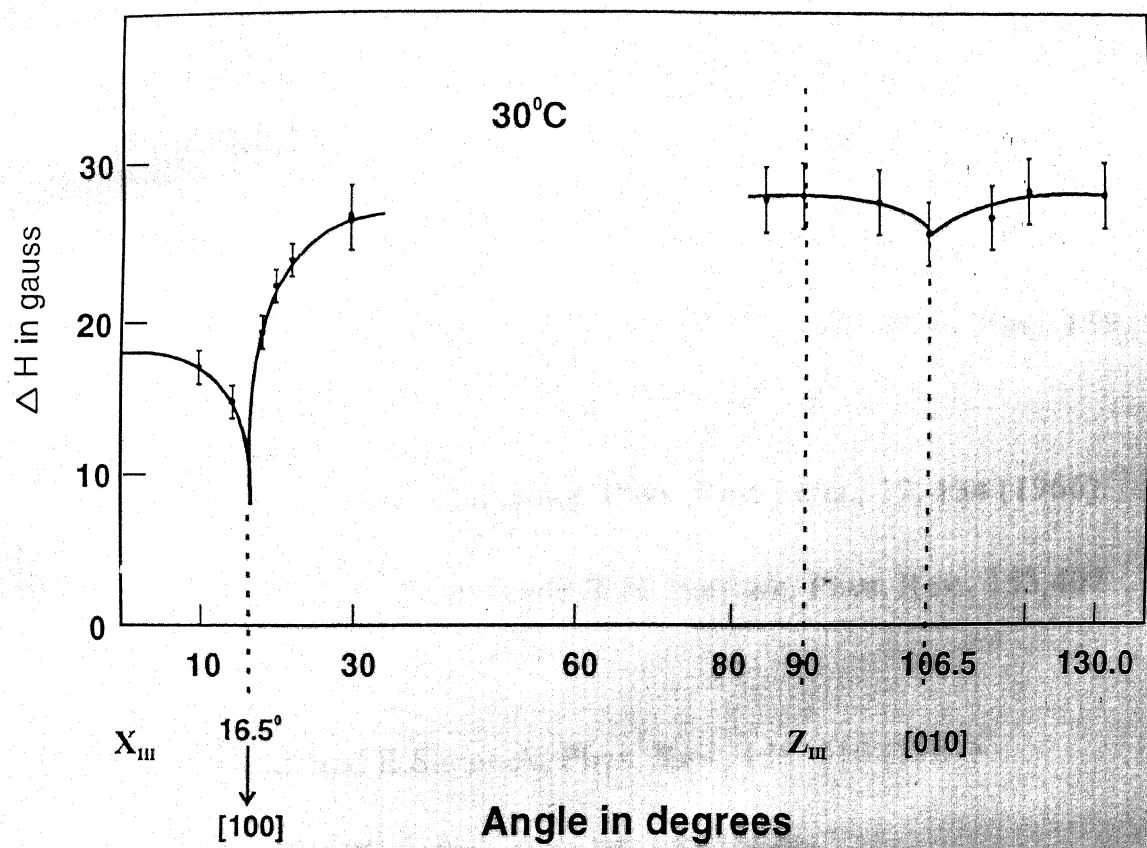


Fig. 6.10 : Angular Variation of the peak to peak derivative linewidth (ΔH) of the $(-5/2 \longleftrightarrow -3/2)$ fine structure sextet of S-III in the Plane (001).

REFERENCES

1. G.W. Smith, J. Appl. Phys., 35, 1217 (1964).
2. R.R. Sharma, T.P. Das and R. Orbach, Phys. Rev., 149, 257 (1966).
3. R.R. Sharma, T.P. Das and R. Orbach, Phys. Rev., 155, 338 (1967).
4. R.R. Sharma, T.P. Das and R. Orbach, Phys. Rev., 171, 378 (1968).
5. B.G. Wybourne, J. Chem. Phys., 43, 4506 (1965).
6. A. Van Heuvelen, J. Chem. Phys., 46, 4903 (1967).
7. W.M. Walsh Jr. , J. Jeener and N. Bloembergen, Phys. Rev., 139., A, 1338 (1965).
8. E. Simanek and NaiLiHuong, Phys. Rev. Letts., 17, 134 (1966).
9. J. Rosenthal, L. Yarmus and R.H. Bartram, Phys. Rev., 153, 407 (1967).
10. R. Orbach and E.Simanek, Phys. Rev., 158, 310 (1967).
11. K. Zdansky, Phys. Stat. Sol., 28, 181 (1968).
12. G. Pfister, W. Dreybrodt and W. Assmus, Phys. Stat. Sol., 36, 351 (1969).
13. R.A. Serway, Phys. Rev. B 3, 608 (1971).
14. K.N. Shrivastava, Phys. Rev., 187, 446 (1969).

15. K.N. Shrivastava, Chem. Phys. Lett., 6, 545 (1970).
16. K.N. Shrivastava, .Phys. Lett., A 42, 385 (1973).
17. K.N. Shrivastava, Chem. Phys. Lett., 22, 622 (1973).
18. A. Leclerc and A. Manoogian, J. Chem. Phys., 63, 4456 (1975).
19. J.A. Hodges, 18th Ampere Congress, Nottingham, 1974, p. 153.
J.A. Hodges, J.Phys. Chem. Solids, 35 ,1385 (1974).
20. J.M. Moret and R. Lacroix, Helvetica Physica Acta, 49, 313 (1976).
21. M. Schlaak and Alarich Weiss, Zeit Fur Naturforschung,28a, 1933
(1973).
22. A. Manooigan and A. Leclerc, J. Chem. Phys., 63, 4450 (1975).
23. R. Biederbick, G. Born,A. Hoftaetter and A. Scharmann, . Z. Physik,
B 22, 219 (1975).
24. K.A. Muller, in 'Structural Phase Transitions and Soft Modes', Edited
by E.J.Samuelson, E. Andersen and J. Feder, Universitets forlaget,
1971, p. 63, p.73,p.85.
25. A.W. Horning, R.C. Rempel and H.E. Weaver J.Phys. Chem. Solids,
10, 1 (1959).
26. L. Rimal and G.A. de Mars, Phys. Rev. 127, 702 (1962).
27. J.H.H. Mooy, Ph.D. Thesis (1974), Universiteit Van Amsterdam.
28. H. Bartuch, and W. Windsch, Phys. Stat. Sol. (a), 14, K 51 (1972);

16, K 121, (1973).

29. W. Windsch, R. Kunze and G. Volkel, Phys. Stat. Sol. (a), 26, K 175 (1974).

30. T. Kato and R. Abe, J. Phys. Soc. Japan, 36, 1065 (1974).

31. T. Kobayashi, J. Phys. Soc. Japan, 35, 558 (1973).

32. M. Maeda, I. Suzuki and R. Abe, J. Phys. Soc. Japan, 39, 1319 (1975).

33. D.E. O'Reilly and G.E. Schacher, J. Chem. Phys., 43, 4222 (1965).

34. K. Hamano, J. Phys. Soc. Japan, 35, 157 (1973).

35. K. Ema, K. Hamano and I. Hatta, J. Phys. Soc. Japan, 39, 726 (1975).

36. N. Maruyama and S. Sawada, J. Phys. Soc. Japan, 20, 811 (1965).

37. S. Nomura, J. Phys. Soc. Japan, 16, 1352 (1961).

38. Y. Yamada, I. Shibuya and S. Hoshino, J. Phys. Soc. Japan, 18, 1594 (1963).

39. S. Tanasaki, J. Phys. Soc. Japan, 16, 579 (1961),
ibid, 18, 1181 (1963).

40. Y. Takagi and K. Gesi, J. Phys. Soc. Japan, 19, 142 (1964).

41. Y. Takagi and K. Gesi, J. Phys. Soc. Japan, 22, 979 (1967).
I. Hatta and A. Ikushima, J. Phys. Chem. Solids, 34, 57 (1973)

42. T. Yagi and I. Tatsuzaki, J.Phys. Soc. Japan, 35, 1675 (1973).
43. S.I. Kwun and K.M. Lee, J. Korean Phys. Soc., 7, 30 (1974).
M.N. Lee and S.I. Kwun, J.Korean Phys. Soc., 3, 9 (1970).
44. C.P. Slichter, 'Principles of Magnetic Resonance', Harper and Row, New York, (1964).
45. C.P. Poole and H.A. Farach, 'Relaxation in Magnetic Resonance', Academic Press (1971).
46. A. Abragam and B. Bleaney, 'Electron Paramagnetic Res. in Trans. Ions', Clarendon Press, Oxford (1970).
47. D. Shaltiel and W.Ilow, Phys. Rev., 124, 1062 (1961).
48. R. Bottcher and J. Dziesiaty, Phys. Stat. Sol. (b), 57, 617 (1973).
49. E.R. Feher, Phys. Rev., 136A, 145 (1964).
50. A.M. Stoneham, Proc. Phys. Soc. A, 89, 909 (1966).
51. A.B. Roitsin, Sov. Phys. Uspekhi, 14, 766 (1972).
52. G. D. Watkins, Phys. Rev., 113, (1959), p. 79 and p. 91.
53. R.F. Tucker Jr., Phys. Rev., 112, 725 (1958).
54. S.U. Cheema and M.J.A. Smith, J. Phys. C: Solid Stat. Phys., 2, 1751 (1969).
55. K. Nishimura and T. Hashimoto, J. Phys. Soc. Japan, 35, 1699 (1973).

56. L.W. Barr and A.B. Lidiard, in 'Physical Chemistry -An Advanced Treatise-Vol. X', Ed. W. Jost, Academic Press (1970).
57. R. Ikeda, M. Mikami, D. Nakamura and M. Kubo, J.Magn. Res. 1, 211 (1969).
58. Y. Sato, K. Gesi and Y. Takagi, J. Phys. Soc. Japan, 16, 2172 (1961).
59. E.V. Chisler and M.S. Shur, Phys. Stat. Sol., 17, 163 and 173 (1966).